Titre: Title:	Modeling of Heat Conduction in Hybrid Nanodispersions
Auteur: Author:	Arash Behrang
Date:	2014
Type:	Mémoire ou thèse / Dissertation or Thesis
Référence: Citation:	Behrang, A. (2014). Modeling of Heat Conduction in Hybrid Nanodispersions [Thèse de doctorat, École Polytechnique de Montréal]. PolyPublie. https://publications.polymtl.ca/1588/

URL de PolyPublie: PolyPublie URL:	https://publications.polymtl.ca/1588/
Directeurs de recherche: Advisors:	Sylvain Turenne, Miroslav Grmela, & Charles Dubois
Programme: Program:	Génie mécanique

UNIVERSITÉ DE MONTRÉAL

MODELING OF HEAT CONDUCTION IN HYBRID NANODISPERSIONS

ARASH BEHRANG
DÉPARTEMENT DE GÉNIE MÉCANIQUE
ÉCOLE POLYTECHNIQUE DE MONTRÉAL

THÈSE PRÉSENTÉE EN VUE DE L'OBTENTION
DU DIPLÔME DE PHILOSOPHIAE DOCTOR
(GÉNIE MÉCANIQUE)
NOVEMBRE 2014

UNIVERSITÉ DE MONTRÉAL

ÉCOLE POLYTECHNIQUE DE MONTRÉAL

Cette thèse intitulée :

MODELING OF HEAT CONDUCTION IN HYBRID NANODISPERSIONS

présentée par : BEHRANG Arash

en vue de l'obtention du diplôme de : Philosophiae Doctor

a été dûment acceptée par le jury d'examen constitué de :

Mme HEUZEY Marie-Claude, Ph. D., présidente

M. TURENNE Sylvain, Ph. D., membre et directeur de recherche

M. GRMELA Miroslav, Doct., membre et codirecteur de recherche

M. DUBOIS Charles, Ph. D., membre et codirecteur de recherche

M. BERNIER Michel, Ph. D., membre

M. JOU David, Doct., membre

DEDICATION

To my beloved parents and my brother,

and my love ; Sara. . .

ACKNOWLEDGMENT

I would like to express my special and sincere gratitude to my research supervisors, Professor Miroslav Grmela, Professor Charles Dubois, Professor Sylvain Turenne, and Professor Pierre G. Lafleur for their extensive support, excellent guidance and warm encouragement during my research as well as for the trust they placed in me to work in my own way. I would like to show my deepest and greatest appreciations to Professor Miroslav Grmela. You are the most knowledgeable, eminent, hard working, considerate, and inspiring professor, I have ever met. I would like to offer my special thanks to Professor Charles Dubois and Professor Sylvain Turenne for their helpful and precious comments and suggestions.

I owe a very important debt to Professor Ahmad Ramazani S.A. who is not only a professor but a friend. He taught me ; not only scientific matters, but much knowledge that will significantly encompass all aspects of my life.

I would also like to convey my gratitude to all my committee members for accepting to be a member of the jury.

I wish to express my gratitude to all secretaries and technical staff of the Chemical Engineering Department in Ecole Polytechnique de Montreal.

Words cannot express how much I am thankful to my dearest parents for their unconditional love, support and dedication. They learned me to never give up on my dreams.

My love Sara, your love was a strong driving force to overcome difficulties during my research journey. I could never have made this, without your love, encouragement and support.

RÉSUMÉ

Pour une large gamme d'applications en ingénierie, allant des matériaux de conversion de l'énergie thermoélectrique aux matériaux d'interface thermique, la conductivité thermique dans les structures à l'échelle nanométrique fût un sujet intéressant et important à la fois dans la recherche fondamentale et appliquée. La théorie classique de Fourier ne permet pas de décrire la conduction thermique dans les matériaux nanostructurés en raison de la négligence des événements de la limite de diffusion qui jouent un rôle très important dans les structures à l'échelle nanométrique. Le but ultime de ce travail est d'établir un cadre général pour étudier la conductivité thermique dans les nanodispersions. Dans cette thèse, en passant en revue les principes de base du transport des phonons dans les nanostructures, les coefficients de conductivité thermique qui se posent dans la théorie de la chaleur macrosopique de Fourier sont modifiés et rendus applicables pour les nanodispersions. Afin d'adapter la conductivité thermique macroscopique aux besoins de cette étude, l'influence de la limite de diffusion des phonons est prise en compte. La majorité des libres parcours moyens de la matrice et des particules dispersées fournis par la théorie cinétique sont modifiés de façon à capturer les effets de la limite de diffusion. Un bon accord entre les prédictions de nos modèles et les résultats expérimentaux et numériques disponibles a été trouvé. Notre analyse théorique permet de comprendre comment la taille des particules, la fraction volumique des particules dispersées, leur forme, les propriétés de l'interface particule-matrice, et l'agglomération des particules influencent la conductivité thermique des nanodispersions. Nous étudions également les nanodispersions hybrides dans lesquelles les particules en suspension sont de différents types (par exemple, des nanofils et des nanosphères). Notre modèle montre que la conductivité thermique augmente à mesure que la spécularité de l'interface augmente. Pour la dispersion de particules anisotropes, l'influence de l'orientation des particules sur la conductivité thermique est mise en évidence. Lorsque plus de nanoparticules sont orientées dans la direction du flux thermique, une conductivité thermique plus élevée est prévue en raison des zones plus

petites pour la limite de diffusion des phonons. Dans l'étude des nanodispersions hybrides, nous utilisons deux approches différentes. On observe que les résultats de ces deux approches sont en très bon accord. Un des avantages les plus importants de notre modèle est qu'il offre la possibilité d'étudier systématiquement la dépendance en température de la conduction thermique des nanodispersions. On constate que la limite de dispersion est dominée pour de faibles températures, tandis que la diffusion phonon-phonon est le mécanisme de diffusion efficace à des températures plus élevées. La dépendance en température de la conductivité thermique dans des dispersions hybrides est étudiée pour différentes tailles de particules, fractions volumiques, formes et orientations. A des températures plus élevées, en raison de la forte incidence de la diffusion phonon-phonon, il est démontré que le changement dans la taille, la composition, l'orientation et la forme des particules ne peut pas changer de manière significative la conductivité thermique.

ABSTRACT

For a wide range of engineering applications, ranging from thermoelectric energy conversion materials to thermal interface materials, the thermal conductivity in nanoscale structures has been an interesting and an important subject in both fundamental and applied research. The classical Fourier theory is not able to describe the heat conduction in nanostructured materials due to the neglect of boundary scattering events that play a very important role at nanoscale structures.

The ultimate purpose of this work is to establish a general framework for studying the thermal conductivity in nanodispersions. In this dissertation, by reviewing the fundamentals of the phonon transport in nanostructures, the heat conductivity coefficients arising in macroscopic Fourier heat theory are modified and made applicable for nanodispersions. In order to adapt the macroscopic thermal conductivity for the purpose of this study, the influence of the phonon-boundary scattering is taken into account. The phonon mean free paths in both the matrix and the dispersed particles, that is provided by kinetic theory, are modified in a way to capture the boundary scattering effects.

A good agreement between predictions of our models and available experimental and numerical results is found. Our theoretical analysis helps to understand how the particle size, the volume fraction of dispersed particles, their shape, the particle-matrix interface properties, and the particle agglomeration influence the thermal conductivity of nanodispersions. We also investigate hybrid nanodispersions in which the suspended particles of are of different types (for example nanowires and nanospheres). Our model shows that the thermal conductivity increases as the specularity of interface increases. For dispersion of anisotropic particles, the influence of particle orientation on the thermal conductivity is highlighted. When more nanoparticles are oriented in the direction of the heat flux, a higher thermal conductivity is expected due to smaller area on which the phonon-boundary scattering takes place. In the investigation of hybrid nanodispersions we use two different approaches and show that results

obtained by following them are in a very good agreement.

One of the most important advantages of our model is that it offers a possibility to investigate systematically the temperature dependence of the heat conduction in nanodispersions. It is observed that the boundary scattering plays a dominant role at lower temperatures, while phonon-phonon scattering is the dominant scattering mechanism at higher temperatures. The temperature dependence of thermal conductivity in hybrid dispersions is studied for particles with different sizes, volume fractions, shapes, and orientations. At higher temperatures, due to strong impact of phonon-phonon scattering, we see that changes made in size, composition, orientation and shape of particles cannot significantly change the thermal conductivity.

TABLE OF CONTENTS

LIST OF TABLES

LIST OF FIGURES

INTRODUCTION

Dispersion of particles of different sizes, of different types, and of different shapes in a continuous matrix is one of the most common and the most successful technique to produce new materials with desired mechanical, electrical, and thermal properties. Miniaturization of the dispersed phase toward the nanoscale has stimulated an interest in understanding the physics underlying the thermal transport in small dimension structures. Modeling the thermal transport in nanostructures such as nanodispersions, thin films, and nanowires, provides an insight that is then very useful for fabrication of electronic devices. In small-scale structures, the assumption of continuum, that is made in conventional heat transport models like the classical Fourier heat conduction theory, breaks down. The thermal conductivity which is generally treated only as a function of material and temperature becomes in small scales also size dependent. Consequently, the conventional Fourier theory cannot be directly applied. The macroscopic models for predicting thermal conductivity in small-scale dispersions become unreliable since they do not take and cannot take into account the complex interactions between heat carriers and boundaries.

Instead of using microscopic approaches, such as those based on the Boltzmann transport equation or on the Monte Carlo and molecular dynamic simulations, that need an extensive numerical calculations, we follow a theoretical approach that is also microscopic but leads to analytical closed-form formulas for the heat conduction coefficients. In our investigation we take into account many different scattering mechanisms of heat carriers. Temperature, particle size, composition, geometry, orientation, and degree of dispersion (well-dispersed or agglomerated) as well as interface properties are some of the parameters on which the effective thermal conductivity of nanodispersions depends. Our main objective is to develop a comprehensive model capable of making accurate predictions of the thermal conductivity of nanodispersions in dependence on the above-mentioned parameters. The results of this study represent a reliable approximation of the thermal conductivity of nanodispersions for either

the thermal management in electronic devices or thermoelectric energy conversion applications. To achieve the objective, a theoretical framework is constructed. In this framework the phonon viewpoint of heat transfer is used to establish a passage from heterogeneous to an effective homogeneous structure. According to this framework, the bulk mean free path of the heat carrier is modified to take into account the influence of multiple scattering events. This methodology will also be useful in studying the thermal conductivity of nanodispersions under more widespread circumstances. Finally, the framework that we use enables us also to extend our investigation to more complex as well as potentially more useful and more interesting structures such as hybrid dispersion of nanoparticles with variety of shapes in a homogeneous matrix.

This dissertation is organized into 9 chapters. The core of the text are four articles that have been published or submitted to scientific journals and is organized as follow :

i. a critical literature review considering the related issues is presented in Chapter 2.

ii. Chapter 3 introduces briefly the objectives.

iii. Chapter 4 describes the organization of the articles.

iv. Four scientific articles written in the scope of this work are included in Chapter 5, 6, 7, and 8.

v. A general discussion regarding to the results obtained in this study is presented in Chapter 9.

vi Finally, Chapter 10 presents the conclusions of this study and the recommendations for future work.

CHAPTER 1

LITERATURE REVIEW

From both practical and fundamental perspectives, thermal properties of nanostructured materials have been an interesting subject of many studies during decades.

From energy and environmental viewpoints, significant researches have been devoted to provide different types of energy conversion technologies which are supposed to be considered as an alternative energy source other than fossil fuels. Among these different technologies, thermoelectric materials have attracted more attentions due to their simplicity, no moving parts, high reliability and miniaturization. However, the operational efficiency of thermoelectric materials is not high enough to be broadly used in a wide range of applications. Nevertheless, a large market is expected for thermoelectric materials in the near future[1, 2]. Figure (1.1) has summarized some applications for thermoelectric materials.

In order to evaluate the efficiency of thermoelectrics, the dimensionless thermoelectric figure of merit $ZT = \frac{S^2\sigma T}{k}$ is defined; where S, σ, T, and k are respectively, the Seebeck coefficient, the electrical conductivity, absolute temperature, and the thermal conductivity. It is pointed out that the higher is ZT, the more efficient is the thermoelectric material[1–5]. In 1950s, bulk structures emerged as the first generation of thermoelectric materials which were discovered to have ZT of $0.8 \sim 1$. The best conversion efficiency of these class of thermoelectric materials was reported not to exceed $5 - 6\%$.

During these years, the basic science of thermoelectric materials developed sufficiently and, simultaneously thermoelectric materials were commercialized for solid-state power generation and cooling system applications. In 1990, after four-decade of stagnancy in research and development, thermoelectric materials became again interesting for new potential applications. It was suggested that miniaturization can improve thermoelectric properties by dramatically suppressing the thermal conductivity; subsequently emergence of small scale materials such

as nanowires, thin films, supperlattices and nanotubes resulted in a remarkable progress in improving thermoelectric properties. Dispersion of nanoscale inclusions in a host has been another approach to improve the efficiency of thermoelectric materials[5–10]. Thermoelectric

Figure 1.1 Some of the thermoelectric applications [9].

materials are capable to act as the power generation or solid-state refrigerators[1–4, 11]. When a temperature gradient is imposed on a thermoelectric couple consisting of n-type (electron-transporting) and p-type (hole-transporting) legs, the mobile charge carriers (electrons or holes) at the hot side will have higher thermal energy and tend to diffuse to the cold side. In this condition, more negative charges are accumulated in the cold side of n-type leg and similarly more positive charges are accumulated in the cold side of p-type leg. It means higher density of mobile carriers are expected to be at the cold side than the hot side. This inhomogeneous density distribution makes an electric field in opposite direction to diffusion. Equilibrium condition is defined when a balance between the rate at which carriers move from the hot end to the cold end due to temperature gradient and the rate at which carriers move from the cold end to the hot end due to electric field is obtained. The electric potential (voltage) produced in response to the temperature gradient in equilibrium

is known as the Seebeck effect (power generation) and the proportionality constant between the amount of voltage produced per unit temperature gradient is named Seebeck coefficient (see Figure (1.2.a)). Figure (1.2.b) shows thermoelectric materials as the solid-refrigerators when a current is made to flow along a thermoelectric couple. This mode is known as the Peltier effect. Depending on the direction of current flow, heat will be generated at one end and absorbed at the other[2–4, 12–14]. It has been experimentally and theoretically observed

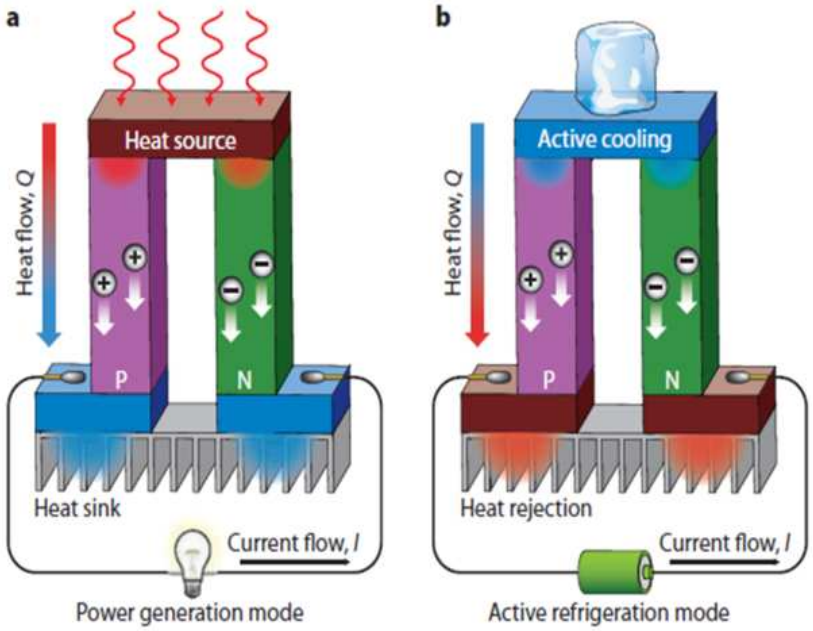

Figure 1.2 Schematic illustrations of thermoelectric devices for (a.) the power generation mode (Seebeck effect) and (b.) the refrigeration mode (Peltier effect)[4].

that a reduction on the thermal conductivity, k would be a successful strategy to increase the efficiency of thermoelectrics [10, 15–20].

Contrary to thermoelectric applications, fast and efficient heat removal has been a crucial issue in electronic and optoelectronics industries where thermally conductive materials are used for thermal interface materials (TIMs). Thermal interface materials with typical thermal conductivity in range of 1-5 W/mK are located between heat sources and heat sinks in order to improve thermal management[21–23]. Conventional thermal interface materials are produced by embedding thermally conductive particles like metals and metal oxides particles

into a polymer matrix. It was reported that dispersion of $50-70$ $vol\%$ of such fillers within the matrix is required to achieve desired properties for thermal interface materials [24–26]. It is remarkable to note that dispersion of nanostructured materials such as carbon nanotubes and graphite nanoplatelets in a polymer matrix can be a promising approach to increase the thermal conductivity of thermal interface materials [22, 27, 28]. It has been reported that a hybrid dispersion of carbon nanotubes and graphite nanoplatelets in a polymer matrix shows higher thermal conductivity than the dispersion utilizing either pure carbon nanotubes or graphite nanoplatelets [29].

Summing up, it has been observed that dispersion of nanostructured particles within a homogeneous matrix would be resulted in an improvement in properties of devices for both above-mentioned applications. Properties of dispersions can be strongly affected by dispersed particle size, volume fraction, shape, orientation, degree of agglomeration and matrix-particle interface properties.

1.1 Macroscopic heat conduction

In the macroscopic view, heat conduction occurs if there is a temperature difference between two points in a medium which may be a solid, a liquid, or a gas. In this condition, the heat conduction is typically a diffuse process and stated by the well-established phenomenological Fourier law as follow

$$\mathbf{q} = -k\nabla T \tag{1.1}$$

where $\mathbf{q}$ and ∇T stand for the heat flux and the temperature gradient, respectively. By k, the thermal conductivity is denoted. Fourier law is the well-known approach in the formulation of the macroscopic heat conduction, where the importance of the size and time on the heat transport could be neglected. The underlying assumption of the Fourier law is that the heat is

conveyed from one spot to another by diffuse collision (experiencing many collisions) between heat carriers in the medium. Depending on the type of the medium, different heat carriers can participate in the heat conduction process. In metals, the majority of heat is carried by electrons while in insulators phonons are dominant heat carriers. For radiative transfer, photons are responsible for thermal energy transport [30–32].

1.2 Lattice vibration in solids

In crystalline solids, atoms are structured in periodical arrays known as lattice. Lattice vibrations contribute to the thermal conductivity. If two atoms in a solid body are far apart, an attractive force will be observed between atoms, while the interaction force will be repulsive (because of the overlap of electronic orbits in the atoms), if two atoms are close to each other. The minimum potential defines the equilibrium positions of atoms where the repulsive and attractive forces balance each other. Atoms in a solid body vibrate about their equilibrium position due to presence of interatomic forces. The vibration of each lattice atom is constrained by its neighbouring atoms through the interatomic potential. A mass-spring system is a simplified picture of the interatomic interaction in crystalline solids. In such a system, the vibration of the atoms is not independent of each other and can cause the vibration of the whole system by creating a lattice wave. Clearly, the atoms near the hot side of the solid have larger vibrational amplitudes, which will be felt by atoms of the other side of the solid through the propagation and interaction of the lattice waves [30, 33].

According to the principle of quantum mechanics, the energy of each lattice wave is discrete and must be a multiple of energy ($\hbar\omega$), where $\hbar$ is the Planck's constant and ω is the frequency. The minimum energy of $h\omega$, a quantized lattice vibrational wave, is called a phonon. For non-metals, it is repeated that heat is transferred by phonons. Under the phonon viewpoint, we can leave behind atoms and consider lattice waves or phonon particles in a crystalline structure. Although phonons can have both wave and particle characteristics, it is more convenient to treat phonons as particles. The length scale associated with the particle

nature of phonons is called the mean free path (Λ_b). When the characteristic length of the medium is in order of the phonon mean free path but larger than the phonon wavelength, the coherence effects are neglected and phonons are treated as particles [30, 32, 34, 35]. Note that the mean free path is the average distance travelled by phonon particle between two subsequent collisions. The mean free path is usually used to estimate whether a transport phenomena belongs to the macro-scale regime or falls into the micro-scale regime.

1.3 Phonon mean free path

When the mean free path of heat carriers is comparable to or larger than the characteristic length of the medium, the diffuse nature of heat conduction breaks down and the conventional Fourier heat conduction leads to erroneous thermal conductivity predictions. In order to distinguish whether the heat conduction belongs to the macroscopic regime or falls into the microscopic regime, the Knudsen (Kn) number is defined as the ratio of the mean free path to the characteristic length of the medium [30–32, 36]. Depending on the value of the Knudsen number, three heat conduction regimes are specified; (i) For $Kn << 1$, the heat conduction regime is called diffuse. Macroscopic laws such as Fourier law are valid and the system is close to local thermal equilibrium. (ii) For $Kn >> 1$, the heat conduction regime can not be described by conventional macroscopic laws. In this condition the heat conduction regime is called ballistic. (iii) For $Kn \approx 1$, the heat conduction regime can be called partially diffuse-partially ballistic [30, 33, 37].

When the mean free path is smaller than the characteristic length of the medium, internal scatterings (phonon-phonon collision) dominate the heat conduction process, suggesting that the heat transfer belongs to the macroscopic regime. Thus, the Fourier law would be able to predict the heat conduction. As the size of the medium decreases (the characteristic length is in order of or smaller than the phonon mean free path), its surface area to volume ratio increases, the probability of phonon-boundary scatterings (surface effects) increases while the probability of volumetric effects such as phonon-phonon scattering decreases, and conse-

quently the thermal boundary resistance affected significantly the heat conduction. However, the microscopic heat conduction regime is dominated and the failure of the Fourier law to predict the thermal conductivity is observed. In such conditions, *ab initio* methods have been engaged to predict the thermal properties where the influence of the thermal boundary resistance due to the size reduction is particularly strong [33, 38–49].

Apart from either macroscopic or microscopic natures of heat conduction, the Boltzmann transport equation under relaxation time approximation can be used to study thermal behaviours of the medium.

1.4 Boltzmann transport equation

The well-known phenomenological transport expressions such as Ohm's law, Fick's law, Fourier's law and hyperbolic heat equations can be derived from the Boltzmann transport equation in the macroscopic limit. Once the particle nature of carriers is considered, the transport phenomena can be described by the Boltzmann transport equation. The equation is established by tracking the statical behaviour of particles over time at different spatial locations.

It is supposed a particle at the spatial location r moves with a group velocity v at time t. At $t+dt$, without a collision with another particle, the particle will reach position $r+dr = r+vdt$ and its velocity will be $v + dv = v + adt$. Where $a = F/m$ is the acceleration in a body force field. Therefore, the initial form of the Boltzmann transport equation in the absence of collision term is written as

$$\frac{f(r+dr, v+dv, t+dt) - f(r,v,t)}{dt} = \frac{\partial f}{\partial t} + v.\frac{\partial f}{\partial r} + a.\frac{\partial f}{\partial v} = 0 \tag{1.2}$$

where $f(r, v, t)$ is the single particle distribution function which shows how a particle is distributed in the phase space at any given time. By assuming that no external forces are applied on particles the third term of equation (1.2) can be neglected. In the presence of the

collision between particles, the Boltzmann transport equation can be written as

$$\frac{\partial f}{\partial t} + v.\frac{\partial f}{\partial r} = [\frac{\partial f}{\partial t}]_{coll} \tag{1.3}$$

The terms on the left side are named drift terms, while that on the right side is called the scattering term. Equation (1.3) is a complicated nonlinear integro-differential equation which can not be solved exactly. To facilitate the solution of the Boltzmann transport equation for a given application, the collision term is linearised by the relaxation time approximation. It provides a linear collision term as follow

$$[\frac{\partial f}{\partial t}]_{coll} = \frac{f_0 - f}{\tau} \tag{1.4}$$

where f_0 and τ stand for the equilibrium distribution and relaxation time, respectively [30, 32, 33, 50].

Consider a phonon as a particle with energy $\hbar\omega$ and momentum $\hbar v$, when the characteristic length of the system is larger than the phonon mean free path. However the influence of the boundary scattering is not taken into account and only collision between phonons becomes important. The internal energy is determined by multiplying $\hbar\omega$ by the number (density) of states $D(\omega)$, and the distribution function of phonons f, and integrating it over the phase space for a large range of frequencies. The internal energy for r-direction $(1 - D)$ is given by

$$e_r = \int_0^{\omega_D} f(r)\hbar\omega D(\omega) d\omega \tag{1.5}$$

Consequently, the heat flux is obtained by multiplying the internal energy expression by the group velocity of the phonon.

$$q_r = \int_0^{\omega_D} f(r)\hbar\omega D(\omega) v_r d\omega \tag{1.6}$$

Where ω_D is the Debye frequency, $\hbar$, and ω are modified Plank's constant, and frequency respectively.

Under steady state condition and making the relaxation time approximation, the 1-D (r-direction) Boltzmann transport equation is reformulated as

$$v_r \frac{\partial f}{\partial r} = \frac{f_0 - f}{\tau} \tag{1.7}$$

It is further assumed that f is not very far away from equilibrium (f_0), so the local thermal equilibrium approximation would be applied

$$\frac{\partial f}{\partial r} = \frac{\partial f_0}{\partial r} = \frac{df_0}{dT}\frac{dT}{dr} \tag{1.8}$$

Substituting equation (1.8) in equation (1.7) leads to the following expression

$$v_r \frac{df_0}{dT}\frac{dT}{dr} = \frac{f_0 - f}{\tau} \tag{1.9}$$

Rearranging the above equation gives

$$f - f_0 = -v_r \tau \frac{df_0}{dT}\frac{dT}{dr} \tag{1.10}$$

Multiplying equation (1.10) by $\hbar\omega D(\omega)v_r$ and integrating it over all frequencies gives

$$q_r = \int_0^{\omega_D} -v_r^2 \tau \hbar\omega D(\omega)\frac{df_0}{dT}\frac{dT}{dr}d\omega \tag{1.11}$$

Note that $\int_0^{\omega_D} f_0 \hbar\omega D(\omega)v_r d\omega = 0$. Because f_0 is equilibrium distribution.

The velocity of phonons is assumed to be identical in all directions ($v_r^2 = v^2/3$) and $\tau.v \equiv \Lambda_b$. By Λ_b, we denote the mean free path of phonons. Thus, equation (1.11) can be rewritten in

the following form

$$q = -\frac{1}{3}\frac{dT}{dr} v\Lambda \int_0^{\omega_D} \frac{df_0}{dT}\hbar\omega D(\omega)d\omega \tag{1.12}$$

where $\int_0^{\omega_D} \frac{df_0}{dT}\hbar\omega D(\omega)d\omega$ is the internal energy with respect to temperature, which is known as the lattice specific heat C. Recalling equation (1.12) in the spirit of the lattice specific heat, we have

$$q = -\frac{1}{3} C v \Lambda_b \frac{dT}{dr} \tag{1.13}$$

by $\frac{1}{3}Cv\Lambda_b$ the phonon thermal conductivity, k is introduced which is exactly the kinetic theory result [30, 32].

1.5 Scattering mechanisms

In addition to phonon-phonon (internal) scattering which is generally dominated in macroscopic heat conduction, phonons can be scattered by various phonon scattering agents such as defects, boundaries, free electrons. These scattering mechanisms can take place if the phonon mean free path is in order of or larger than the characteristic length of the medium. The phonon mean free path and consequently the phonon thermal conductivity would be significantly affected by resistances produced by above mentioned scattering mechanisms [10, 51–55].

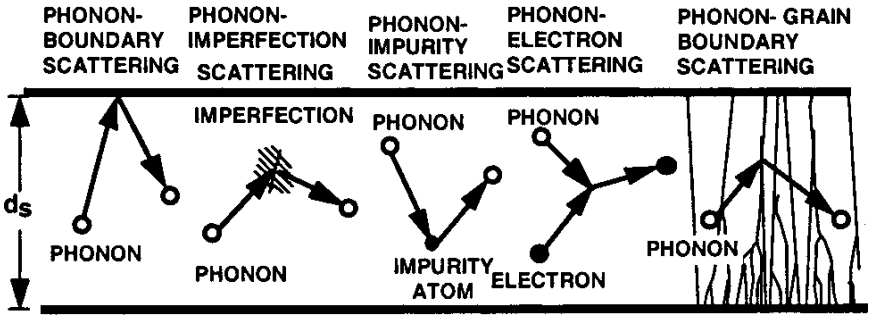

Figure 1.3 Different phonon scattering mechanisms that reduce the thermal conductivity of the medium, d_s is the film thickness [51].

Figure (1.3) illustrates phonon scattering mechanisms that decrease the thermal conduc-

tivity. In order to show the influence of different scattering mechanisms on the phonon mean free path, Matthiessen's rule is employed. According to the Matthiessen's rule, the resistivity due to one scattering event is independent of the existence of any other scattering event[49]. Thus,

$$\frac{1}{\Lambda} = \sum_i \frac{1}{\Lambda_i} \tag{1.14}$$

1.5.1 Phonon-phonon scattering

Contributions of phonon-phonon scatterings on heat conduction are summarized into two *Umklapp* (U-process) and *normal* (N-process) processes.

Probability of interactions between four or higher phonons on the thermal resistance is considered to be too rare, however, for phonon-phonon scattering usually interactions involving three phonons are taken into account. Note that interactions between at least three phonons are required for the energy conservation. In a three-phonon process, either a single phonon can break into two phonons or two phonons can merge to form a third one. Spontaneous appearance or disappearance of three phonons can not occur due to energy conservation. Conditions to conserve the phonon energy and momentum are given by

$$\hbar\omega_1 + \hbar\omega_2 = \hbar\omega_3 \;\; or \;\; \hbar\omega_1 = \hbar\omega_2 + \hbar\omega_3 \tag{1.15}$$

and

$$\hbar\kappa_1 + \hbar\kappa_2 = \hbar\kappa_3 + \zeta\hbar G \;\; or \;\; \hbar\kappa_1 = \hbar\kappa_2 + \hbar\kappa_3 + \zeta\hbar G \tag{1.16}$$

where κ is the wavevector, ζ is an integer and G is a reciprocal lattice vector. If interactions between phonons stay inside the first Brillouin zone, the N-process is observed. The N-process does not change the direction of the heat flux (both the energy and momentum are conserved),

hence, in equation (1.16) $\zeta = 0$ and consequently the N-process does not contribute to the thermal resistance.

For U-process, interactions between phonons can form a third one whose wavevector stays outside the Brillouin zone, then the process can be completed with introducing the addition of what is called the reciprocal lattice vector.

In such condition, phonon momentum is not conserved during the U-process (ζ is nonzero), which creates resistance against heat flow and thus reduces the thermal conductivity of the medium. It is noted that an infinite thermal conductivity is predicted, if the N-process is only taken into account [30, 33, 49, 50, 56].

Schematic illustration of phonon-phonon scattering processes have been shown in Figure (1.4).

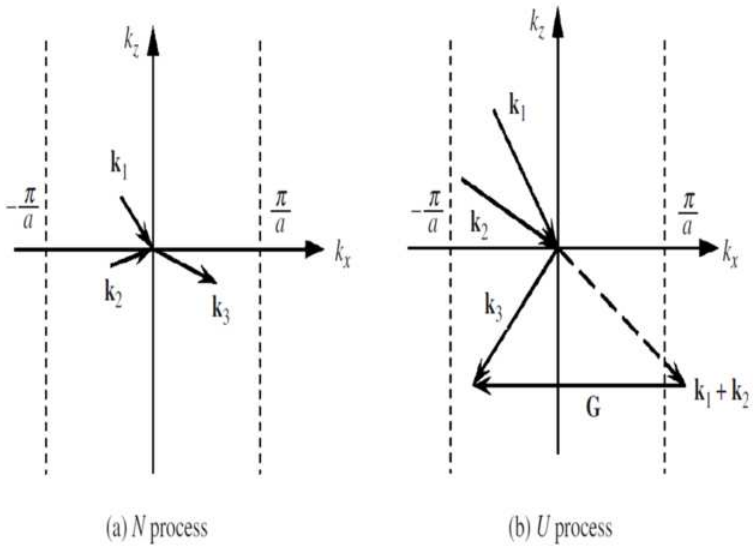

Figure 1.4 Schematic illustration of normal and Umklapp phonon-phonon scatterings [30].

1.5.2 Influence of temperature on phonon scattering mechanisms

Phonon wavelength is strongly affected by the temperature according to the Wien's displacement law. Therefore, different phonon scattering mechanisms can dominate at different

temperatures. According to Wien's displacement law, the phonon wavelength depends inversely on temperature. Therefore, the wavelength of dominant phonons significantly decreases as the temperature rises. The effect of temperature on the thermal conductivity has been well-explained by Figure (1.5). Figure (1.5) is a plot of the thermal conductivity of $CoSb_3$ as a function of temperature. At low temperatures, the phonon wavelength is long and the Umklapp scattering does not make a significant contribution to the thermal conductivity. However, it would be said that the boundary scattering is dominating and the role of medium size on the thermal conductivity is significant. As the temperature gradually increases, the phonon wavelength obviously decreases and becomes comparable to the size of defects. Thus, defect scattering becomes important. Finally, at higher temperatures, the phonon wavelength is shortened and the Umklapp scattering becomes important.

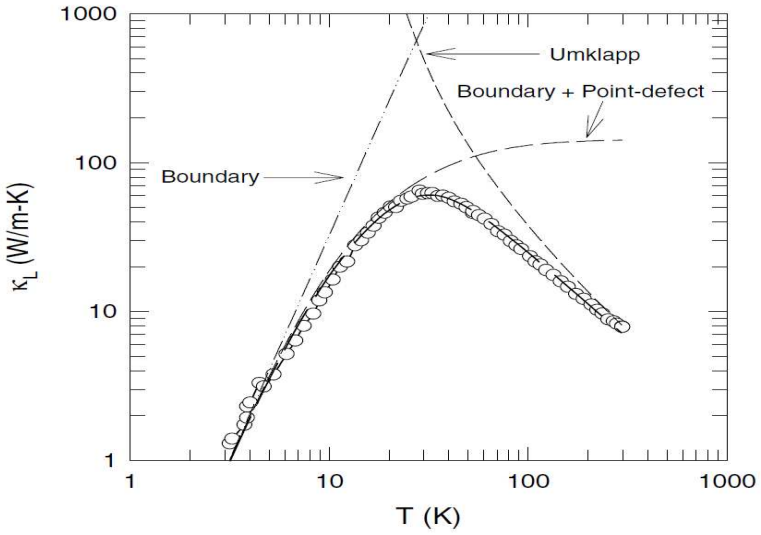

Figure 1.5 Thermal conductivity of $CoSb_3$ as a function of temperature. The dots and solid lines represent the experimental and theoretical results[57].

The empirical expression for the temperature dependence phonon bulk mean free path can be written as [30, 54, 58]

$$\Lambda_b(T,\omega) = \frac{\exp(\frac{\theta}{T})}{BT\omega^2} \tag{1.17}$$

Here, θ and B are constant parameters. In order to find θ and B, the temperature dependent expression of the thermal conductivity is fitted by experimental results. The general expression of the thermal conductivity can be predicted by using Callaway's model [49, 53, 54]

$$k = \int_0^{\omega_D} \frac{\hbar^2}{2\pi^2 v^2 k_B T^2} \frac{\omega^4 \exp(\hbar\omega/k_B T)\Lambda_b(T,\omega)}{[\exp(\hbar\omega/k_B T) - 1]^2 d\omega} \tag{1.18}$$

Figure (1.6) shows how well equation (1.18) is fitted with experimental results [59] of Bi_2Te_3. $B = 3.242 \times 10^{-21} s^2 m^{-1} K^{-1}$ and $\theta = 5.45K$ are led to the best fit. For Bi_2Te_3, the phonon group velocity is assumed to be $2950 ms^{-1}$[46], and the Debye frequency cuttoff is $2.029 \times 10^{13} s^{-1}$[60].

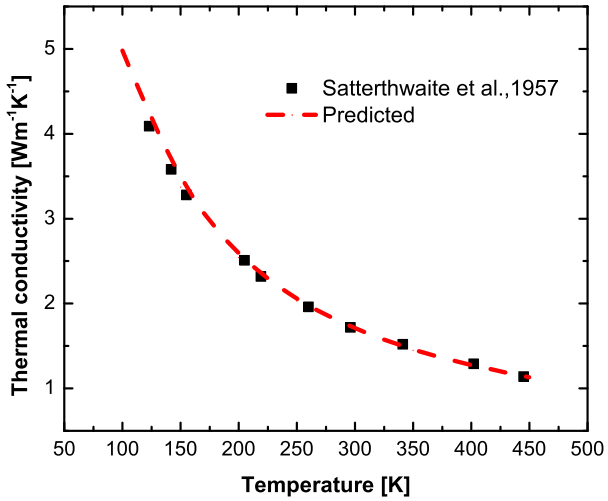

Figure 1.6 Predicted temperature dependent thermal conductivity of Bi_2Te_3 compared with the experimental results obtained from Ref.[59].

In Figure (1.6), a continuous reduction of the bulk thermal conductivity versus temperature is observed. Since the bulk thermal conductivity of Bi_2Te_3 is not influenced by the thermal boundary resistance, the only dominant scattering mechanism is the phonon-phonon scattering. At lower temperatures, the phonon-phonon scattering is not significantly contributing to the thermal conductivity, and a higher thermal conductivity is observed. While, the

higher is temperature, the more significant is the resistance produced by the phonon-phonon scattering, and consequently the lower is the thermal conductivity.

1.6 Thermal boundary resistance

The interface between two dissimilar materials produces a barrier against heat flow which depends on densities and phonon propagation speeds of the two materials. This barrier is often referred as the thermal boundary resistance, $R_{BD} = \frac{q}{\Delta T}$ where q is the heat flux across the interface and ΔT is the interfacial temperature drop [30, 49].
The effect of the thermal boundary resistance manifests itself as a discontinuity in the temperature across the interface of two materials when the heat flow is imposed.

The heat flux across the interface from side (1) to side (2) can be expressed by

$$q_{interface} = \iint_{2\pi} [t_{12} v_1 \cos\theta_1 \hbar\omega [f(\omega, T_{e1}) - f(\omega, T_{e2})] \frac{D_1(\omega)}{4\pi} d\omega] d\Omega_1 \tag{1.19}$$

where t_{12} is the phonon transmission probability from side (1) to side (2), $D_1(\omega)$ is the density of states, $f(\omega, T)$ is the Bose-Einstein phonon distribution function, ω is the phonon frequency, $d\Omega = \sin\theta d\theta d\phi$ is the differential angle[32]. The rearranging equation (1.19) gives

$$q_{interface} = (T_{e1} - T_{e2}) \int_0^{2\pi} \int_0^{\pi/2} \int_0^{\omega_D} t_{12} v_1 \hbar\omega \frac{df}{dT} \frac{D_1(\omega)}{4\pi} \cos\theta_1 \sin\theta_1 d\omega d\theta_1 d\phi \tag{1.20}$$

where T_{e1} and T_{e2} are emitted temperatures of side (1) and (2), respectively. Considering the definition of the volumetric specific heat capacity of phonons, the general equation for the thermal boundary resistance becomes

$$\frac{1}{R_{BD}} = \frac{1}{2} \int_0^1 t_{12}(\mu_1) C_1 v_1 \mu_1 d\mu_1 \tag{1.21}$$

where μ_1 is $\cos\theta_1$. Depending on properties of the interface, i.e. specular or diffuse, the transmission coefficient is determined. At room temperature, it has been theoretically and

experimentally observed that values of the thermal boundary resistance typically range from $10^{-9}m^2KW^{-1}$ to $10^{-7}m^2KW^{-1}$ [61–66]. These values do not have a significant influence on the thermal conductivity when heat transport belongs to macroscopic regime.

The influence of the thermal boundary resistance is more significant in low dimensional structures when the dimension of the structure is comparable to the mean free path. In this condition, phonons will be propagated more ballistically which have less contribution to thermal transport. Therefore, it is pointed out that the thermal boundary resistance is size dependent. In other words, the thermal boundary resistance decreases as the characteristic length of the medium increases. It happens due to an increase in probability of phonon-phonon scattering as compared to phonon-boundary scattering [61, 66, 67].

There have been two well-known theoretical ways developed to predict the thermal boundary resistance [49]. The acoustic mismatch model (AMM) was proposed to take the specular scattering of phonons at the interface between two dissimilar materials into account. This model is successful to predict the thermal boundary resistance at low temperatures where the wave nature of phonons is considered [68]. Also the diffuse mismatch model (DMM) was proposed to account for the diffuse scattering of phonons at the interface [69].

1.6.1 Acoustic Mismatch Model

An incident phonon at the interface can be either reflected or transmitted. The phonon transmission probability at the interface is influenced by properties of the interface. For a perfect interface and at lower temperatures when the phonon wavelength is long, the wave nature of the incident phonon at the interface between two materials can be considered. Note that conditions for perfect interface can be satisfied if the roughness of the interface is assumed to be smaller than the incident phonon wavelength. Thus, the specular scattering of phonons is probable at low temperatures. In order to show the degree of specularity of

phonons at the interface, the specularity parameter, s is defined as

$$s = \exp[-\frac{16\pi^2\delta_{rms}^2}{\Delta^2}] \tag{1.22}$$

Note that δ_{rms} and Δ are the asperity parameter of the interface and the coherence length, respectively. The expression for Δ is hv/k_BT, where h is the Plank's constant, v is the phonon velocity and k_B and T are the Boltzmann's constant and temperature, respectively. The specular (smooth) interface is defined, if the specularity parameter is unity. For totally diffuse phonon scattering, $s = 0$. It is obvious that temperature rising results in an increase of the probability of diffuse scattering [70, 71].

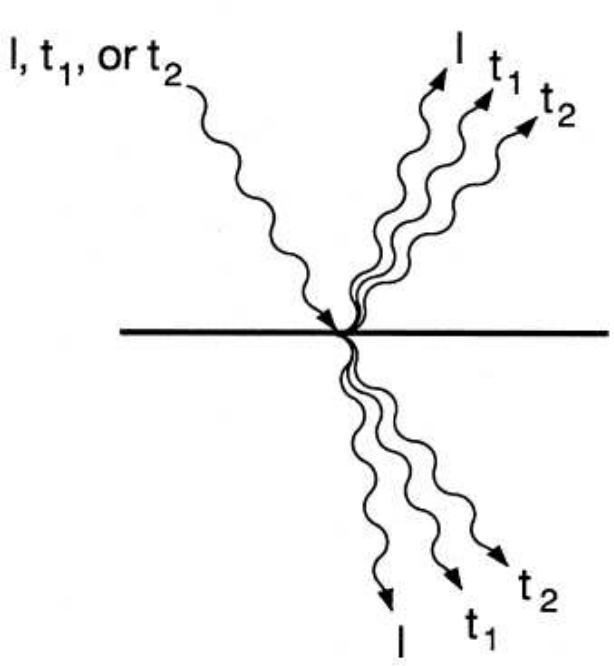

Figure 1.7 Schematic of many possibilities of an incident phonon at the interface between two dissimilar materials [69].

For specular interface, when a phonon is incident at the interface, four general possible conditions as shown in Figure (1.7) can be expected. The phonon can specularly reflect, reflect and mode convert, refract or refract and mode convert.

The probability of the specular phonon transmission from side (1) to side (2) is given by

$$t_{12}^{(s)} = \frac{4\rho_1 v_1 \rho_2 v_2 \cos\theta_1 \cos\theta_2}{(\rho_1 v_1 \cos\theta_1 + \rho_2 v_2 \cos\theta_2)^2} \tag{1.23}$$

By $t_{12}^{(s)}$, the probability of specular transmission is noted, and ρ_i and θ_i are the material density and the angle of incidence of the phonons in each side, respectively. The relation between the angles of reflection and refraction with or without mode converts are calculated by the Snell's law for acoustic waves[32, 72, 73].

$$\frac{\sin\theta_1}{v_1} = \frac{\sin\theta_2}{v_2} \tag{1.24}$$

For a case of $v_1 > v_2$, above equations can be used without any restriction. While the critical angle, $\theta_c = \arcsin(\frac{v_1}{v_2})$ is required to define in a case of $v_1 < v_2$. If $\theta_1 < \theta_c$, the above equations are still valid, while the probability of phonon transmission will be vanished, $t_{12}^{(s)} = 0$ and only internal reflection occurs, if $\theta_1 > \theta_c$[73, 74]. For totally specular interface, the thermal boundary resistance can be expressed as

$$R_{BD}^{(s)} = \frac{2}{C_1 v_1 \int t_{12}^{(s)}(\mu_1) d\mu_1} \tag{1.25}$$

1.6.2 Diffuse Mismatch Model

Under the diffuse mismatch model assumption, incident phonons at the interface totally lose their memory. Therefore, the probability of transmission from side (1) is equal to the probability of reflection from side (2).

$$t_{21}^{(d)} = r_{12}^{(d)} = 1 - t_{12}^{(d)} \tag{1.26}$$

t_{ij} and r_{ij} stand for probabilities of transmission and reflection from side (i) to side (j), respectively. Note that upper index (d) shows the totally diffuse phonon scattering at the interface. It is also assumed that both sides of the interface are at the same temperature, thus applying the principle of energy balance yields

$$t_{12}^{(d)} \int \hbar\omega v_1 D_1(\omega) f(\omega) d\omega = t_{21}^{(d)} \int \hbar\omega v_2 D_2(\omega) f(\omega) d\omega \tag{1.27}$$

Under elastic scattering limit, a phonon with frequency ω from side (1) can only emit a phonon from side (2) with same frequency. Recalling equation (1.27), the elastic diffuse transmission coefficient can be written as

$$t_{ij}^{(d)} = \frac{\frac{1}{v_j^2}}{\frac{1}{v_j^2} + \frac{1}{v_i^2}} \tag{1.28}$$

At higher temperatures, the accuracy of the above expression is under doubt, however inelastic scattering of phonons at the interface is taken into account. Under inelastic scattering, phonons of all frequencies can participate in transmission process through the interface. The transmission coefficient under the inelastic diffuse scattering is given by [32, 69–73]

$$t_{ij}^{(d)} = \frac{C_j v_j}{C_i v_i + C_j v_j} \tag{1.29}$$

Under the totally diffuse phonon-boundary scattering limit, the thermal boundary resistance (equation (1.21)) is written as follow

$$R_{BD}^{(d)} = \frac{4}{t_{12}^{(d)} C_1 v_1} \tag{1.30}$$

Note that the transmission coefficient under the diffuse mismatch model is a rough approximation and is obviously not applicable when the two materials are very similar. In the case of similar materials, equation (1.29) predicts the transmission coefficient approaching 0.5 while

the $t_{12}^{(d)} = 1$ is expected.

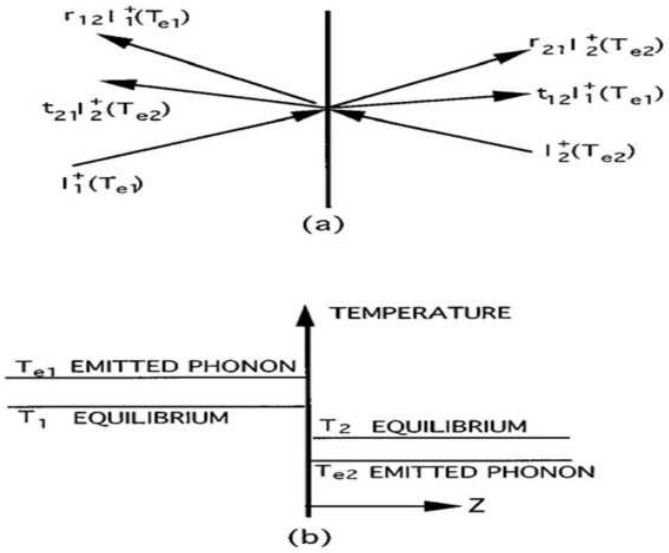

Figure 1.8 Presentations of (*a.*) phonon transport at the interface between side (1) and side (2) and (*b.*) equilibrium and emitted phonon temperature at interface[73].

It would be considered that the phonon scattering process at the interface can be treated as partially diffuse-partially specular rather than extreme situations of either totally diffuse or totally specular. Introducing specularity parameter, s the overall thermal boundary resistance is given by [32, 72, 74]

$$R_{BD} = (1-s)R_{BD}^{(d)} + sR_{BD}^{(s)} = \frac{2}{C_1 v_1}\left(\frac{s}{\int t_{12}(\mu_1)^{(s)} d\mu_1} + \frac{2(1-s)}{t_{12}^{(d)}}\right) \tag{1.31}$$

It is noted that the thermal boundary resistance under the diffuse phonon scattering is higher than the specular thermal boundary resistance due to higher confinement of phonon transport at the interface.

An obvious trouble can be observed by definition of the thermal boundary resistance under the temperature of emitted phonons. For the interface between the two very similar materials or where the transmissivity is assumed to be one, the thermal boundary resistance should approach zero. But the diffuse and specular thermal boundary resistance expressions presented by equations (1.25) and (1.30) give finite thermal boundary resistances. This dilemma can

arise from the definition of temperature at the interface. The thermal boundary resistances represented in equations (1.25) and (1.30) have been derived based on the temperature of emitted phonons, T_e. As presented in Figure (1.8.a), three groups of phonons can contribute in energy transport at the interface; incident, reflected and transmitted phonons. However, the thermal boundary resistance can not only be defined based on the emitted temperature. Since the phonon energy transport at the interface, specially for low dimensional structures is highly non-equilibrium, thus the concept of the temperature at the interface is defined by the equivalent equilibrium temperature which represents the average energy of all phonons around a local point. The relation between the equivalent equilibrium temperature, T and emitted temperature can be expressed by

$$T_1 = T_{e1} - (T_{e1} - T_{e2}) \int t_{12}(\mu_1)\mu_1 d\mu_1 \tag{1.32}$$

and

$$T_2 = T_{e2} + (T_{e1} - T_{e2}) \int t_{21}(\mu_2)\mu_2 d\mu_2 \tag{1.33}$$

therefore

$$T_1 - T_2 = (T_{e1} - T_{e2})[1 - \int t_{12}(\mu_1)\mu_1 d\mu_1 - \int t_{21}(\mu_2)\mu_2 d\mu_2] \tag{1.34}$$

Based on the equivalent equilibrium temperature, the diffuse and specular thermal boundary resistances are expressed as

$$R_{BD}^{(d)} = \frac{4[1 - 0.5(t_{12}^{(d)} + t_{21}^{(d)})]}{t_{12}^{(d)} C_1 v_1} \tag{1.35}$$

and

$$R_{BD}^{(s)} = \frac{2[1 - \int_0^1 t_{12}^{(s)}(\mu_1)\mu_1 d\mu_1 - \int_0^1 t_{21}^{(s)}(\mu_2)\mu_2 d\mu_2]}{C_1 v_1 \int_0^1 t_{12}^{(s)}(\mu_1)\mu_1 d\mu_1} \tag{1.36}$$

Thus, the diffuse and specular thermal boundary resistances based on the emitted and equivalent equilibrium temperatures are presented in Table 1.1.

Table 1.1 Thermal boundary resistance based on acoustic and diffuse mismatch models.

Thermal boundary resistance	Emitted temperature	Equivalent equilibrium temperature
Diffuse mismatch model	$\frac{4}{t_{12}^{(d)} C_1 v_1}$	$\frac{4[1-0.5(t_{12}^{(d)}+t_{21}^{(d)})]}{t_{12}^{(d)} C_1 v_1}$
Diffuse mismatch model	$\frac{2}{C_1 v_1 \int t_{12}^{(s)}(\mu_1) d\mu_1}$	$\frac{2[1-\int_0^1 t_{12}^{(s)}(\mu_1)\mu_1 d\mu_1 - \int_0^1 t_{21}^{(s)}(\mu_2)\mu_2 d\mu_2]}{C_1 v_1 \int_0^1 t_{12}^{(s)}(\mu_1)\mu_1 d\mu_1}$

1.7 Thermal conductivity of dispersions

Embedding of particles with specific properties within a homogeneous matrix can result in outstanding properties of the dispersion which can be used in a large variety of applications ranging from mechanical to thermal and electrical. It has been observed that several elements such as particle size, shape and volume fraction, orientation and degree of dispersion (from fully dispersed to fully agglomerated) of particles, temperature as well as the interface properties between matrix and dispersed particles can be affected on the final properties of dispersions. For heat transfer subject, several attempts have been made to predict theoretically and numerically the thermal conductivity of dispersions. The early theoretical model to calculate the thermal conductivity of spherical particles in the matrix was presented by Maxwell[75].

Later some theoretical models have been proposed to capture the influence of the thermal boundary resistance on the thermal conductivity. There are several works which have focused on thermal conductivity of dispersions with either imperfect[76–78] or perfect [79] interfaces between dispersed phase and the matrix. Nan *et al*. introduced a general expression for the thermal conductivity of dispersions which is applicable for the wide variety of dispersed phase shapes and also includes the thermal boundary resistance[77]. Although those models are considerably successful to predict the thermal conductivity under the macroscopic heat conduction regime, they are generally failing to estimate the thermal conductivity of nanodispersions where the characteristic length of dispersed particles are comparable to the carrier mean free path. This is because thermal conductivities of dispersed particles and the matrix

in a nanodispersion significantly differ from their corresponding bulk thermal conductivities due to strong influence of the interface scattering.

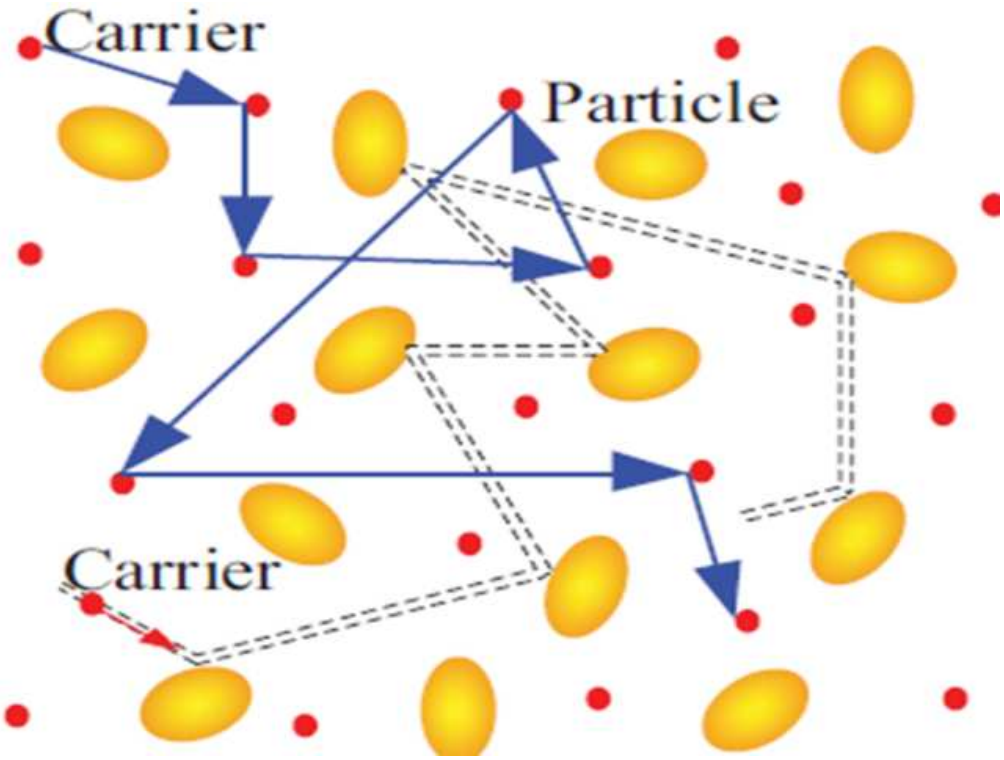

Figure 1.9 Schematic illustration of carrier-particle collision in a heterogeneous dispersion[80].

To study the thermal conductivity of dispersions when the heat transport does not belong to macroscopic regime, plenty of numerical and theoretical attempts can be found in the literature. In numerical point of view, several *ab initio* methods have been employed to predict the thermal conductivity of nanodispersions. Some researchers have used the Boltzmann transport equation simulations to numerically address the effect of boundary scatterings created by nanoscale particles[40, 43, 44]. In the context of first-principles calculation also, either equilibrium with Green-Kubo formula or nonequilibrium molecular dynamic simulations [41, 42] are carried out to characterize the scattering events in nanoscale structures due to calculate the thermal conductivity.

A modified view of the Maxwell's homogenization has been presented to theoretically predict

the thermal conductivity of nanodispersions. In these attempts, the bulk mean free path of the dispersed particles and the matrix are modified in a way to take the influence of the carrier-boundary scattering into account. It is worthwhile to note that embedding nanoscale particles within the matrix shortens the mean free path of carriers in the matrix phase (see Figure(1.9)). In order to manifest the influence of carrier-particle collision, the collision mean free path, Λ_{coll} is defined as the distance travelled by the heat carrier before being scattered by the dispersed particles divided by the number of collisions[80, 81]. According to the unit cell approach, it is assumed that an individual particle is embedded in the unit cell from the matrix with effective length of α. Thus, for a spherical particle with radius of a_p, the volume fraction, ϕ is defined as

$$\phi = \frac{4/3\pi a_p^3}{\alpha^3} \tag{1.37}$$

If a phonon travels a distance L, it will experience $n\pi a_p^2 L$ collisions. Note that $n = 1/\alpha^3$ stands for the density of nanoparticles. Thus, the collision mean free path for a dispersion consisting of spherical particles can be written as[81] :

$$\Lambda_{coll} = \frac{L}{n(\pi a_p^2 L)} = \frac{4a_p}{3\phi} \tag{1.38}$$

The mean free path of the carrier inside the dispersed phase also decreases by boundary scattering events. Obviously, this reduction will be more significant, if the mean free path is in order or greater than the characteristic length of the particle phase. Thus, the effective mean free path should be defined for the particle phase[80–83].

There are different models which have been introduced to calculate the thermal conductivity of nanoscale materials with different geometries such as thin films, and nanowires. The analytical model presented by McGaughey *et. al* has been successful to predict the thermal conductivity of thin films in longitudinal direction, while their model has not been in good agreement with experimental results for transverse direction[84]. From direct solution of the Boltzmann transport equation under relaxation time approximation, the thermal conducti-

vity of the thin film in the longitudinal direction has been expressed as follow

$$k = \frac{1}{3} C v \Lambda_b (1 - \frac{1-s}{\delta} \frac{1-\exp(-\delta)}{1-s\exp(-\delta)}) \tag{1.39}$$

where $\delta = \frac{L}{\Lambda_b}$. Note that L stands for the thickness of the film[38]. In another work, it has also been observed that the solution of the Boltzmann transport equation for thin films lead to the following expression[30, 85] :

$$\frac{k}{k_{bulk}} = 1 - \frac{3Kn}{2} \int_0^\infty (\frac{1}{t^3} - \frac{1}{t^5})(1 - \exp(\frac{-t}{Kn}))dt \tag{1.40}$$

Majumdar has introduced another model to show the influence of the thickness on the thermal conductivity reduction of thin films[86]. His model is presented as follow :

$$\frac{k}{k_{bulk}} = \frac{1}{1 + \frac{3\Lambda_b}{8L}} \tag{1.41}$$

Based on the kinetic theory of transport processes, Maldovan has studied the effects of phonon boundary scattering on the thermal conductivity of semiconductor thin films. His results are in good agreement with experimental observations[87].

It is pointed out that the influence of boundary scattering on the thermal conductivity of thin films and nanowires with different cross-sections can be addressed by using phonon hydrodynamic models[88–91].

1.8 Influence of dispersed particle anisotropy and orientation on the thermal conductivity

Dispersion of anisotropic particles such as nanowires, nanotubes, and thin films with different aspect ratio in an isotropic matrix can provide highly anisotropic thermal conductivity of the nanodispersion. For thermal interface materials application, a higher thermal conductivity has been observed when dispersed phase is aligned parallel to heat flow direction. For

dispersion of $11wt\%$ graphite nanoplatelet in epoxy matrix, it was observed that the in-plane thermal conductivity is about four times of the cross-plane thermal conductivity[50]. For dispersion of $0.4vol\%$ carbon nanotube in the polymer $S160$, the thermal conductivities of the dispersions with aligned and randomly dispersed carbon nanotubes were reported as 1.21 and $0.59Wm^{-1}K^{-1}$, respectively. Note that the thermal conductivity of the pure $S160$ was reported as $0.52Wm^{-1}K^{-1}$[92]. The perpendicular thermal conductivity of neat $Elvax$ 260 has changed from $0.311Wm^{-1}K^{-1}$ to $0.356Wm^{-1}K^{-1}$ when $20wt\%$ multi-walled carbon nanotube is dispersed in the matrix. While for the parallel thermal conductivity, a significant increase has been observed (from $0.324Wm^{-1}K^{-1}$ to $2.318Wm^{-1}K^{-1}$)[93].

It is remarkable to note that the alignment of thermally conductive fillers in the heat flow direction can effectively facilitate heat transfer through the dispersion by making less barriers against the heat carrier motion which is resulted in an increase in the thermal conductivity of the dispersion. Recently, the Monte Carlo simulation was performed to study anisotropic thermal conductivity of the $PEEK$ matrix containing single-walled carbon nanotube and tungsten disulfide. Results clearly showed that the more aligned are the carbon nanotubes in heat flow direction, the higher is thermal conductivity[94]. Three possible orientations of anisotropic particles for heat removal in electronic packaging applications have been presented in Figure (1.10).

For dispersion of nano-silicon wires in germanium matrix, numerical results have shown that lower thermal conductivity can be achieved if nanowires are oriented perpendicular to heat flow direction[40, 95].

Only a few theoretical attempts have been made to comprehensively study the sensitivity of the thermal conductivity of nanodispersions to all possible governing parameters. It is pointed out that the influence of volume fraction, particle size, and the totally diffuse phonon-boundary scattering on the thermal conductivity of nanodispersions has been addressed in previous works available in literature[80–83, 96, 97]. However, the role of other important parameters, in particular including temperature, the properties of the interface (i.e. totally

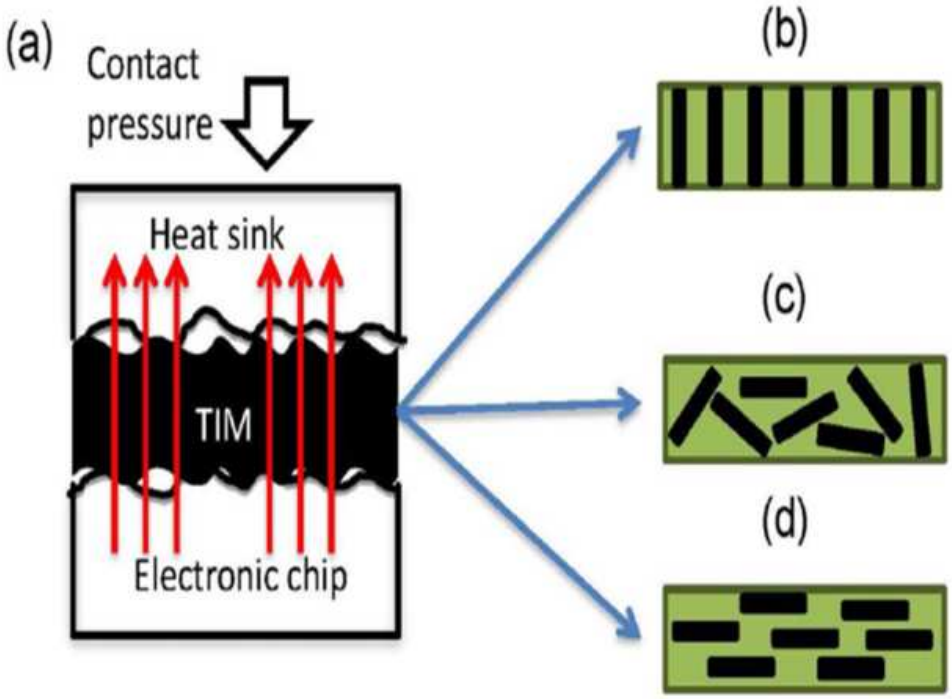

Figure 1.10 (a). Schematic description of thermal interface materials for heat removal in electronic packaging. Possible alignments of anisotropic particles in thin thermal interface material layer : (b). parallel, (c). random, and (d). perpendicular to the thickness[28].

specular or partially diffuse-partially specular) between particle phase and the matrix, orientation, and degree of dispersion of the dispersed phase as well as the hybrid dispersion of dispersed phases has not been addressed.

CHAPTER 2

OBJECTIVES

Predictions of the thermal conductivity of nanodispersions are needed in order to design products with desired properties. Nanodispersions have attracted a large interest due to their quicker and cheaper fabrications as well as their remarkable features to merge the mechanical, electrical and thermal properties for a particular application. Despite unique and tunable properties of nanodispersions, their theoretical investigation is lacking a systematic investigation of the importance of different factors such as particle size, volume fraction and particle geometry, interface properties and temperature on the thermal conductivity. Thus, the main objective of this study is :

To construct a general framework for a systematic theoretical investigation of the thermal conductivity of nanodispersions

To meet this objective, a particular attention is paid to the phonon viewpoint of heat conduction in nanodispersions. The phonon transport, in both the matrix and dispersed phase, is crucial for the study of the role of boundary scattering on the thermal conductivity. In each phase, the impact of the phonon-phonon and the phonon-boundary scattering is taken into account in the effective mean free path expressions represented by Mattheissen's rule.
Depending on the dispersed phase geometry, different collision and thermal boundary resistance mean free paths are defined. The influence of the size, the shape, and the orientation of dispersed particles as well as their volume fraction on the heat conductivity is investigated. Finally, a new approach is presented to study the thermal conductivity of hybrid dispersions consisting dispersed particles with different shapes and sizes. This approach is performed on two different nanodispersions ; first, on hybrid dispersion of sphere particles and their

agglomerates, and second on hybrid dispersion of spheres and wires.

CHAPTER 3

ORGANIZATION OF THE ARTICLES

The following four chapters are four articles in which results of our investigation are presented :

The first article, presented in Chapter 4, is entitled *"Influence of particle-matrix interface, temperature, and agglomeration on heat conduction in dispersions"*. In this work, the phonon viewpoint of heat conduction is employed to modify the Fourier heat conduction expression for dispersion of nanospheres in order to take the microscopic nature of heat transfer into account. The collision and the thermal boundary resistance mean free paths under specular and diffuse scatterings of phonons at boundaries are defined. Results are compared with available experimental and numerical simulation data. For different particle sizes and volume fractions, the impact of temperature on the thermal conductivity of dispersions consisting of nanosphere particles is demonstrated. Finally, using a homogenization approach, the thermal conductivity of nanodispersions consisting of nanospheres and their agglomerates are studied. This article has been published in *Journal of Applied Physics, 2013 Vol. 114, pp 014305.*

The article in Chapter 5 is entitled *"Effective heat conduction in dispersion of wires"*. The approach used in the first article is extended to study the thermal conductivity of anisotropic nanowires in a homogeneous matrix. Influence of the size, volume fraction, specularity of the interface as well as the orientation of nanowires on the thermal conductivity of nanodispersions is entirely studied. As the conclusion, a good agreement between numerical results obtained from the Boltzmann transport equation simulations and our analytical results is observed. This article has been published in *Applied Physics Letters, 2014 Vol. 104, pp 063106.*

The third article, presented in Chapter 6 is entitled *Effective heat conduction in hybrid sphere & wire nanodispersions*. In this work, two different approaches of homogenization are used to

predict the thermal conductivity of dispersion of sphere and wire nanoparticles in a homogeneous matrix. It is seen that predicted results from both approaches are in good agreement. During this part of study, the influence of different effective parameters consisting volume fraction, size, orientation and properties of the interface on the thermal conductivity of hybrid dispersion is evaluated. This article has been published in *Applied Physics Letters, 2014 Vol. 104, pp 233111.*

The fourth article in Chapter 7 is entitled *Temperature dependence of thermal conductivity in hybrid nanodispersions*. In this work, our previous model is extended to predict the thermal conductivity of nanodispersions consisting of cuboid nanowires. The results show a good agreement with available numerical data. Afterwards, the influence of the temperature on the thermal conductivity of hybrid dispersion of nanospheres and nanowires in a homogeneous matrix is studied. It is observed that the influence of interface produced by embedding nanoparticles in the matrix is only significant at lower temperatures while the possible benefit of hybrid nanodispersions in fabricating electronic devices diminishes with increasing the temperature. This article has been published in *RSC Advances, 2014, DOI : 10.1039/C4RA12368A.*

CHAPTER 4

ARTICLE1 : Influence of particle-matrix interface, temperature, and agglomeration on heat conduction in dispersions

A. Behrang, M. Grmela, C. Dubois, S. Turenne and P. G. Lafleur

Journal of Applied Physics, 2013 Vol. 114, pp 014305

Abstract

A combination of the effective medium and the phonon approaches is used to investigate heat conduction in heterogeneous media composed of a homogeneous matrix in which spherical particles of micro and nano sizes are dispersed. In particular, we explore the effect of different types of scattering on the particle-matrix interface, temperature dependence of the effective heat conduction coefficient, and the effect of various degrees of agglomeration of the particles. Predictions, calculated explicitly for Si nanoparticles dispersed in Ge matrix, agree with available results from Monte Carlo simulations. Moreover, our predictions show that the higher is the temperature, the lower is the heat conductivity and the smaller is the influence of the details of the particle-matrix interface. Regarding the agglomeration, we predict both decrease and increase of the heat conductivity depending on the degree of agglomeration.

4.1 Introduction

We investigate heat conduction in two component heterogeneous media. One component is a homogeneous matrix in which the second component is dispersed in the form of spherical particles. If the dimension of the spheres is larger than the phonon mean free path then the heat conduction is well described by the classical Fourier theory. Its application results in a complex system of partial differential equations and boundary conditions. It has been shown in Refs.[1, 2] that the system can be approximately reduced to a much simpler system of

equations corresponding to a homogenized effective medium. This type of reduction is called an effective medium approach (introduced originally in the context of electric conductivity in Ref.[3]). The heat conductivity k_{eff} of the effective medium that arises in Ref. [2] is given by

$$k_{eff} = k_m \frac{2k_m + (1+2\alpha)k_p + 2\phi[(1-\alpha)k_p - k_m]}{2k_m + (1+2\alpha)k_p - \phi[(1-\alpha)k_p - k_m]} \tag{4.1}$$

The symbol ϕ stands for the volume fraction of the dispersed particles, and k_m and k_p for the heat conductivity coefficient of the matrix and the dispersed particle. The influence of the particle-matrix interface is expressed in Eq.(4.1) in the dimensionless parameter $\alpha = \frac{a_K}{a_p}$ where a_p is the radius of the spherical particle and $a_K = Rk_m$ is defined as the thickness of the matrix-filled layer surrounding the particle in which the same temperature drop occurs as that at the interface. The coefficient R is called a thermal boundary resistance coefficient. If $a_K = 0$ and thus $\alpha = 0$, then the interface is called a perfect interface.

If, on the other hand, the dimension of the spheres is smaller than the phonon mean free path then the heat conduction has to be approached with the Boltzmann-Peierls theory in which heat is seen as a gas of phonons (see Refs.[4–7]). The mathematical formulation consists of the Boltzmann-type equation governing the time evolution of the one-phonon distribution function in the heterogenous medium under consideration. We shall not take this route.

In this paper we follow a third route, introduced originally in Refs.[8, 9], that is a hybrid of the previous two. The starting point is the expression Eq.(4.1) for the heat conductivity of an effective homogeneous medium. The phonon viewpoint of heat is introduced into Eq.(4.1) in expressions for the coefficients k_m, k_p and α that arise in the Boltzmann-Peierls phonon theory. Our contribution consists in : (i) a new consideration of the matrix-particle interface (Section 4.2), (ii) an explicit investigation of the temperature dependence of k_{eff} that follows from its phonon representation (Section 4.3), and (iii) an investigation of the influence of various degrees of agglomeration of the dispersed particles (Section 4.4). Our motivation and a potential domain of application is an attempt to increase the efficiency of thermoelectric devices measured by $S^2\sigma T/k$, where S is the Seebeck coefficient, σ is the electric conductivity,

T the absolute temperature, and k the thermal conductivity[10, 11]. In this paper we are addressing only the heat conductivity. Previous experimental observations[12–17] indicate that it is the reduction in thermal conductivity that plays a dominant role in increasing the thermoelectric efficiency.

4.2 Phonon representation of the effective Fourier heat conduction

We recall first the phonon representation of Eq.(4.1) derived in Refs.[8, 9]. The Boltzmann-Peierls phonon theory applied to a homogeneous medium leads to the following expression for the heat conductivity coefficient k,

$$k = \frac{1}{3}\int C(\omega)v(\omega)\Lambda(\omega)d\omega \approx \frac{1}{3}Cv\Lambda \tag{4.2}$$

where C is the volumetric specific heat per unit frequency at the frequency ω, v the phonon group velocity, and Λ the phonon mean free path. The heterogeneity of the medium is taken into account in Refs.[8, 9] by using Matthiessen's rule expressing Λ in the form

$$\frac{1}{\Lambda_j} = \frac{1}{\Lambda_{b,j}} + \frac{1}{\Lambda_{coll,j}} \qquad j = m, p \tag{4.3}$$

where the subscript p and m denote "particle" and "matrix" respectively, b stands for "bulk", and *coll* for "collisions". Alternatively, the expression Eq.(4.3) is also written in the form $\Lambda_j = F_j\Lambda_{b,j}, i = p, m$ which defines the scaling factor F_j by requiring that this expressions and Eqs.(4.3) are equivalent. For the collision contribution to the mean free paths, the expressions $\Lambda_{coll,m} = \frac{4a_p}{3\phi}$ and $\Lambda_{coll,p} = 2a_p$ are used in Minnich and Chen[8]. As for the coefficient α representing in Eq.(4.1) the medium-particle interface, its phonon representation used by Chen in Ref.[18] is $\alpha = \frac{Rk_m}{a_p}$ with $R = 4\left(\frac{C_m v_m + C_p v_p}{C_m v_m C_p v_p}\right)$. By inserting these expressions into Eq.(4.1), one obtains the phonon representation of Eq.(4.1) derived in Refs.[8, 9].

Now we proceed to present our alternative approach. Our intention is to pay more attention to the medium-particle interface. We do not account for it in (4.1) in the parameter α

(we put $\alpha = 0$ in Eq.(4.1)). Instead, we do it in modified expressions for the heat conductivity coefficients. In addition to considering in Λ the effect of collisions, as it is done in Eq.(4.3), we also consider in Λ the effect of the interface. This alternative approach will give us a possibility to consider both diffuse and specular scattering of phonons on the interface. Instead of Eq.(4.3), we write

$$\frac{1}{\Lambda_j^{(i)}} = \frac{1}{\Lambda_{b,j}^{(i)}} + \frac{1}{\Lambda_{coll,j}^{(i)}} + \frac{1}{\Lambda_{TBR,j}^{(i)}} \qquad i = s, d \quad j = m, p \tag{4.4}$$

The upper index "(s)" stands for "specular" and "(d)" for "diffuse" and Λ_{TRB} is the thermal boundary resistance mean free path. With this modification, we are able to consider two types of scatterings on the interface : diffuse (considered in Refs. [8, 9]) and also specular. For diffuse collisions and for particles, we use $\Lambda_{coll,p}^{(d)} = \frac{3a_p}{4}$ proposed in Ref.[19]. For the matrix, we keep the same $\Lambda_{coll,m}^{(d)}$ as in Minnich and Chen analysis [8] (i.e. $\Lambda_{coll,m} = \frac{4a_p}{3\phi}$ and $\Lambda_{coll,p} = 2a_p$). For the specular collisions we make the same choice as for the diffuse collisions except that, following Ref.[20], we replace the particle radius a_p with an effective particle radius $a_p^{(s)} = a_p \frac{1+s}{1-s}$, where the parameter $0 \leq s \leq 1$ is the probability of the specular scattering of phonons on the particle-matrix interface, $1 - s$ is the probability of the diffuse scattering. Consequently, $\Lambda_{coll,m}^{(s)} = \frac{4a_p^{(s)}}{3\phi}$ and $\Lambda_{coll,p}^{(s)} = \frac{3a_p^{(s)}}{4}$. We note that for the pure specular collisions $(\Lambda_{coll,m}^{(s)})^{-1} = 0$ and consequently (see Eq.(4.4)) collisions do not contribute to the effective mean free path.

Now we turn to Λ_{TBR}. Following Refs.[18, 21], we use expressions based on the equivalent equilibrium temperature :

$$
\begin{aligned}
\Lambda^{(i)}_{TBR,p} &= 0 \; for \; i = s, d \\
\Lambda^{(d)}_{TBR,m} &= \frac{a_p t^{(d)}_{mp}}{\phi\left[1 - \frac{1}{2}(t^{(d)}_{mp} + t^{(d)}_{pm})\right]} \\
\Lambda^{(s)}_{TBR,m} &= \frac{2a_p \int_0^{\mu_{crit}} t^{(s)}_{mp}(\mu_m)\mu_m d\mu_m}{\phi\left[1 - \int_0^{\mu_{crit}} t^{(s)}_{mp}(\mu_m)\mu_m d\mu_m - \int_0^{\mu_{crit}} t^{(s)}_{pm}(\mu_p)\mu_p d\mu_p\right]}
\end{aligned} \tag{4.5}
$$

The symbol $t^{(d)}_{jl}$ denotes the probabilities of transmission from side "j" to side "l" in the diffuse scattering. They are given by $t^{(d)}_{jl} = \frac{C_l v_l}{C_j v_j + C_l v_l}$, $j, l = p, m$; $j \neq l$. The symbol $t^{(s)}_{jl}$ denotes the probabilities of transmission from side "j" to side "l" in the specular scattering. They are given by $t^{(s)}_{pm} = \frac{4\rho_p v_p \rho_m v_m \mu_p \mu_m}{(\rho_p v_p \mu_p + \rho_m v_m \mu_m)^2}$ and $t^{(s)}_{mp} = \frac{C_p v_p^3}{C_m v_m^3} t^{(s)}_{pm}$, where $\mu_m = \cos\theta_m$ and $\mu_p = \cos\theta_p$ are related by Snell's law $\frac{\sin\theta_m}{v_m} = \frac{\sin\theta_p}{v_p}$, the critical angle θ_{crit} appearing in the formula for $F^{(s)}_m$ is given by $\theta_{crit} = \arcsin\frac{v_p}{v_m}$ if $v_m > v_p$ and $= 0$ if $v_m < v_p$ for phonon transmission from particle to matrix. In the opposite case for phonon transmission from matrix to particle, $\theta_{crit} = \arcsin\frac{v_m}{v_p}$ if $v_p > v_m$ and $= 0$ if $v_p < v_m$. By $a^{(s)}_p = a_p\frac{1+s}{1-s}$, we denote the effective particle radius, ρ_m and ρ_p denote the mass density of the matrix and the particle, respectively. The expressions for the probabilities of specular transmission are valid when the incident angle is smaller than a critical angle θ_c. Otherwise, there is no transmission of phonons[18]. With these expressions for the heat conductivity coefficients, the expression Eq.(4.1) takes the form

$$
k_{eff} = s k^{(s)}_{eff} + (1 - s) k^{(d)}_{eff} \tag{4.6}
$$

where

$$k_{eff}^{(i)} = \frac{1}{3} C_m v_m \Lambda_{b,m} F_m^{(i)} \times$$
$$\frac{\frac{2}{3} C_m v_m \Lambda_{b,m} F_m^{(i)} + \frac{1}{3} C_p v_p \Lambda_{b,p} F_p^{(i,1)} + 2\phi \left(\frac{1}{3} C_p v_p \Lambda_{b,p} F_p^{(i,2)} - \frac{1}{3} C_m v_m \Lambda_{b,m} F_m^{(i)} \right)}{\frac{2}{3} C_m v_m \Lambda_{b,m} F_m^{(i)} + \frac{1}{3} C_p v_p \Lambda_{b,p} F_p^{(i,1)} - \phi \left(\frac{1}{3} C_p v_p \Lambda_{b,p} F_p^{(i,2)} - \frac{1}{3} C_m v_m \Lambda_{b,m} F_m^{(i)} \right)}$$
$$i = s, d \tag{4.7}$$

where F, scaling coefficients related to the mean free paths Λ by the relation ($\Lambda_j = F_j \Lambda_{b,j}, i = p, m$), are given by

$$F_p^{(i,1)} = F_p^{(i,2)};\ i = s, d$$
$$F_m^{(d)} = \frac{4 \frac{a_p}{\Lambda_{b,m}} t_{mp}^{(d)}}{4 \frac{a_p}{\Lambda_{b,m}} t_{mp}^{(d)} + \phi [t_{mp}^{(d)} - 2 t_{pm}^{(d)} + 4]}$$
$$F_m^{(s)} = (4 \frac{a_p}{\Lambda_{b,m}} \int_0^{\mu_{crit}} t_{mp}^{(s)}(\mu_m) \mu_m d\mu_m) / (4 \frac{a_p}{\Lambda_{b,m}} \int_0^{\mu_{crit}} t_{mp}^{(s)}(\mu_m) \mu_m d\mu_m +$$
$$\phi [2(1 - \int_0^{\mu_{crit}} t_{pm}^{(s)}(\mu_m) \mu_m d\mu_m) + \int_0^{\mu_{crit}} t_{mp}^{(s)}(\mu_p) \mu_p d\mu_p (\frac{3 a_p}{a_p^{(s)}} - 2)])$$
$$F_p^{(d)} = \frac{3 \frac{a_p}{\Lambda_{b,p}}}{3 \frac{a_p}{\Lambda_{b,p}} + 4}$$
$$F_p^{(s)} = 1 \tag{4.8}$$

The formulas derived in Refs.[8, 9] are a particular case of Eqs.(4.6), (4.7) corresponding to no specular scattering (i.e. $s = 0$ and thus also $F_m^{(s)} = 0, F_p^{(s,1)} = 0, F_p^{(s,2)} = 0$) and $F_m^{(d)} = \frac{4a_p}{\Lambda_{b,m}} (\frac{4a_p}{\Lambda_{b,m}} + 3\phi)^{-1}$, $F_p^{(d,1)} = \left(\frac{2a_p}{\Lambda_{b,p}} \right) (1 + 2\alpha(\phi, a_p)) (\frac{2a_p}{\Lambda_{b,p}} + 1)^{-1}$, $F_p^{(d,2)} = \left(\frac{2a_p}{\Lambda_{b,p}} \right) (1 - \alpha(\phi, a_p)) (\frac{2a_p}{\Lambda_{b,p}} + 1)^{-1}$, together with $\alpha = a_K / a_p$ with the thermal boundary resistance coefficient (i.e. R).

4.2.1 Comparison with results of Monte Carlo simulations and experimental observations

We illustrate the expression (4.6) on $SiGe$ nanocomposite with Si nanoparticles dispersed in a Ge matrix. The material parameters used in calculation are presented in Table 4.1.

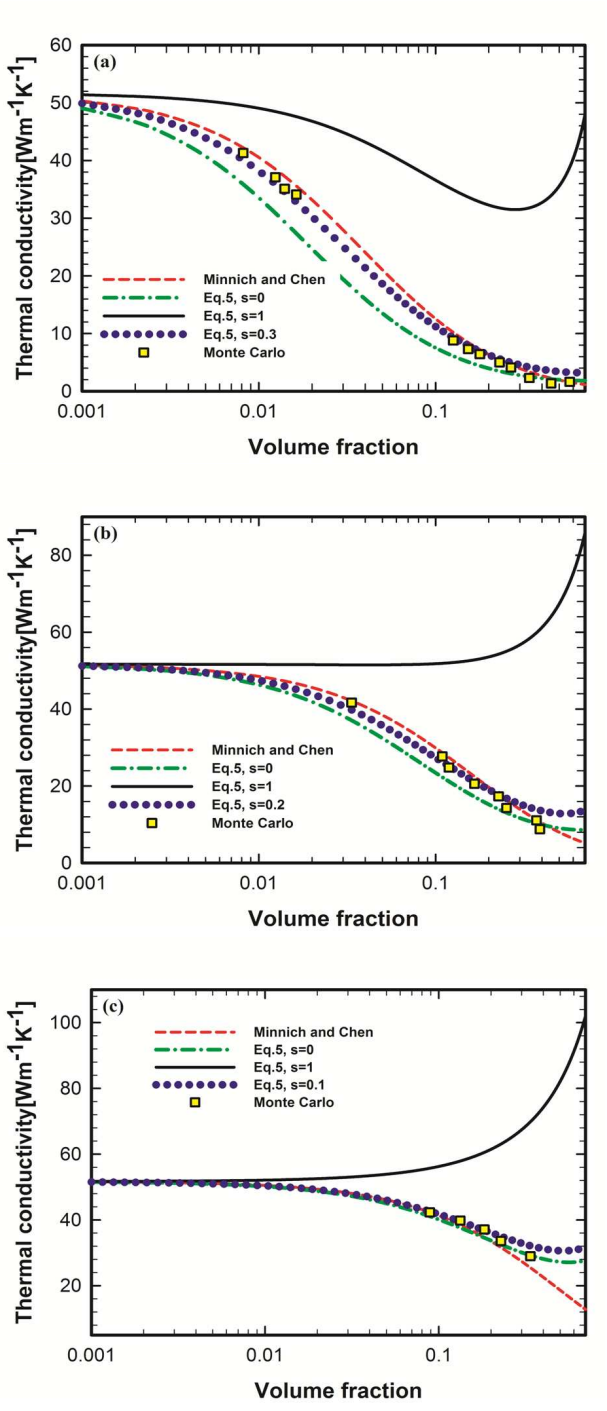

Figure 4.1 (Color online) Effective thermal conductivity of a SiGe nanocomposite comprising spherical Si particles with the radius : (a) $a_p = 5nm$, (b) $a_p = 25nm$, and (c) $a_p = 100nm$ as a function of the particle volume fraction ϕ.

This nanocomposite has also been previously simulated by Monte Carlo method [22]. Fig.4.1 compares our results with the Minnich-Chen [8] formula and with Monte Carlo simulations for a_p =5, 25, 100 nm. We see that in the case $s = 1$ (i.e. for pure specular reflection) the predictions implied by Eqs.(4.6) and (4.7) differ substantially from the Monte Carlo simulations. On the other hand, in the case of pure diffuse scattering (i.e. when $s = 0$) we see an agreement for all volume fractions. A significant difference between the specular and diffuse effective thermal conductivities is observed in particular in higher volume fractions. It is worthwhile to remark that our results (except in the case when $s = 1$) are similar to those implied by the Minnich and Chen formula for smaller particle volume fractions. For all particle sizes and in the case of pure diffuse scattering (i.e. $s = 0$), the formulas (4.6), (4.7) predict higher values than does the Minnich-Chen formulas. Moreover, the effective heat conductivity calculated from Eqs.(4.6)and(4.7) approaches the effective thermal conductivity k_p of dispersed nanoparticles when $\phi \to 1$. This difference between our results and the Minnich-Chen formulas becomes more pronounced when the particle radius increases. A difference is also seen for smaller particle sizes in moderate volume fractions. By choosing an appropriate value for s (in other words, choosing an appropriate combination of specular and diffuse scattering), we are able to bring predictions implied by Eqs.(4.6)and (4.7) closer to results of Monte Carlo simulation for all particle sizes. Our results also indicate how the effective thermal conductivity of the nanocomposite would change if the particle-matrix surfaces were modified (for example lowering the temperature to a few Kelvin or changing the roughness of the nanoparticle) to favor specular reflections.

Finally, our results are compared with the experimental data[26] for the effective thermal conductivity of nanocomposites with silicon dioxide (SiO_2) and aluminium nitride (AlN) particles embedded in epoxy matrix. The material parameters required for calculations are presented in Table 4.1. Fig.4.2 depicts the nanocomposite with SiO_2 particles. Our predictions appear to be in a very good agreement with the experimental data. This is not however the case for the nanocomposite with AlN particles. This maybe due to the fact that our model

Table 4.1 Material parameters used in calculations.

Material	C $[\times 10^6 Jm^{-3}K^{-1}]$	v $[ms^{-1}]$	Λ_b $[nm]$	ρ $[kgm^{-3}]$
Si	0.93[1]	1804[1]	268[1]	2330[1]
Ge	0.87[1]	1042[1]	171[1]	5330[1]
SiO_2	1.687[2]	4400[2]	0.558[2]	2278[2]
AlN	2.7[3]	6972[3]	51[4]	3300[3]
$Epoxy$	1.91[5]	2400[5]	0.11[6]	1970[5]

[1] Ref[18].
[2] Ref[23].
[3] Ref[24].
[4] Calculated from $\Lambda_b = 3k/Cv$ by considering $k = 320Wm^{-1}K^{-1}$ from Ref[24].
[5] Ref[25].
[6] Calculated from $\Lambda_b = 3k/Cv$ by considering $k = 0.168Wm^{-1}K^{-1}$ from Ref[26].

assumes spherical particles of the same size and AlN nanoparticles are not spherical and nor their size distribution is wide. On the other hand, the SiO_2 nanoparticles are spherical and they have a narrow size distribution.

Summing up, our results confirm an anticipated conclusion that the more obstacles the phonons encounter (in particular the larger is the particle-matrix interface and the more diffuse is the scattering on it) the lower is the thermal conductivity.

4.3 Temperature dependence of k_{eff}

The transformation that we have made in Section 4.2, namely the transformation from Eq.(4.1) to Eq.(4.7), provides also the dependence of k_{eff} on the temperature T. We have lost it in the previous section in the approximation made in the second equality in Eq.(4.2). The temperature dependence of k enters in Eq.(4.2) as a parameter in the dependence of C, v and Λ on ω. We shall now repeat the calculations made in the previous section but without the approximation. We restrict ourselves in this section to diffuse scattering (i.e. we put $s = 0$ in Eq.(4.6)). In order to deduce from (4.2) the temperature dependence, we need the functions

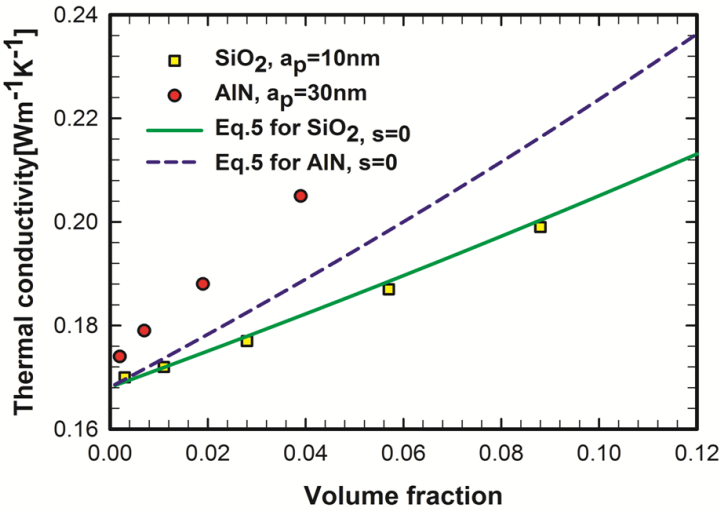

Figure 4.2 (Color online) Experimental and calculated values of the effective thermal conductivity as a function of the volume fractions ϕ of SiO_2 and AlN embedded in epoxy resin.

$C(T,\omega), v(T,\omega), \Lambda^{(d)}_{b,i}(T,\omega), \Lambda^{(d)}_{coll,i}(T,\omega)$, and $\Lambda^{(d)}_{TBR,i}(T,\omega)$, $i = p, m$. They all are well known in the Boltzmann-Peierls theory of phonon propagation.

Following Refs.[21, 27, 28], we use the Debye approximation, take the phonon group velocity v to be a constant independent of ω and T, and the volumetric specific heat per unit frequency at the frequency ω, $C(T,\omega)$, given by

$$C(T,\omega) = \frac{3\hbar^2}{2\pi^2 v_i^3 k_B T^2} \frac{\omega^4 \exp(\hbar\omega/k_B T)}{[\exp(\hbar\omega/k_B T) - 1]^2} \quad i = m, p \tag{4.9}$$

where $\hbar$ is the reduced Planck's constant, k_B is the Boltzmann constant. The limits of integration in Eq.(4.2) are 0 and ω_D that is the Debye frequency cutoff.

Next, we turn to the phonon mean free paths. As for the collision contribution, we see that both $\Lambda^{(d)}_{coll,m}$ and $\Lambda^{(d)}_{coll,p}$ are independent of ω and T. As for the $\Lambda^{(d)}_{b,m}$ and $\Lambda^{(d)}_{b,p}$, we use the expression $\frac{1}{\Lambda^{(d)}_{b,i}} = B_i T \omega^2 \exp(-\frac{\theta_i}{T})$; $i = m, p$. B and θ are constant parameters determined by fitting experimental data[54].

Finally, we address $\Lambda^{(d)}_{TBR,m}$ and $\Lambda^{(d)}_{TBR,p}$. We use the expressions given in Eq.(4.5) with

$$t_{jl}^{(d)} = \frac{\frac{3\hbar^2}{2\pi^2 v_l^2 k_B T^2} \int_0^{\omega_{D,l}} \frac{\omega^4 \exp(\hbar\omega/k_B T)}{[\exp(\hbar\omega/k_B T)-1]^2} d\omega}{\frac{3\hbar^2}{2\pi^2 v_l^2 k_B T^2} \int_0^{\omega_{D,l}} \frac{w^4 \exp(\hbar\omega/k_B T)}{[\exp(\hbar\omega/k_B T)-1]^2} d\omega + \frac{3\hbar^2}{2\pi^2 v_j^2 k_B T^2} \int_0^{\omega_{D,j}} \frac{\omega^4 \exp(\hbar\omega/k_B T)}{[\exp(\hbar\omega/k_B T)-1]^2} d\omega}$$
$$j, l = p, m;\ j \neq l \tag{4.10}$$

We have now all what we need to evaluate the effective heat conductivity coefficient k_{eff} given in Eq.(4.7). We shall make the evaluation explicitly for the dispersion of Si particles in Ge discussed already in Section 4.2.1. We need the parameters B and θ, appearing in bulk mean free path expression, for both Si and Ge. We find them by fitting the experimental data reported in Ref.[29]. For Si, we obtain $B = 5.753 \times 10^{-23} s^2 m^{-1} K^{-1}$ and $\theta = 199.2K$ and we expect the best fit coefficients for the Ge as $B = 1.655 \times 10^{-22} s^2 m^{-1} K^{-1}$ and $\theta = 78.92K$. Fig.4.3 shows how well the bulk thermal conductivity model fits the experimental data for both silicon and germanium. The Debye frequency cutoff of Si and Ge are $9.12 \times 10^{13} s^{-1}$ and $5.14 \times 10^{13} s^{-1}$[30] respectively, and the phonon group velocities for Si and Ge 6400 m/s and 3900 m/s[18]. Fig.4.4 shows the thermal conductivity of $SiGe$ nanocomposites as a function of volume fraction of silicon for different temperatures and different silicon particle sizes. The thermal conductivity decreases from 72 $Wm^{-1}K^{-1}$ at $\phi = 1\%$ to 26 $Wm^{-1}K^{-1}$ at $\phi = 20\%$ for 200 K, while there is almost no difference in the thermal conductivity of the nanocomposite (14 $Wm^{-1}K^{-1}$ at $\phi = 1\%$ to 10 $Wm^{-1}K^{-1}$ at $\phi = 20\%$) at high temperatures around 1000 K. This observation may be explained by the fact that the effect of the interface scattering is more important at lower temperatures, while the Umklapp (internal) scattering has a strong effect at high temperatures[31]. Another argument explaining Fig.4.4 is the following : An increase in the temperature causes a reduction in the transmission coefficient from matrix to particles. This reduction then increases the thermal boundary resistance, and consequently the thermal conductivity of the dispersion is reduced. Thermal conductivities of nanocomposites calculated for different particle sizes and volume fractions as a function of

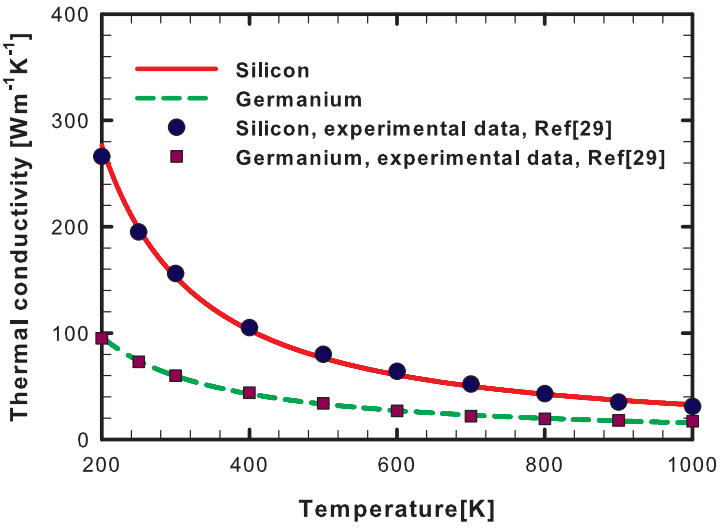

Figure 4.3 (Color online) Temperature dependence of theoretical phonon thermal conductivities for bulk silicon and germanium fitted to experimental data.

temperature are plotted in Fig.4.5. As shown in Fig.4.5(a), the thermal conductivity is significantly reduced with increasing the temperature for all particle sizes at the concentration of 1%. In this condition, due to small amount of nanoparticles, probability of phonon-interface scattering decreases, while, possibility of phonon-phonon (internal) scattering rises. As we expect, the thermal conductivities are the smallest at high temperatures.

At elevated volume fractions and smaller particle sizes, the thermal conductivity of nanocomposites is seen to become almost independent of the temperature (Fig.4.5(b) for $a_p = 10nm$). This is due to the dominance of the interface scattering. However, it is remarkable to note that the influence of the internal scattering (phonon-phonon Umklapp scattering) may even become weaker than that of the interface scattering. This happens when nanocomposites have high volume fractions and smaller particle sizes. Despite the insensitivity of the heat conductivity to temperature changes at higher volume fractions and smaller particle sizes, the smallest thermal conductivities are expected to arise precisely in such conditions due to the relative increase in the interface scattering area per unit volume [32] implying strong confinement of phonon transport at the particle matrix interface.

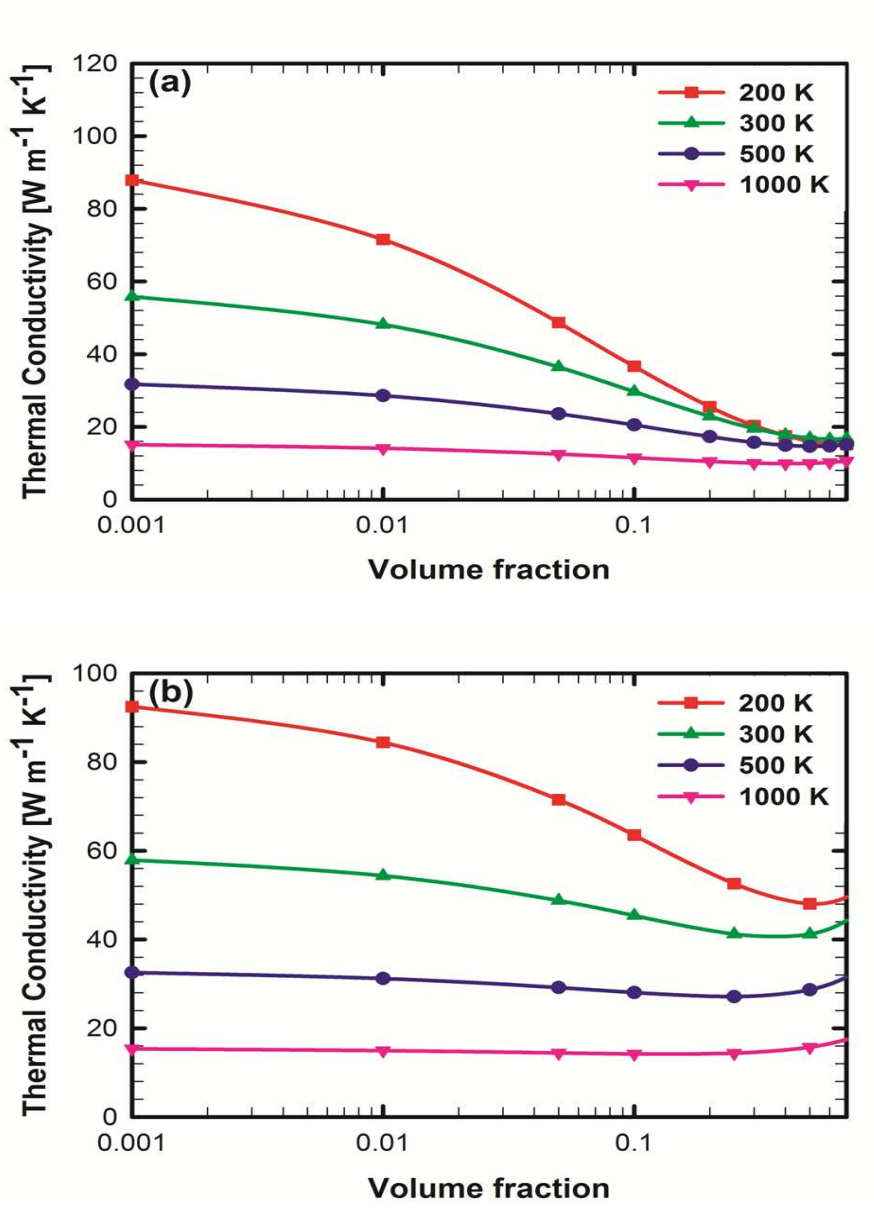

Figure 4.4 (Color online) Effective thermal conductivity of a SiGe nanocomposite comprising spherical Si particles with the radius : (a) $a_p = 10nm$, and (b) $a_p = 50nm$ as a function of the particle volume fraction ϕ in different temperatures.

Summing up, we see the heat conductivity decreases with increasing the temperature. Moreover, we see again that the larger are obstacles for phonons (i.e. the larger is the particle-boundary interface) the smaller is the heat conductivity. The difference becomes however significantly smaller for high temperatures.

4.4 Influence of various degrees of agglomeration on k_{eff}

The distribution of dispersed particles has been so far always uniform (i.e. independent of the spatial coordinate). We now allow the particles to agglomerate. Some of the original particles will form clusters (agglomerates) and the dispersion becomes a dispersion of two types of "particles" : the remaining original particles (their number is $N^{(out)}$) and the agglomerates (their number is $N^{(agg)}$). Both the original particles and the agglomerates are assumed to be uniformly distributed (i.e. their distribution is assumed to be independent of the spatial coordinate). If $N^{(in)}$ is the number of the original particles in a single agglomerate and $N^{(p)}$ is the number of the original particles in the dispersion without agglomeration then, $N^{(p)} = N^{(out)} + N^{(in)}N^{(agg)}$, which then implies a similar relation for the volume fractions ϕ,

$$\phi^{(p)} = \phi^{(out)} + \phi^{(in)}\phi^{(agg)} \tag{4.11}$$

where

$$\phi^{(p)} = \frac{N^{(p)}V^{(p)}}{V};\;\; \phi^{(out)} = \frac{N^{(out)}V^{(p)}}{V};$$

$$\phi^{(in)} = \frac{N^{(in)}V^{(p)}}{V^{(agg)}};\;\; \phi^{(agg)} = \frac{N^{(agg)}V^{(agg)}}{V} \tag{4.12}$$

V is the total volume of the dispersion, $V^{(p)}$ is the volume of a single original particle, and $V^{(agg)}$ volume of a single agglomerate.

To investigate heat conduction in media with agglomerates, we use the same effective medium approach that we have used in previous sections for media without agglomerates.

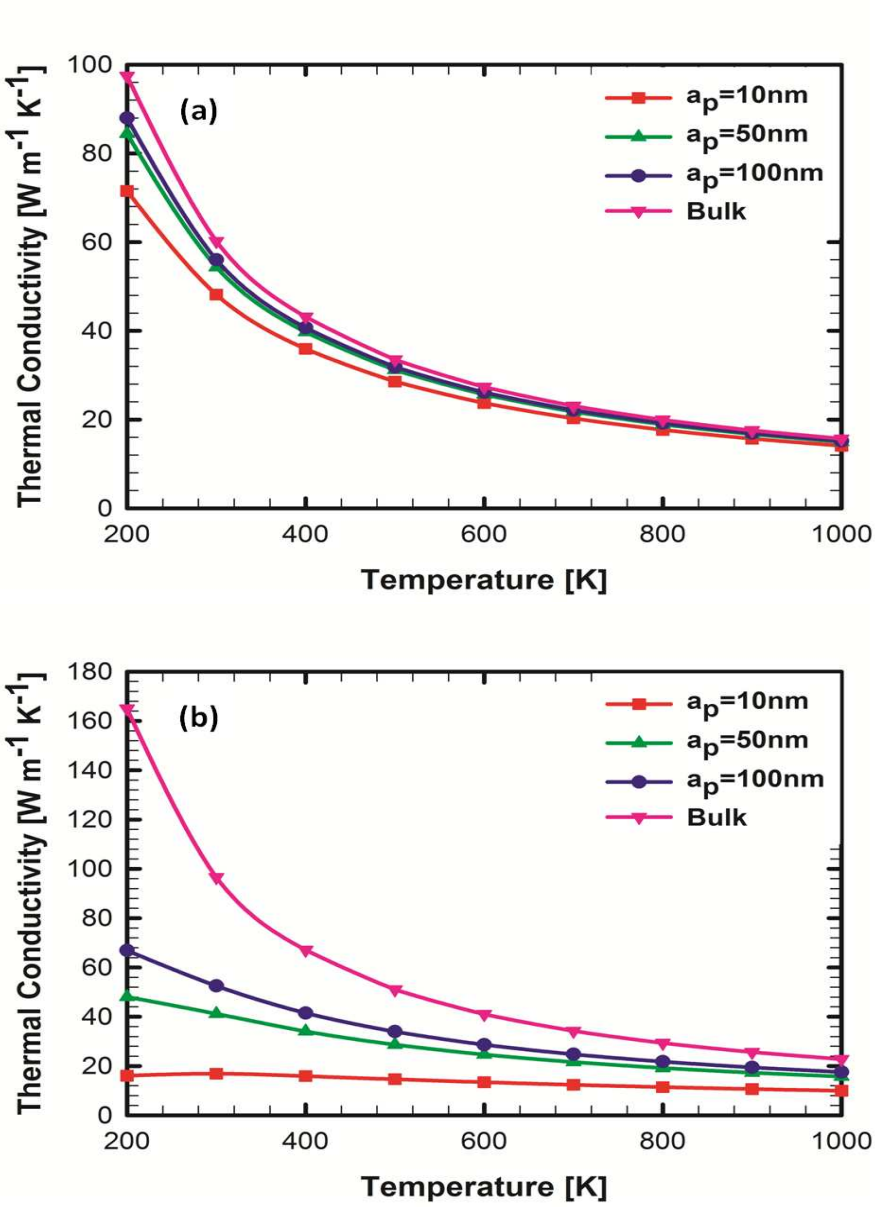

Figure 4.5 (Color online) Calculated temperature-dependent thermal conductivity of a Si/Ge nanocomposite for a three differences particle sizes and volume fraction (a) $\phi = 0.01$, and (b) $\phi = 0.5$.

We apply it now in three steps : (*Step 1*), we homogenize inside a single agglomerate, (*Step 2*), we homogenize outside the agglomerates, and finally (*Step 3*), we homogenize the dispersion of agglomerates. For each step of inhomogeneity, we use the formula (4.6) derived in Section 4.2.

For *Step 1* and *Step 2*, we apply Eq.(4.6) with related volume fractions $\phi^{(in)}$ and $\phi^{(out)}$, respectively. Note that the specific heat capacity, phonon group velocity and bulk mean free path of the matrix and the dispersed particles in *Step 1* and *Step 2* are presented in Table 4.1 ; also the size of dispersed particles for these steps is the same and equal to the size of the original particles in the dispersion without agglomeration. After performing the first two steps, the equivalent bulk thermal conductivities of the matrix and dispersed particles are determined. It means that we have now a heterogeneous media consisting an equivalent bulk matrix phase resulted from *Step 2* and an equivalent bulk dispersed phase (agglomerates) resulted from *Step 1*. In *Step 3*, we need the specific heat capacities C_m, C_p, and the phonon group velocities v_m, v_p. We calculate them by using the mixing rule (i.e. $C_m^{(agg)} = C_m^{(out)}(1-\phi^{(out)}) + C_p^{(out)}\phi^{(out)}$ and similarly for C_p, v_m, v_p). The mean free paths of the matrix and agglomerates are calculated by using Eq.(4.2). Eventually, we use Eqs.(4.6) and (4.7) to determine the effective thermal conductivity of the dispersion. The particle size in *Step 3* is the size of the agglomerate.

Figs.4.6(a-b) illustrate the evolution of thermal conductivity of dispersion with $\phi^{(in)}$. As a case study, we look at the thermal conductivity of $SiGe$ dispersion. The material parameters used in this calculation have been already presented in Table 4.1. The radius of the original particles is 20 nm and the gyration radius of the agglomerates are assumed 5 times the radius of original particles. The x-axis is the volume fraction $\phi^{(out)}$ of the original particles outside agglomerates. Passing from left to right is thus passing from low to higher degrees of agglomeration.

The matrix-agglomerate scattering is assumed to be purely diffuse. This is because we expect the matrix-agglomerate interface to be, in general, rougher than the particle-matrix

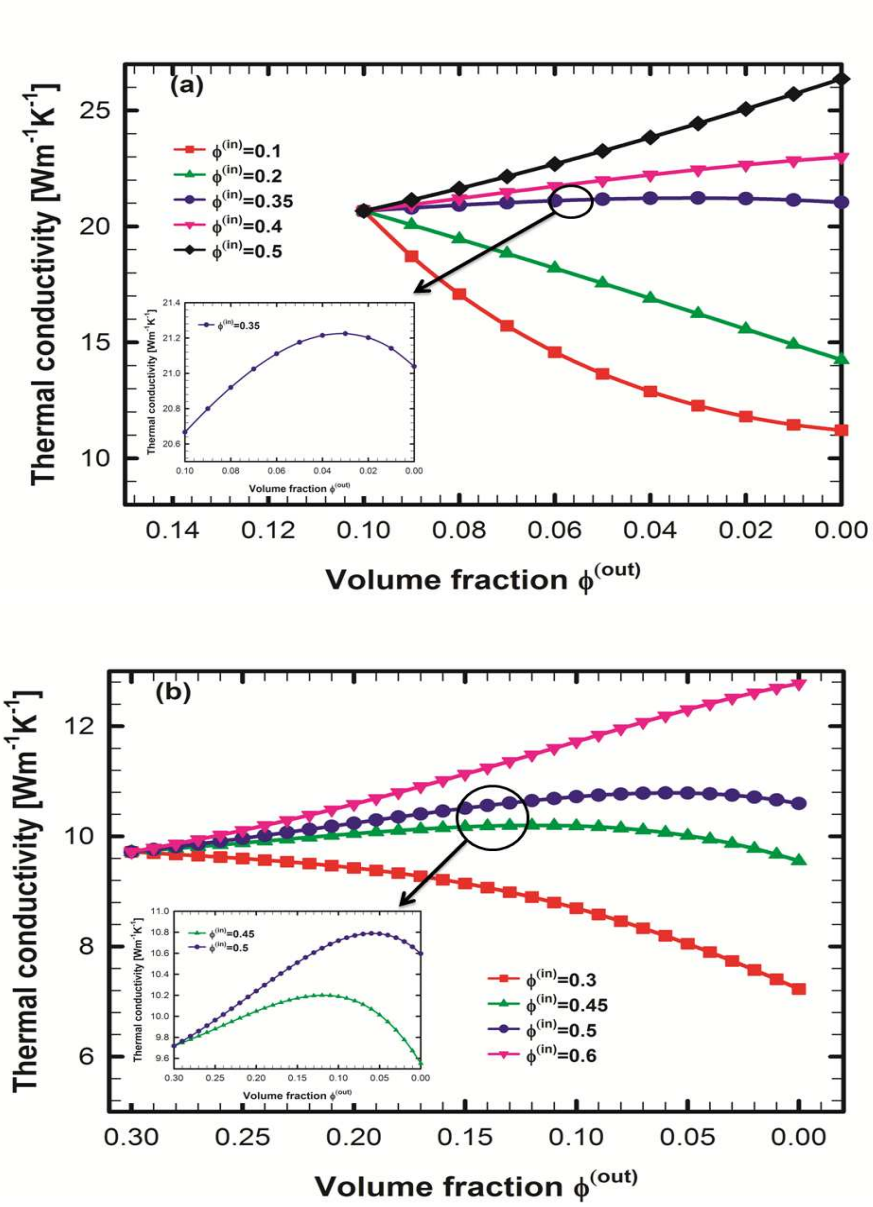

Figure 4.6 (Color online) Effect of agglomeration on the thermal conductivity of dispersion. (a) $\phi^{(p)} = 0.1$, and (b) $\phi^{(p)} = 0.3$ as a function of the volume fraction of well-dispersed particles, $\phi^{(out)}$ for different degree of agglomeration.

interface. In Figs. 4.6(a-b) we also assume that the matrix-particle scattering is purely diffuse. The effect of specularity in the particle-matrix scattering leads to an increase in the thermal conductivity.

Results show that agglomeration can either decrease or increase the thermal conductivity. The increase occurs for compact agglomerates (i.e. for large $\phi^{(in)}$) and decrease for agglomerates that are less compact. For intermediate degrees of compactness of the agglomerates (i.e. intermediate values of $\phi^{(in)}$) the heat conductivity first increases with increasing the degree of agglomeration (i.e. with decreasing $\phi^{(out)}$) and then, after reaching a certain critical value of the agglomeration, starts to decrease. We believe that the possibility to influence the heat conductivity by nonuniform distribution of particles may be of particular importance for optimizing efficiency of thermoelectric devices.

4.5 Concluding remarks

We have used the well known combination of the effective medium approach and the phonon approach to study heat conduction in heterogeneous media composed of a homogeneous matrix in which spherical particles are dispersed. In particular, we have investigated how the effective heat conductivity coefficient k_{eff} of the composite is influenced by the type of phonon scattering on the particle-matrix interface, by changes in the temperature, and by various degrees of agglomeration of the dispersed particles. The influence of the interface enters the analysis in the thermal boundary resistance phonon mean free path. The temperature dependence, implicitly appearing in the frequency dependencies of all the phonon-related quantities entering the formula for k_{eff}, is made explicit with the assistance of computers. In the investigation of the influence of agglomeration, we apply homogenization separately to the medium inside the agglomerate, outside the agglomerates, and finally to the dispersion of agglomerates.

Our results show that the more obstacles the phonons encounter in the composites the lower is the thermal conductivity. The main obstacle is the particle-matrix interface. Given the

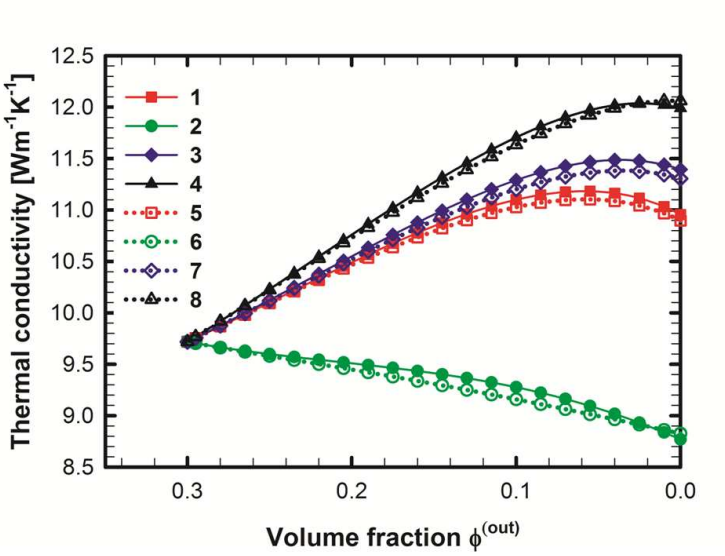

Figure 4.7 (Color online) Thermal conductivity of dispersions consisting two different agglomeration sizes as a function of the volume fraction of well-dispersed particles,$\phi^{(out)}$ for different degree of agglomeration. Parameters used in calculation for curve (1) are $\phi^{(p)} = 0.3$, $\phi^{(inA)} = 0.35$, $\phi^{(inB)} = 0.4$, $\phi^{(aggA)} = 0.1\phi^{(aggB)}$, $a_p^{(A)} = 60nm$, $a_p^{(B)} = 200nm$ and $a_p^{(out)} = a_p^{(inA)} = a_p^{(inB)} = 20nm$. Parameters in curve (2) are same as curve (1) but $\phi^{(aggA)} = 1.5\phi^{(aggB)}$. For curves (3) and (4), parameters presented in curve (1) are considered but $\phi^{(inA)} = 0.5$ for curve (3) and $a_p^{(B)} = 300nm$ for curve (4). Note that in these curves the order of homogenization is : phase $in \rightarrow$ phase $inA \rightarrow$ phase $aggA \rightarrow$ phase $inB \rightarrow$ phase $aggB$. Curves (5 to 8) are corresponded to curves (1-4), but the method of homogenization is phase $in \rightarrow$ phase $inB \rightarrow$ phase $aggB \rightarrow$ phase $inA \rightarrow$ phase $aggA$.

volume fraction of the particles, the particle-matrix interface can be increased by decreasing the size of the particles and increasing their number. We also show that the more diffuse is the phonon-interface scattering the lower is the thermal conductivity. By comparing our predictions with results of experimental observations we have seen that the diffuse scattering is dominant but a small amount of the specular scattering is needed to improve the fit.

As for the temperature dependence, we see the decrease of the heat conductivity with increasing the temperature. Moreover, we also see that the differences caused by changes in the size of the particle-matrix interface and the type of phonon-particle scattering, become considerably smaller for higher temperatures.

Particularly interesting results arise in the study of the influence of the agglomeration on the effective heat conductivity coefficient k_{eff}. Our investigation shows that both decrease and increase of k_{eff} can be achieved. The increase occurs in general for compact agglomerates and the decrease for agglomerates that are only slightly more compact than the initial nonagglomerated composite. We do not investigate in this paper the influence of the agglomeration on the electric conductivity coefficient. In a future paper we intend to explore the potential of agglomeration as a tool to increase the efficiency of thermoelectric devices.

4.6 Acknowledgments

This article was partially supported by Natural Sciences and Engineering Research Council of Canada.

Bibliographie

[1] Hasselman DPH, L. F. Johnson, *moshi J. Compos. Mater.* **21**, 508 (1987).

[2] C.-Wen Nan, R. Birringer, David R. Clarke and H. Gleiter. *J. Appl. Phys.* **81**, 6692 (1997).

[3] J.C. Maxwell, *Treatise on Electricity and Magnetism*, 2nd ed. (Clarendon, Oxford 1881)

[4] R. Peierls , *Ann. Phys.* **395**, 1055 (1929).

[5] J.A. Reissland, *The Physics of Phonons*(John Willey and Sons, London, 1973).

[6] W. Dreyer, H. Struchtrup, *Continuum Mech. Thermodyn.* **5**, 3 (1993)

[7] M. Grmela, G. Lebon, C. Dubois, *Phys. Rev E* **83**, 061134 (2011)

[8] A. J. Minnich and G. Chen, *Appl. Phys. Lett.* **91**, 073105 (2007).

[9] J. Ordonez-Miranda, R. Yang, and J. J. Alvarado-Gil, *Appl. Phys. Lett.* **98**, 23311 (2011).

[10] M. S. Dresselhaus, G. Chen, M. Y. Tang, R. G. Yang, H. Lee, D. Z. Wang, Z. F. Ren, J. P. Fleurial, and P. Gogna,, *Adv. Mater.* **19**, 1043 (2007).

[11] A. Minnich, M. S. Dresselhaus, Z. F. Ren, and G. Chen,, *Energy Environ. Sci.* **2**, 466 (2009).

[12] K. F. Hsu, S. Loo, F. Guo, W. Chen, J. S. Dyck, C. Uher, T. Hogan, E. K. Polychroniadis, and M. G. Kanatzidis, *Science* **303**, 818 (2004).

[13] G. H. Zhu, H. Lee, Y. C. Lan, X. W. Wang, G. Joshi, D. Z. Wang, J. Yang, D. Vashaee, H. Guilbert, A. Pillitteri, M. S. Dresselhaus, G. Chen, and Z. F. Ren, *Phys. Rev. Lett.* **102**, 196803 (2009).

[14] B. Poudel, Q. Hao, Y. Ma, Y. Lan, A. Minnich, B. Yu, X. Yan, D. Wang, A. Muto, D. Vashaee, X. Chen, J. Liu, M. S. Dresselhaus, G. Chen, and Z. F. Ren, *Science* **320**, 634 (2008).

[15] A. I. Boukai, Y. Bunimovich, J. Tahir-Kheli, J. K. Yu, W. A. Goddard III, and J. R. Heath, *Nature* **451**, 168 (2008).

[16] X. W. Wang, H. Lee, Y. C. Lan, G. H. Zhu, G. Joshi, D. Z. Wang, J. Yang, A. J. Muto, M. Y. Tang, J. Klatsky, S. Song, M. S. Dresselhaus, G. Chen and Z. F. Ren, *Appl. Phys. Lett.* **93**, 193121 (2008).

[17] G. Joshi, H. Lee, Y. Lan, X. Wang, G. Zhu, D. Wang, R. W. Gould, D. C. Cuff, M. Y. Tang, M. S. Dresselhaus, G. Chen, and Z. F. Ren, *Nano Lett.* **8**, 4670 (2008).

[18] Chen, G., *Phys. Rev. B.* **57**, 14958 (1998).

[19] G. Chen, *J. Heat Transfer* **118**, 539 (1996).

[20] C. Dames and G. Chen, *J. Appl. Phys.* **95**, 682 (2004).

[21] G. Chen, *Nanoscale Energy Transport and Conversion : A Parallel Treatment of Electrons, Molecules, Phonons, and Photons : A Parallel Treatment of Electrons, Molecules, Phonons, and Photons* (Oxford University Press, Oxford, New York, 2005).

[22] M.-S. Jeng, R. Yang, D. Song, and G. Chen, *J. Heat Transfer* **130**, 042410 (2008).

[23] T. Zeng and G. Chen, *J. Heat Transfer* **123**, 340 (2001).

[24] Y. Zhao, C. Zhu, S. Wang, J. Z. Tian, D. J. Yang, C. K. Chen, H. Cheng and P. Hing, *J. Appl. Phys.* **96**, 4563 (2004).

[25] H. M. Duong, N. Yamamoto,K. Bui,D. V. Papavassiliou, S. Maruyama, and B. L. Wardle, *J. Phys. Chem. C* **114**, 8851 (2010).

[26] R. Kochetov and A. V. Korobko and T. Andritsch and P. H. F. Morshuis and S. J. Picken and J. J. Smit, *J. Phys. D-Appl. Phys* **44**, 395401 (2011).

[27] J. Callaway, *J. Phys. Rev.* **113**,1046 (1959).

[28] N. Mingo, L. Yang, D. Li and A. Majumdar, *Nano Lett.* **3**,1713 (2003).

[29] C. J. Glassbrenner and G. A. Slack, *Phys. Rev.* **134**, A1058 (1964).

[30] K. Kádas, L. Vitos and R. Ahuja, *Appl. Phys. Lett.* **92**, 052505 (2008).

[31] Q. Hao, G. Zhu, G. Joshi, X. Wang, A. Minnich, Z. Ren and G. Chen, *Appl. Phys. Lett.* **97**, 063109 (2010).

[32] R, Yang, G. Chen and M. S. Dresselhaus, *Phys. Rev. B.* **72**, 125418 (2005).

CHAPTER 5

ARTICLE2 : Effective heat conduction in dispersion of wires

A. Behrang, M. Grmela, C. Dubois, S. Turenne, P. G. Lafleur and G. Lebon

Applied Physics Letters, 2014 Vol. 104, pp 063106

Abstract

We derive a formula for the heat conductivity coefficient of dispersions of wires in a homogeneous matrix. Such formula is particularly useful for thermoelectric applications. The method used to derive this type of formula in [A. Behrang, M. Grmela, C. Dubois, S. Turenne, P. Lafleur , J. Appl. Phys., **114**, 014305 (2013)] for spherical particles is adapted to generally oriented wires of a finite length. Both diffuse and specular scattering on the wire-matrix interface is considered. The results obtained previously from numerical solutions of the phonon kinetic equation under the assumption of diffuse scattering agree with predictions based on the formula.

The overall heat conductivity coefficient, k, of a dispersion of particles in a homogeneous matrix depends on the following factors :

(i) The factors determining heat conductivity of particles and the matrix when they are separated one from the other. We denote them by the symbols $bulk_p$ and $bulk_m$ addressing respectively the bulk of the particles and the matrix.

(ii) The volume fraction of particles, ϕ.

(iii) The temperature, T.

(iv) The shape of the particles (denoted *shape*).

(v) The way the particles are dispersed and oriented (denoted *dispersion*).

(vi) The matrix-particle interface (denoted *interface*).

Our objective in this paper is to derive a formula

$$k = k(bulk_p,\, bulk_m,\, T, \phi,\, shape,\, dispersion,\, interface) \tag{5.1}$$

for a dispersion of fibers in a homogeneous matrix.

There are essentially three routes that can be taken in such investigation.

Route 1 : Maxwell's homogenization. On this route one begins and remains in the setting of the classical Fourier heat conduction theory. The passage from a heterogeneous to an effective homogeneous medium has been worked out by Maxwell in Ref. [1] (in the context of electric conductivity) and by Nan et al. (using an alternative approach) in Ref. [2]. The bulk properties are represented on this route by the bulk heat conductivity coefficients (i.e. $bulk_p = k_p$, $bulk_m = k_m$). The temperature dependence enters (5.1) only through the temperature dependence of k_p and k_m. The shapes for which the formula (5.1) has been worked out include ellipsoids, wires and flat plates. The particles are assumed to be distributed homogeneously and if their shape is not isotropic then all have the same orientation. Certain types of inhomogeneous distributions of isotropic particles can be however considered. For example, let isotropic particles be dispersed in the form of a homogeneous distribution of agglomerates (i.e. regions with higher volume fraction ϕ). To investigate this type of dispersion we make the homogenization in two steps : first we homogenize inside the agglomerates and then we homogenize the homogeneous dispersion of the agglomerates (see Ref. [3]). As for the influence of the interface, this factor is represented in (5.1) by one scalar parameter (denoted usually by the symbol α) that involves the Kapitza radius (see more in Ref. [2]).

The formula (5.1) obtained in this way is applicable to dispersions in which the particle dimensions are sufficiently large (larger than the phonon mean free path).

Route 2 : Mesoscopic analysis. When the size of particles is smaller than the phonon

mean free path then the investigation has to be conducted in a setting that is more microscopic (mesoscopic) than the setting of the Fourier theory. It can be for example the setting of the Boltzmann-Peirels kinetic theory of phonons (see Ref. [4]) or the setting of various phonon hydrodynamic theories as for instance the Cattaneo or the Guyer-Krumhansl theories used in the investigation presented in Refs. [5, 6]. The bulk properties are represented on this route in the material parameters entering the mesoscopic theories. The more microscopic viewpoint makes it possible to investigate details of the temperature, the shape, and the interface dependence of the heat transfer that are beyond the reach of the classical Fourier theory. The main problem in this approach is that the microscopic information needed as the input of the analysis is usually difficult to acquire and that the mathematical formulation is complex. The passage from the governing equations to predictions of the effective heat conductivity coefficient k involves complex numerical analysis of partial differential equations.

Route 3 : Maxwell's homogenization followed by a mesoscopic analysis. The question arises as to whether the passage from dispersions of large particles to dispersions of nano particles can also be achieved by a mesoscopic adaptation of the Maxwell homogenization. Minnich et Chen have suggested in Ref. [7] to apply the mesoscopic setting only after making the Maxwell homogenization. The factors $bulk_p$, $bulk_m$, $interface$ entering the Maxwell formula (5.1) are subsequently investigated and expressed in Ref. [7] in the settings of the kinetic theory of phonons. The advantage of this combined approach is that the final outcome is still a closed form formula of the type of (5.1) and complex numerical analysis is not needed. Our goal in this paper is to extend this type of investigation made in Ref. [3] for spherical particles to wires.

We begin by considering dispersions of wires of infinite length that are all aligned in one direction. The formulas arising in the Maxwell homogenization for such dispersions (without taking into account the influence of the interface, or in other words, for the so called perfect

interface - see Ref. [2]) are :

$$k^{\perp} = k_m \frac{k_p + k_m + \phi(k_p - k_m)}{k_p + k_m - \phi(k_p - k_m)}$$
$$k^{\parallel} = (1-\phi)k_m + \phi k_p \tag{5.2}$$

where the superscript $\perp$ (resp. $\parallel$) denotes that the direction of the heat flux is perpendicular (resp. parallel) to the direction of the wires. Now we want to adapt this formulas to nanowires. We follow closely the physical considerations that we have made in the adaptation from spheres to nanospheres in Ref. [3].

We leave the Fourier theory and continue in the setting of the phonon kinetic theory. We express in this mesoscopic setting the bulk heat conductivity coefficients k_p and k_m appearing in (5.2). In this analysis we shall consider the influence of the interface, shape, and also a general orientation of nanowires and the heat flux. As for the interface, we consider two types of phonon scattering : specular and diffuse. We introduce a phenomenological parameter $0 \leq s \leq 1$ having the physical interpretation of the probability of the specular scattering of phonons on the particle-matrix interface. Regarding the shape of the particles, we consider only wires of the radius a_p and length L. In the case of the general orientation of the wires and heat flux, we denote the angle between the two orientation by the symbol θ. The overall heat conductivity coefficient as well as the bulk heat conductivity coefficients k_p and k_m become now functions of the four parameters (s, L, a_p, θ) :

$$\begin{aligned} k(s, L, a_p, \theta) &= s \left[k^{(\parallel, spec)}(s, L, a_p, \theta) \cos^2\theta \right. \\ &\left. + k^{(\perp, spec)}(s, L, a_p, \theta) \sin^2\theta \right] \\ &+ (1-s) \left[k^{(\parallel, diff)}(s, L, a_p, \theta) \cos^2\theta \right. \\ &\left. + k^{(\perp, diff)}(s, L, a_p, \theta) \sin^2\theta \right] \end{aligned} \tag{5.3}$$

We recall that in the previous investigations reported in Refs. [8–10] the length L is infinite,

phonon interface scattering is totally diffuse (i.e. $s = 0$), and θ is only either zero or $\pi/2$.

What remains is to express $k^{(i,j)}$ ($i = \|, \perp$ refers to the Maxwell formulas (5.2), and $j = spec, diff$) appearing in (5.3) in the setting of the phonon kinetic theory. The bulk heat conductivity coefficients entering these formulas take the form (see Refs. [7, 11])

$$\begin{aligned} k_l^{(j)}(s, L, a_p, \theta) &= \frac{1}{3}\int C(\omega)v(\omega)\Lambda_l^{(j)}(\omega, s, L, a_p, \theta))d\omega \\ &\approx \frac{1}{3}Cv\Lambda_l^{(j)}(s, L, a_p, \theta) \quad j = spec,\ diff,\ \ l = m, p \end{aligned} \tag{5.4}$$

where ω is the phonon frequency, C denotes the volumetric specific heat capacity per unit frequency at the frequency ω, v the phonon group velocity, and Λ the phonon bulk mean free path. By using Matthiessen's rule, we express Λ in terms of the bulk Λ_b, the collision Λ_{coll}, and the thermal boundary resistance Λ_{TBR} mean free paths :

$$\Lambda^{-1} = \Lambda_b^{-1} + \Lambda_{coll}^{-1} + \Lambda_{TBR}^{-1} \tag{5.5}$$

We now investigate the mean free paths for the matrix and then for the particles.

First, we turn to the matrix. The bulk mean free path $\Lambda_{b,m}$ for the matrix is a material parameter (it remains the same for the specular and the diffuse scattering) in which the individual features of the matrix are expressed in the phonon kinetic theory.

In the collision mean free path Λ_{coll}, we shall make no distinction between specular and diffuse scattering but we let it depend on the parameter s. We thus use $\Lambda_{coll}^{(spec)} = \Lambda_{coll}^{(diff)} = \Lambda_{coll}(s)$, where

$$\frac{1}{\Lambda_{coll}(s)} = \phi\frac{1-s}{1+s}\left(\frac{1}{\Xi^{(\perp)}} + \frac{1}{\Xi^{(\|)}}\right) \tag{5.6}$$

with $1/\Xi^{(\|)} = (1/L + 2\zeta/(\pi a_p))\cos\theta$ and $1/\Xi^{(\perp)} = 2\sin\theta/(\pi a_p)$ denoting characteristic lengths of the nanowires of length L and angle θ with respect to the heat flux direction ($\theta = 0$ when all of nanowires are aligned in heat flow direction and $\theta = \pi/2$ for nanowires

perpendicular to heat flow). By multiplying the characteristic length by $\frac{1+s}{1-s}$ we obtain an effective characteristic length. By the symbol ζ we denote the probability of the phonon-wire scattering when phonon travels in the longitudinal direction : $\zeta = \sqrt{\phi}/(\sqrt{\phi}+1)$.

We now turn to the thermal boundary resistance mean free path Λ_{TBR}. We write it in the form

$$\frac{1}{\Lambda_{TBR}^{(j)}} = \frac{\phi}{\Gamma^{(j)}}\left(\frac{1}{\Xi^{(\perp)}} + \frac{1}{\Xi^{(\parallel)}}\right), \;\; j = spec, \;\; diff \tag{5.7}$$

where $\Gamma^{(diff)} = \frac{3t_{mp}^{(diff)}}{4(1-\frac{1}{2}(t_{mp}^{(diff)}+t_{pm}^{(diff)}))}$ and $\Gamma^{(spec)} = \frac{3\int_0^{\mu_{crit}} t_{mp}^{(spec)}(\mu_m)\mu_m d\mu_m}{2(1-\int_0^{\mu_{crit}} t_{mp}^{(spec)}(\mu_m)\mu_m d\mu_m - \int_0^{\mu_{crit}} t_{pm}^{(spec)}(\mu_p)\mu_p d\mu_p)}$. By the symbols t_{mp} and t_{pm} we denote probabilities of transmission from matrix "m" to particles "p" and vis-versa. Explicit expressions for these quantities in both specular and diffuse transmissions are given in Ref. [3].

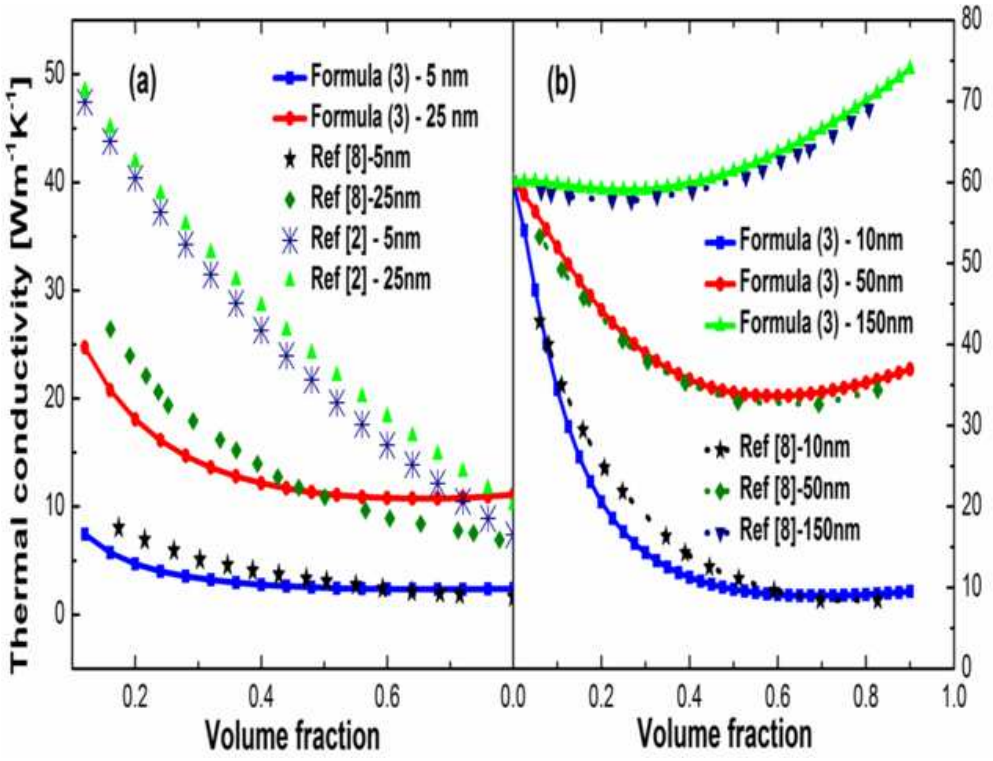

Figure 5.1 (Color online) Influence of the radius of wires a_p and the volume fraction ϕ on : (a) transverse thermal conductivity $k^{\perp}$, (b) longitudinal thermal conductivity $k^{\parallel}$ of $SiGe$ nanocomposite.

Next, we discuss the particles. Following Refs. [3, 8], we take $\Lambda_{TBR}^{-1} = 0$ and

$$\Lambda^{(\perp)} = \Lambda_{b,p}\left(\frac{a_p(s)/\Lambda_{b,p}}{a_p(s)/\Lambda_{b,p}+1}\right) \tag{5.8}$$

where $\Lambda_{b,p}$ is the material parameter in which the individual features of the particles are expressed in the phonon kinetic theory, $a_p(s) = a_p\frac{1+s}{1-s}$ is the effective wire radius.

As for $\Lambda^{(\|)}$, we write it (following Ref. [12]) in the form

$$\frac{1}{\Lambda^{(\|)}(L)} = \frac{1}{\Lambda^{(\|)}}\left(1+\frac{\Lambda^{(\|)}}{2L(s)}\right) \tag{5.9}$$

where $L(s) = L\frac{1+s}{1-s}$, $\Lambda^{(\|)} = \Lambda_{b,p}\times[1-\frac{12}{\pi}\int_0^1(1-x^2)^{0.5}B_4(\frac{2a_p(s)x}{\Lambda_{b,p}})dx]$ is the effective longitudinal mean free path for a infinite nanowire; $B_4(x) = \int_0^{\pi/2}\exp[\frac{-x}{\sin\theta}]\cos^2\theta\sin\theta d\theta$ [9]. When the angle between the orientation of wires and the heat flux is θ, then (5.8) and (5.9) combine to give

$$\Lambda(a_p, L, \theta) = \Lambda^{(\|)}(L)\cos^2\theta + \Lambda^{(\perp)}\sin^2\theta \tag{5.10}$$

The formula (5.3) for the effective heat conductivity of suspensions of wires is now complete. The material parameters entering it are :

$$C_m, C_p, v_m, v_p, \Lambda_{b,m}, \Lambda_{b,p}, a_p, L, \theta, s, \phi, T \tag{5.11}$$

If the length, L, and the orientation, θ, of the dispersed particles is not fixed but instead we know the distribution functions $f(\theta)$ and $f(L)$ then the heat conduction coefficient is obtained by averaging.

As a case study, we apply the formula (5.3) to two-dimensional $SiGe$ nanodispersion with Si nanowires aligned in the direction of the heat flux embedded in Ge matrix. This dispersion has been extensively studied in Si-based applications such as high efficiency thermoelectric materials. We use the same material parameters as the ones used in Ref. [8] (namely : $C_m = 0.87\times10^6, C_p = 0.93\times10^6 Jm^{-3}K^{-1}, v_m = 1042, v_p = 1804ms^{-1}, \Lambda_m = 198.6, \Lambda_p = 268.2nm$)

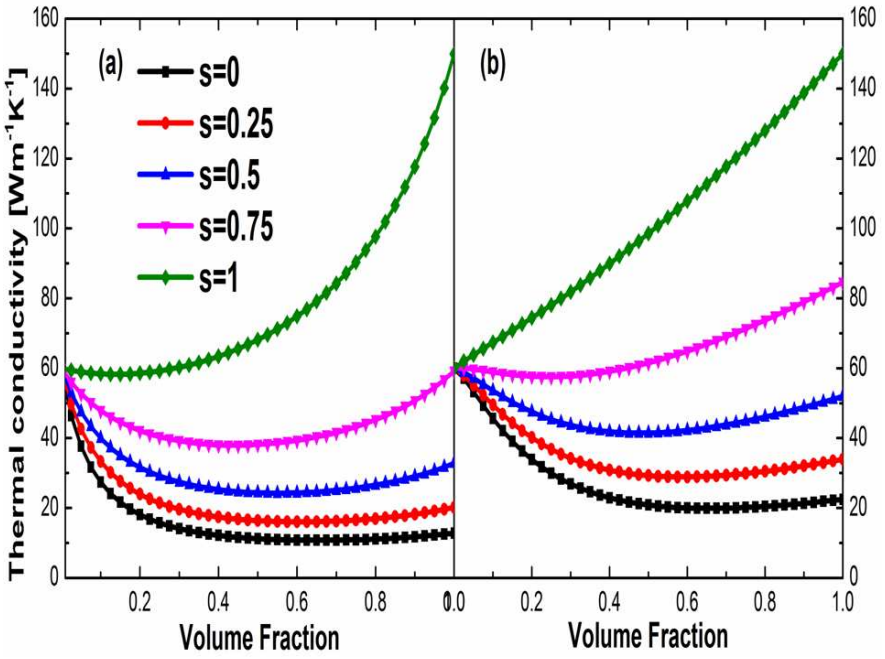

Figure 5.2 (Color online) Influence of the interface specularity parameter s and the volume fraction ϕ on : (a) $k^{\perp}$, (b) $k^{\parallel}$ of $SiGe$ nanocomposites ; Si wires are long ($L \to \infty$) and their radius $a_p = 25nm$.

and compare our results with results obtained by taking the mesoscopic Route 2 (i.e. with results based on numerical solutions of the Boltzmann kinetic equation) presented in Ref. [8].

Figure 5.1(a,b) depicts the dependence of the longitudinal and the transverse thermal conductivities of the dispersion of Si wires in Ge matrix on the size and the volume fraction of the wires. This figure illustrates that predictions based on the formula (5.3) (in which we consider only the totally diffuse interface scattering) essentially coincide with predictions based on numerical solutions of the phonon kinetic equation presented in Ref. [8]. We note that for a fixed volume fraction ϕ, the effective longitudinal thermal conductivity decreases with decreasing the radius a_p of the wires. Indeed, when a_p decreases and $\phi = const.$ then the effective area of the wire-matrix interface increases and the phonon-interface scattering plays more important role in hindering the passage of phonons. When the volume fraction increases we see two different scenarios. For small wire radius, the heat conductivity decreases as the volume fraction increases (due to the enlargement of the wire-matrix interface) while for

larger wire radius the heat conductivity increases as the volume fraction increases (due to the reduction of the wire-matrix interface). We also note that the influence of phonon-interface scattering decreases as the wire radius increases and $1/\Lambda_{coll}, 1/\Lambda_{TBR} \to 0$. Then, the principal contribution to the resistance of the phonons comes from phonon-phonon collisions expressed mathematically in the bulk mean free path. Therefore, the thermal conductivities of the matrix and of the dispersed phase tend to their corresponding bulk thermal conductivities. Since the bulk thermal conductivity of silicon (the dispersed phase) is higher than germanium (the matrix phase), we expect an increase on the thermal conductivity as the volume fraction increases. We thus conclude that if in applications we aim at low thermal conductivity then we should use thin nano-size wires and high volume fractions. In the opposite case, if we need to disperse the heat, wires of larger radius are recommended.

Comparison between predictions based on the formula (5.3) for the thermal conductivity in $\perp$ direction with those based on numerical solutions of the phonon kinetic equation is depicted in Figure 5.1(a). Again, our results are in good agreement with results based on numerical solution of the Boltzmann transport equation especially at small wire radius. We note that the dependence on the wire radius and the volume fraction is qualitatively the same as for the longitudinal thermal conductivity.

In the next step we examine influence of the type of the phonon-interface scattering. We recall that only one type of scattering, namely diffuse scattering, was previously investigated in Refs. [7, 9, 10]. With the formula (5.3) we are in position to include into the investigation also the specular scattering that, as it has been suggested in Ref. [13], may possibly play an important role. Figure 5.2(a,b) shows the influence of the specular parameter s (we recall that $0 \leq s \leq 1$ and if $s = 0$ the scattering is totally diffuse) of interface on the longitudinal and transverse thermal conductivities of dispersions with long silicon nanowires. The thermal conductivity in both longitudinal and transverse directions increases with increasing the specularity of interface. We see that the higher is the specularity parameter s, the lower is the phonon confinement at the interface and consequently the larger is the thermal conductivity.

When the specularity parameter s increases the phonon confinement at the interface decreases and consequently the thermal conductivity of the dispersion increases in both directions.

In Figure 5.3(a), the influence of nanowire length on the longitudinal thermal conductivity of dispersion is qualitatively illustrated. Our results show that for all volume fractions the longitudinal thermal conductivity of dispersions increases with L and approaches a plateau at larger lengths. We note that the plateau corresponds to the value of k for nanowires of infinite length. Obviously, the longitudinal thermal conductivity decreases with increasing the volume fraction of silicon nanowire due to relative enhancement in phonon-interface scattering.

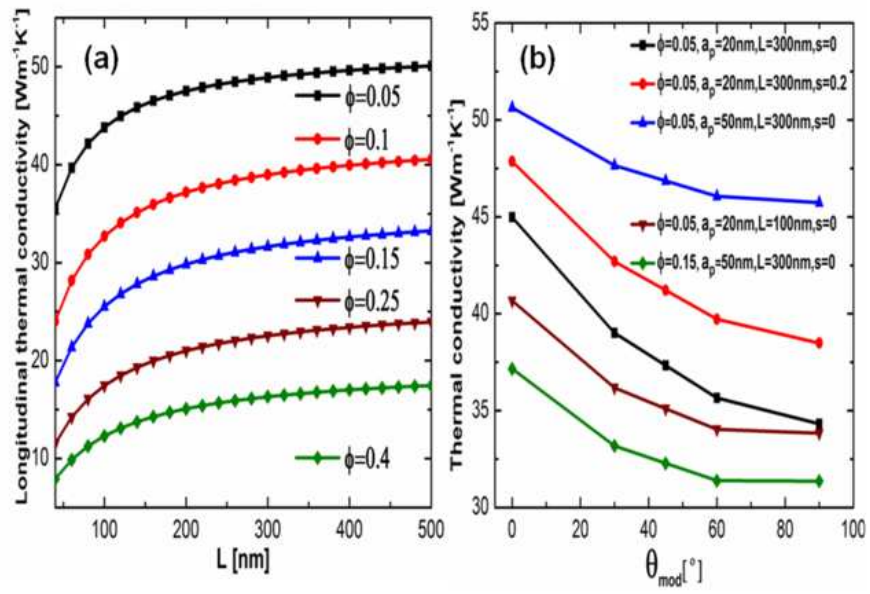

Figure 5.3 (Color online) (a)Influence of the length of wires L and volume fraction ϕ on thermal conductivity ($k^{\|}$) of $SiGe$ dispersion; the radius $a_p = 20nm$. (b) Influence of the nanowire orientation distribution $f(\theta)$ on the thermal conductivity of dispersions.

In Figure 5.3(b), we show the role of the nanowire orientation on the thermal conductivity. As an illustration, we take the orientation distribution function $f(\theta)$ used in Ref. [14] :

$$f(\theta) = \frac{(\sin\theta)^{2p-1}(\cos\theta)^{2q-1}}{\int_{\theta_{min}}^{\theta_{max}}(\sin\theta)^{2p-1}(\cos\theta)^{2q-1}d\theta} \tag{5.12}$$

where p and q are the shape parameters. We note that when $p = q = 1$ then the most probable

orientation angle $\theta_{mod} = \pi/4$; $p = 1$ and $q > 1$, $\theta_{mod} < \pi/4$; $p > 1$ and $q = 1$, $\theta_{mod} > \pi/4$; when $p = 1/2$, $\theta_{mod} = 0$; $q = 1/2$, $\theta_{mod} = \pi/2$. The nanowires are distributed randomly if $p = q = 1/2$. In Figure 5.3(b) we see that the thermal conductivity of nanodispersions increases as the angle of the orientation of the most probable nanowire shifts from $\theta_{mod} = \pi/2$ toward $\theta_{mod} = 0$. This is due to a decrease of the effective area for phonon-interface scattering. We also observe that the thermal conductivity increases if either the specularity parameter s or the size of the wire increase. Depending on the size of the wire and on s, the parameter β defined by $\beta = (k^{\parallel} - k^{\perp})/k^{\parallel} \times 100$ is about $10 - 24\%$; lower β corresponds to nanodispersions with larger sizes of the nanowires. The parameter β could be made larger by changing the size and volume fraction of nanowires (e.g. $\beta \approx 42\%$ for $\phi = 0.1, a_p = 10nm, L = 300nm$ and $s = 0$).

The investigation presented in this paper is a part of the larger investigation whose objective is to increase efficiency of thermoelectric devices. Such efficiency is measured by the parameter $ZT = \frac{S^2\sigma T}{k}$, where S is the Seebeck coefficient, σ the electrical conductivity coefficient, T the absolute temperature, k the thermal conductivity coefficient[15–17].

The formula for k presented in this paper has the advantage of being simple (no numerical solution of partial differential equations are needed), and of taking into account : (i) details of the phonon scattering on the wire-matrix interface (both diffuse and specular scattering are considered), (ii) finite length and general orientation of the wires.

This article was partially supported by Natural Sciences and Engineering Research Council of Canada.

Bibliographie

[1] J.C. Maxwell, *Treatise on Electricity and Magnetism*, 2nd ed. (Clarendon, Oxford 1881)

[2] C.-Wen Nan, R. Birringer, David R. Clarke and H. Gleiter. *J. Appl. Phys.* **81**, 6692 (1997).

[3] A. Behrang, M. Grmela, C. Dubois, S. Turenne, and P. G. Lafleur, *J. Appl. Phys.*, **114**, 014305 (2013).

[4] R. Peierls, Z. Kinetischem, *Ann. Phys.* **3**, 1025 (1929).

[5] A. Sellitto, F. X. Alvarez and D. Jou, *J. Appl. Phys.*, **109**, 064317 (2011).

[6] F. X. Alvarez, D. Jou and A. Sellitto, *J. Heat Transfer*, **133**, 022402 (2010).

[7] A. J. Minnich and G. Chen, *Appl. Phys. Lett.*, **91**, 073105 (2007).

[8] R, Yang, G. Chen and M. S. Dresselhaus, *Phys. Rev. B.*, **72**, 125418 (2005).

[9] R. Prasher, *J. Appl. Phys.*, **100**, 034307 (2006).

[10] X. L*ü*, *J. Appl. Phys.*, **106**, 064305 (2009).

[11] J. Ordonez-Miranda, R. Yang, and J. J. Alvarado-Gil, *Appl. Phys. Lett.* **98**, 23311 (2011).

[12] E. S. Landry M. I. Hussein, A. J. H and McGaughey, *Phys. Rev. B.*, **77**, 184302 (2008).

[13] Chen, G., *Phys. Rev. B.* **57**, 14958 (1998).

[14] Shao-Yun Fu, B. Lauke, *Compos. Sci. Technol.*, **56**, 1179 (1996).

[15] M. S. Dresselhaus, G. Chen, M. Y. Tang, R. G. Yang, H. Lee, D. Z. Wang, Z. F. Ren, J. P. Fleurial, and P. Gogna,, *Adv. Mater.* **19**, 1043 (2007).

[16] A. Minnich, M. S. Dresselhaus, Z. F. Ren, and G. Chen„ *Energy Environ. Sci.* **2**, 466 (2009).

[17] A. I. Boukai, Y. Bunimovich, J. Tahir-Kheli, J. K. Yu, W. A. Goddard III, and J. R. Heath, *Nature* **451**, 168 (2008).

CHAPTER 6

ARTICLE3 : Effective heat conduction in hybrid sphere & wire nanodispersions

A. Behrang, M. Grmela, C. Dubois, S. Turenne, P. G. Lafleur and G. Lebon

Applied Physics Letters, 2014 Vol. 104, pp 233111

Abstract

Heat conductivity of dispersions can be modified by varying shapes of dispersed particles and also by making hybrid dispersions containing particles of different shapes and sizes. Spheres and their agglomerates that we have investigated previously are replaced in this paper by spheres and wires. The method used to derive the formulas for the overall effective heat conductivity is based on the Maxwell homogenization (adapted to hybrid dispersions) followed by a mesoscopic analysis in which heat transfer is regarded as transport of phonons. The mesoscopic formulation provides then also a setting for investigation the role of particle-matrix nanoscale interfaces.

Electric and thermal conductivity of materials used in the fabrication of electronic devices have a large influence on their overall efficiency. In this paper we concentrate on the thermal conductivity and investigate theoretically its changes caused by dispersing nano-size particles into a homogeneous matrix. In Refs. [1, 2] we have conducted such investigation for disper-

sions of spherical particles and wires respectively. In Ref. [1] we have also explored hybrid particle-agglomerate dispersions. The sensitive dependence of the thermal conductivity on the composition of the hybrid dispersion seen in this study motivates us to investigate also other types of hybrid dispersions. In this paper the dispersed particles are spheres and wires. As in Refs. [1, 2], we begin with Maxwell's homogenization (see Refs. [3, 4]) but we need to adapt it to hybrid dispersions. We make two types of adaptation : one developed in Refs. [1, 2] in the context of dispersions with agglomerates (we call it *Hybrid I*), and the other, called *Hybrid II*, developed in Ref. [16]. Subsequently, due to the nanometric size of the dispersed particles, we introduce (following Refs. [1, 2, 6]) into the analysis the microscopic (phonon) viewpoint of the heat transport. The effective heat conductivity coefficients of dispersions arise in our investigation in the form of closed formulas that are easily evaluated.

In the context of the Fourier heat conduction theory, the effective thermal conductivity coefficient k_{eff} of a dispersion composed of a matrix in which particles of a single shape and size are distributed is given by the formula (see Refs. [3, 4], and Refs. [5, 7])

$$k_{eff} = \frac{\sum\limits_{i=m,p} k_i \phi_i \frac{\gamma\beta}{(\gamma-1)\beta+k_i}}{\sum\limits_{i=m,p} \phi_i \frac{\gamma\beta}{(\gamma-1)\beta+k_i}} \tag{6.1}$$

where ϕ is the volume fraction, k is the thermal conductivity, and subscripts "m" and "p" stand for matrix and dispersed phases respectively. We shall use hereafter particles of two shapes : spheres (denoted by the subscript "sph"), and wires (denoted by the subscript "w") Depending on the shape of the dispersed particles, the parameters γ and β take different values. Namely : $\gamma = 3$ and $\beta = k_m$ for spheres, $\gamma \to \infty$ or $\beta = k_i$ for wires oriented in the direction of the heat flow (denoted by $\|$), and $\gamma = 2$ and $\beta = k_m$ for wires oriented in the direction that is perpendicular to the heat flow (denoted by $\perp$) (see Ref. [5]).

In this paper we explore heat conduction in hybrid dispersions composed of a matrix in which particles having the shape of both spheres and wires are uniformly distributed. The formula (6.1) has to be therefore extended to this more general situation. There are in fact

many ways to do it. We shall follow two routes (denoted *(Hybrid I)* and *(Hybrid II)*) and compare the results. We shall see at the end that the values of the effective heat conductivity coefficients k_{eff} obtained on both routes remain very close. Next, we describe the routes *(Hybrid I)* and *(Hybrid II)*.

(Hybrid I)extension of (6.1). On this route we follow the method introduced in Ref. [1] to investigate heat conductivity in hybrid spherical-particle&agglomerate dispersions. This method, if adapted to the hybrid sphere&wire dispersions, consists of the following two steps. First, we homogenize (by following Ref. [1]) the matrix and the spheres. We obtain in this way a new matrix that we denote (m&sph). In the second step we homogenize (by following Ref. [2]) this new matrix and the wires. This then results in a homogeneous material ((m&sph)&w). Of course, we can also begin with the wires and then include the spheres to obtain another homogeneous material ((m&w)&sph). It has been shown in Ref. [1] that the effective heat conductivity coefficients do not change much by changing the order of the homogenization. When presenting the results in Section , we shall always present the average $k_{(m\&sph\&w)} = \frac{\phi_p^{(sph)}}{\phi_p^{(sph)}+\phi_p^{(w)}} k_{((m\&sph)\&w)} + \frac{\phi_p^{(w)}}{\phi_p^{(sph)}+\phi_p^{(w)}} k_{((m\&w)\&sph)}$ and the average of the difference between the results obtained in the two homogenizations ((m&sph)&w) and ((m&w)&sph). The difference between $k_{((m\&sph)\&w)}$ and $k_{((m\&w)\&sph)}$ is presented in the results in one number $\eta = (\int (k_{((m\&sph)\&w))}(x) - k_{((m\&w)\&sph)}(x))^2 dx / \int dx)^{1/2}$ where x is the $x-axis$ of the graphs.

(Hybrid II)extension of (6.1). On this route we follow Ref. [5]. We briefly recall this method and adapt it to the dispersion under investigation. We assume a homogeneous matrix with two dispersed phases of wires and spheres. It is assumed that the matrix phase is to be divided between the two dispersions with a volume fraction Δ_m belonged to the dispersion of wires and $1-\Delta_m$ belonged to the dispersion of spheres. By considering the role of Δ_m, it is assumed that the effective thermal conductivity k_{eff} of the hybrid dispersion of particles in the shape of sphere and wires is identical to the effective thermal conductivities of dispersions of particles of the shape "$j = sph, w$".

We now proceed to specify separately the effective thermal conductivity of the hybrid

dispersion of wires and spheres for the wires oriented in the direction of the heat flow (" $\parallel$ ") and the wires oriented in the direction that is perpendicular to the heat flow (" $\perp$ "). The appropriate form of the Eq.(6.1) for dispersions in which wires are oriented in the direction of the heat flow is

$$k_{eff}^{(\parallel)} = \frac{k_m^{(w,\parallel)}(1-\phi_p^{(w)})\Delta_m + k_p^{(w,\parallel)}\phi_p^{(w)}}{(1-\phi_p^{(w)})\Delta_m + \phi_p^{(w)}} \tag{6.2}$$
$$= \frac{k_m^{(sph)}(1-\phi_p^{(sph)})(1-\Delta_m) + k_p^{(sph)}\phi_p^{(sph)}\frac{3k_m^{(sph)}}{2k_m^{(sph)}+k_p^{(sph)}}}{(1-\phi_p^{(sph)})(1-\Delta_m) + \phi_p^{(sph)}\frac{3k_m^{(sph)}}{2k_m^{(sph)}+k_p^{(sph)}}}$$

Now, we specify Δ_m. We assume that the thermal conductivity of the matrix phase in both dispersions of spheres and wires is identical, i.e. $k_m^{(w,l)} = k_m^{(sph)} = k_m^{(l)}, \quad l = \parallel, \perp$. Finally, we obtain

$$\begin{aligned} k_{eff}^{(\parallel)} &= (k_p^{(w,\parallel)}k_p^{(sph)}(\phi_p^{(sph)}-1)\phi_p^{(w)} + k_m^{(\parallel)}(k_p^{(sph)}(1+2\phi_p^{(sph)})(\phi_p^{(w)}-1) + 2k_p^{(w,\parallel)} \\ &\quad (\phi_p^{(sph)}-1)\phi_p^{(w)}) + 2k_m^{2(\parallel)}(\phi_p^{(sph)} - 1 + \phi_p^{(w)} - \phi_p^{(sph)}\phi_p^{(w)}))/(k_p^{(sph)}(\phi_p^{(sph)}-1) + \\ &\quad k_m^{(\parallel)}(-2 + \phi_p^{sph}(3\phi_p^{(w)}-1))) \end{aligned} \tag{6.3}$$

In a similar way we arrive at the effective heat conductivity $k_{eff}^{(\perp)}$ of the hybrid dispersion in which the wires are oriented in the direction that is perpendicular to the direction of the heat flow. In this case Eq.(6.1) takes the form

$$k_{eff}^{(\perp)} = \frac{k_m^{(\perp)}(1-\phi_p^{(w)})\Delta_m^* + k_p^{(w,\perp)}\phi_p^{(w)}\frac{2k_m^{(\perp)}}{k_m^{(\perp)}+k_p^{(w,\perp)}}}{(1-\phi_p^{(w)})\Delta_m^* + \phi_p^{(w)}\frac{2k_m^{(\perp)}}{k_m^{(\perp)}+k_p^{(w,\perp)}}} \tag{6.4}$$
$$= \frac{k_m^{(sph)}(1-\phi_p^{(sph)})(1-\Delta_m^*) + k_p^{(sph)}\phi_p^{(sph)}\frac{3k_m^{(sph)}}{2k_m^{(sph)}+k_p^{(sph)}}}{(1-\phi_p^{(sph)})(1-\Delta_m^*) + \phi_p^{(sph)}\frac{3k_m^{(sph)}}{2k_m^{(sph)}+k_p^{(sph)}}}$$

Finally, we arrive at

$$
\begin{aligned}
k_{eff}^{(\perp)} &= -(k_m^{(\perp)}(2k_m^{2(\perp)}(\phi_p^{(sph)}-1)(\phi_p^{(w)}-1)+k_p^{(sph)}k_p^{(w,\perp)}(1+\phi_p^{(sph)}(2-4\phi_p^{(w)}) \qquad (6.5)\\
&\quad +\phi_p^{(w)})+k_m^{(\perp)}(-k_p^{(sph)}(1+2\phi_p^{(sph)})(\phi_p^{(w)}-1)-2k_p^{(w,\perp)}(\phi_p^{(sph)}-1)\\
&\quad (1+\phi_p^{(w)}))))/(k_p^{(sph)}k_p^{(w,\perp)}(\phi_p^{(sph)}-1+\phi_p^{(w)}-\phi_p^{(sph)}\phi_p^{(w)})+k_m^{(\perp)}(k_p^{(w,\perp)}\\
&\quad (2+\phi_p^{(sph)})(\phi_p^{(w)}-1)+k_p^{(sph)}(\phi_p^{(sph)}-1)(1+\phi_p^{(w)}))+k_m^{2(w,\perp)}(-2(1+\phi_p^{(w)})\\
&\quad +\phi_p^{(sph)}(5\phi_p^{(w)}-1)))
\end{aligned}
$$

In order to be able to apply the formulas (6.3) and (6.5) to nanodispersions (where the particle size is comparable to the phonon mean free path), we have to modify them. Following Refs. [1, 2, 6], we make the modification by expressing the bulk heat conductivity coefficients $k_i^{(j)}$, where $i = m, p$ and $j = sph, w$, appearing in (6.3) and (6.5) in the form in which they arise in the phonon kinetic theory. In these expressions we then take into consideration the specificity of interactions of the phonons with the matrix-particle interface. Importance of such interactions in the heat conduction has also been revealed in microscopic *ab initio* calculations in Refs. [8–13].

In this paper we follow the extension of the formulas arising in the Maxwell homogenization to formulas involving quantities characterizing propagation of phonons developed in Refs. [1, 2]. Adaptation of the extension to the hybrid dispersion is straightforward. We therefore recall only the essential steps.

The nanospheres in the dispersion have radius $a_p^{(sph)}$ and the nanowires have length $L^{(w)}$ and radius $a_p^{(w)}$. Let $\theta^{(w)}$ be the angle between the direction of the wire and the direction of the heat flux (note that $\theta^{(w)} = 0$ if all the nanowires are aligned in the direction of the heat flow and $\theta^{(w)} = \pi/2$ if the nanowires are aligned in the direction that is perpendicular to the direction of the heat flow).

From the phonon kinetic theory we use the expression

$$
\begin{aligned}
& k_i^{(j,l)}(s^{(j)}, L^{(j)}, a_p^{(j)}, \theta^{(j)}) = \\
& \frac{1}{3}\int C(\omega)v(\omega)\Lambda_i^{(j,l)}(\omega, s^{(j)}, L^{(j)}, a_p^{(j)}, \theta^{(j)})d\omega \\
& \approx \frac{1}{3}Cv\Lambda_i^{(j)}(s^{(j)}, L^{(j)}, a_p^{(j)}, \theta^{(j)}) \\
& i = m,\ p,\quad j = sph,\ w,\ \ l = spec,\ \ diff
\end{aligned}
\tag{6.6}
$$

where ω is the phonon frequency, C denotes the volumetric specific heat capacity per unit frequency at the frequency ω, v the phonon group velocity, and Λ the phonon mean free path. We note that for $j = sph$ in Eq.(6.6), $L^{(sph)}$ and $\theta^{(sph)}$ are not defined. The remaining parameter in Eq.(6.6) is $0 \leq s \leq 1$ which is the probability of the specular scattering of phonons on the particle-matrix interface. We denote the specular (i.e. $s = 1$) and diffuse (i.e. $s = 0$) types of scattering of phonons at the matrix-particle interface by "$spec$" and "$diff$", respectively.

Next, we find the phonon mean free paths of the matrix and the dispersed phases. By using Matthiessen's rule, we express them in terms of the bulk phonon mean free paths Λ_b, the phonon mean free path Λ_{coll} addressing the collisions of the phonons on the interface, and the thermal boundary resistance phonon mean free path Λ_{TBR} :

$$
\Lambda^{-1} = \Lambda_b^{-1} + \Lambda_{coll}^{-1} + \Lambda_{TBR}^{-1} \tag{6.7}
$$

In our previous work[1, 2], the collision and the thermal boundary resistance mean free paths in dispersions of wires and spheres have been expressed separately. Now, for the hybrid dispersion of wires and spheres, the phonon mean free path of the matrix is written as follows

$$
\begin{aligned}
\frac{1}{\Lambda_m} \;=\; & \frac{1}{\Lambda_{b,m}} + \phi_p^{(w)}\left(\frac{1-s}{1+s} + \frac{1}{\Gamma^{(w,l)}}\right)\left(\frac{1}{\Xi^{(w,\parallel)}} + \frac{1}{\Xi^{(w,\perp)}}\right) \\
& + \left(\frac{1-s}{1+s} + \frac{1}{\Gamma^{(sph,l)}}\right)\left(\frac{\phi_p^{(sph)}}{\Xi^{(sph)}}\right)
\end{aligned}
\tag{6.8}
$$

Note that $1/\Xi^{(w,\|)} = (1/L + 2\xi/(\pi a_p^{(w)}))\cos\theta^{(w)}$, $1/\Xi^{(w,\perp)} = 2\sin\theta^{(w)}/(\pi a_p^{(w)})$, and $1/\Xi^{(sph)} = 3/(4a_p^{(sph)})$ are the characteristic lengths of nanowires in $\|$, $\perp$ directions to the heat flux and the characteristic length of nanospheres, respectively. By $\xi = \sqrt{\phi_p^{(w)}}/(1+\sqrt{\phi_p^{(w)}})$, we denote the probability of the phonon-wire scattering when phonon travels in the longitudinal direction. The specular and diffuse properties of the particle-matrix interface take the following form $\Gamma^{(j,diff)} = \frac{3t_{mp}^{(diff)}}{4(1-\frac{1}{2}(t_{mp}^{(diff)}+t_{pm}^{(diff)}))}$ and $\Gamma^{(j,spec)} = \frac{3\int_0^{\mu_{crit}} t_{mp}^{(spec)}(\mu_m)\mu_m d\mu_m}{2(1-\int_0^{\mu_{crit}} t_{mp}^{(spec)}(\mu_m)\mu_m d\mu_m - \int_0^{\mu_{crit}} t_{pm}^{(spec)}(\mu_p)\mu_p d\mu_p)}$, $j = w,\ sph$. By the symbols t_{mp} and t_{pm} we denote probabilities of the transmission from matrix "m" to particles "p" and vis-versa. Explicit expressions for these quantities in both specular and diffuse transmissions are given in Ref. [1].

Next, we turn our attention to the mean free paths of the dispersed phases.

For the wires we have $\frac{1}{\Lambda_p^{(w,\perp)}} = \frac{1}{\Lambda_{b,p}^{(w)}} + \frac{1}{a_p(s)^{(w)}}$ and $\frac{1}{\Lambda_p(L)^{(w,\|)}} = \frac{1}{\Lambda_p^{(w,\|)}} + \frac{1}{2L(s)}$[14], where $L(s) = L\frac{1+s}{1-s}$ is the effective wire length, $\Lambda_p^{(w,\|)} = \Lambda_{b,p}^{(w)} \times [1 - \frac{12}{\pi}\int_0^1 (1-x^2)^{0.5} B_4(\frac{2a_p^{(w)}(s)x}{\Lambda_{b,p}^{(w)}})dx]$ is the effective longitudinal mean free path for a infinite nanowire; $B_4(x) = \int_0^{\pi/2} \exp[\frac{-x}{\sin\theta}]\cos^2\theta\sin\theta d\theta$ [15] and $a_p(s)^{(w)} = a_p^{(w)}\frac{1+s}{1-s}$ is the effective wire radius[16].

For the spheres we have [17] $\frac{1}{\Lambda_p^{(sph)}} = \frac{1}{\Lambda_{b,p}^{(sph)}} + \frac{4}{3a_p(s)^{(sph)}}$.

When the angle between the orientation of wires and the heat flux is $\theta^{(w)}$, then these expressions combine to give $\Lambda_p(a_p^{(w)}, L, \theta^{(w)}) = \Lambda_p^{(w,\|)}(L)\cos^2\theta^{(w)} + \Lambda_p^{(w,\perp)}\sin^2\theta^{(w)}$.

By using (6.6) we arrive at the coefficients of the effective thermal conductivity of each individual phase in the hybrid dispersion of wires and spheres.

Finally, when we take into account the influence of the orientation of wires, the overall heat conductivity coefficient of the hybrid dispersion of wires and spheres takes the form

$$
\begin{aligned}
&k_{eff}(s, L, a_p^{(w)}, a_p^{(sph)}, \theta^{(w)}) = s\left[k_{eff}^{(\|,spec)}(s, L, a_p^{(w)}, a_p^{(sph)}, \theta^{(w)})\cos^2\theta^{(w)}\right.\\
&\left.+k_{eff}^{(\perp,spec)}(s, L, a_p^{(w)}, a_p^{(sph)}, \theta^{(w)})\sin^2\theta^{(w)}\right]\\
&+(1-s)\left[k_{eff}^{(\|,diff)}(s, L, a_p^{(w)}, a_p^{(sph)}, \theta^{(w)})\cos^2\theta^{(w)}\right.\\
&\left.+k_{eff}^{(\perp,diff)}(s, L, a_p^{(w)}, a_p^{(sph)}, \theta^{(w)})\sin^2\theta^{(w)}\right] \qquad (6.9)
\end{aligned}
$$

In order to illustrate expression (6.9), we consider the hybrid dispersion of silicon nano-

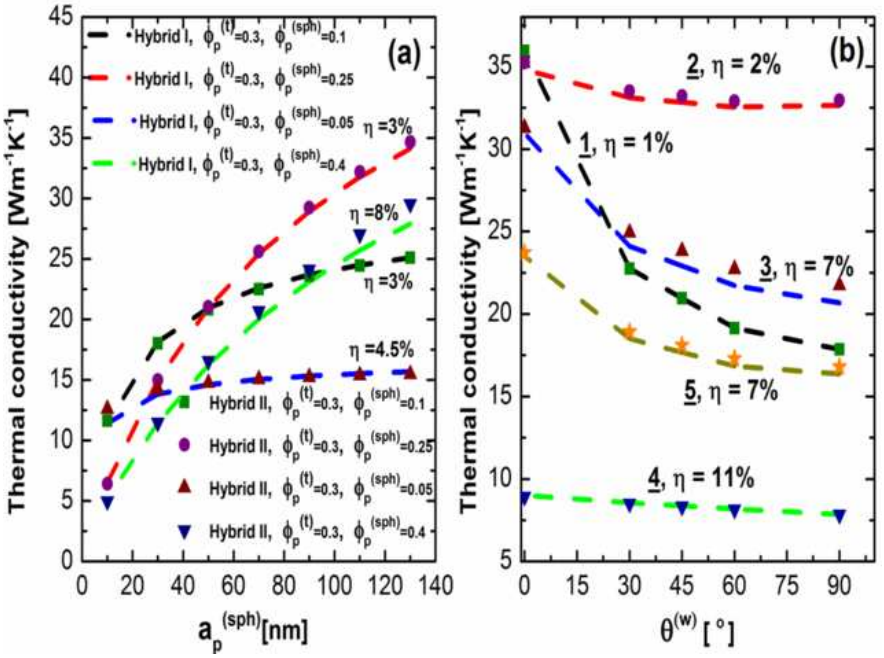

Figure 6.1 (Color online) (a.)Dependence of the diffuse thermal conductivity of the hybrid dispersion on the size of dispersed nanospheres for $\theta^{(w)} = 0$, $a_p^{(w)} = 20nm$ and $L = 300nm$.(b) Influence of the nanowire orientation on the thermal conductivity of hybrid dispersion under totally diffuse interface and $L = 600nm$, 1. $a_p^{(w)} = 10nm$, $a_p^{(sph)} = 100nm$, $\phi^{(t)} = 0.1$ and $\phi^{(w)} = 0.08$, 2. $a_p^{(w)} = 100nm$, $a_p^{(sph)} = 10nm$, $\phi^{(t)} = 0.1$ and $\phi^{(w)} = 0.08$, 3. $a_p^{(w)} = 10nm$, $a_p^{(sph)} = 100nm$, $\phi^{(t)} = 0.25$ and $\phi^{(w)} = 0.05$, 4. $a_p^{(w)} = 100nm$, $a_p^{(sph)} = 10nm$, $\phi^{(t)} = 0.25$ and $\phi^{(w)} = 0.05$, 5. $a_p^{(w)} = 25nm$, $a_p^{(sph)} = 80nm$, $\phi^{(t)} = 0.4$ and $\phi^{(w)} = 0.2$

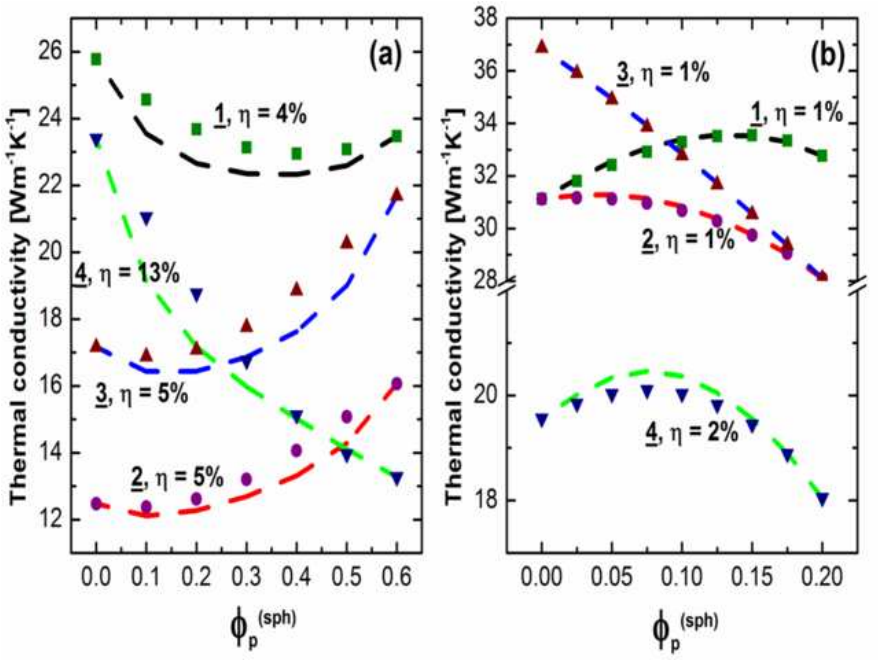

Figure 6.2 (Color online)(a.)Thermal conductivity of the hybrid dispersion of silicon nanowires and spheres in germanium matrix as a function of $\phi_p^{(sph)}$ when $\theta^{(w)} = \pi/4$, $L = 400nm$ and 1. $a_p^{(w)} = 70nm$, $a_p^{(sph)} = 80nm, s = 0$, 2. $a_p^{(w)} = 25nm$, $a_p^{(sph)} = 50nm, s = 0$,3. $a_p^{(w)} = 25nm$, $a_p^{(sph)} = 50nm, s = 0.2$, 4. $a_p^{(w)} = 60nm$, $a_p^{(sph)} = 40nm, s = 0$.(b.)Thermal conductivity of the hybrid dispersion of silicon nanowires and spheres in germanium matrix as a function of $\phi_p^{(sph)}$ when $\theta = 0$, $s = 0$, $L = 600nm$ and 1. $a_p^{(w)} = 25nm$, $a_p^{(sph)} = 80nm$, 2. $a_p^{(w)} = 25nm$, $a_p^{(sph)} = 60nm$,3. $a_p^{(w)} = 40nm$, $a_p^{(sph)} = 60nm$, 4. $a_p^{(w)} = 10nm$, $a_p^{(sph)} = 30nm$

wires and nanospheres in the germanium matrix. This is one of the most promising composition that is widely used in thermoelectric application in which low thermal conductivity is sought[18–20]. Uniform dispersions of only nanospheres[1, 6] or nanowires [2, 8, 9, 15] of Si embedded in Ge have already been extensively studied. Here, we used the same material parameters as in Ref. [8]. Figure (6.1).a shows the diffuse thermal conductivity of the hybrid dispersion ($k_{eff}^{(\|)}, s = 0$) as a function of the size $a_p^{(sph)}$ of the nanosphere silicon particle for different volume fractions. Note that $\phi_p^{(t)} = \phi_p^{(sph)} + \phi_p^{(w)}$ where $\phi_p^{(t)}$ is the total volume fraction of the particle phase. We see that the predicted results from $Hybrid\ I$ and $Hybrid\ II$ are in good agreement. Apart from the dependence on the volume fraction, we also observe that the thermal conductivity of hybrid dispersion increases monotonically with increasing $a_p^{(sph)}$. This is expected due to reduce phonon scattering by interface. In other words, phonons are less hindered by the interface for larger particle sizes and the role of the phonon-phonon scattering (i.e. internal resistance) becomes more significant than the role of the phonon-interface scattering (i.e. the interface resistance). Note that the internal resistance is expressed in the bulk mean free path Λ_b while the collision Λ_{coll} and the thermal boundary resistance Λ_{TBR} mean free paths represent the interface scattering. When the hybrid dispersion is filled mainly with the nanospheres then the slope of $k_{eff}\ \ vs.\ \ a_p^{(sph)}$ is greater than in the hybrid dispersion with less volume fraction of nanospheres. It means that the higher is $\phi_p^{(sph)}$, the more significant is the contribution of nanospheres on the thermal conductivity. In other words, an increase in the particle size of nanospheres does not play a significant role on the thermal conductivity of the hybrid dispersion if $\phi_p^{(sph)}$ is much smaller than $\phi_p^{(w)}$. However, the major contribution to the thermal conductivity comes from nanowires. A gentle slope is observed for $k_{eff}\ \ vs.\ \ a_p^{(sph)}$. The same pattern is expected to be seen in the influence of $a_p^{(w)}$ on the thermal conductivity of hybrid dispersions. In Figure (6.1).b, the influence of nanowire orientation $\theta^{(w)}$ on the diffuse thermal conductivity of hybrid dispersion is shown. We take the same orientation distribution function used in our previous study in Ref. [2]. Again, results obtained from the $Hybrid\ I$ method agree well with results of the $Hybrid\ II$ method. It is

clearly seen that the thermal conductivity decreases when the $\theta^{(w)}$ moves toward $\pi/2$. We can say that the effective area for phonon-interface scattering and eventually resistance against heat flow will increase if more wires are oriented perpendicularly to heat flow direction, thus the thermal conductivity decreases. As presented in this figure, we see an almost plateau line under some circumstances. This means that the thermal conductivity is less sensitive on orientation of the nanowirs. Figure (6.2).a depicts the behavior of the thermal conductivity of hybrid dispersion when $\theta = \pi/4$ and $\phi_p^{(t)}$ changes between two extremes of $\phi_p^{(sph)} = 0$ which is dispersion of nanowires and $\phi_p^{(sph)} = \phi_p^{(t)}$ which is dispersion of nanospheres. Depending on the specularity of the interface, nanoparticle sizes and volume fractions, the thermal conductivity of the hybrid dispersion changes in different ways. For instance, an undershoot is observed for curve 1, while by changing the size of nanoparticles, we can see either an increase or decrease in the thermal conductivity of the hybrid dispersion. It is obvious that the thermal conductivity increase with increasing the specularity of interface (compare curves 2 and 3 in Figure (6.2).a). In other words, the higher is the specularity of the interface s, the lower is phonon confinement at the interface and the higher is the thermal conductivity.

As another illustration in Figure (6.2).b, we present the longitudinal ($\theta^{(w)} = 0$) thermal conductivity of the hybrid dispersion for different values of $a_p^{(w)}$ and $a_p^{(sph)}$ when the interface is totally diffuse. Here, overshoots can be observed for curves 1 and 4. For regions where the contribution of nanowires is significant (i.e. $\phi_p^{(sph)} \to 0$), it is observed that the thermal conductivity of hybrid dispersion increases with increasing the nanowire size due to less confinement of phonon transport by the boundary for larger particle sizes. Depending on the thermal conductivity of the dispersion of nanowires (i.e. $\phi_p^{(sph)} = 0$) and nanospheres (i.e. $\phi_p^{(w)} = 0$), we can see either increase or decrease with or without overshoot or undershoot of the thermal conductivity curve of hybrid dispersions against volume fraction of nano particles.

An important part of the search for suitable materials in the fabrication of electronic devices is an investigation of thermal and electric conductivities. The goal is to identify modifications of the materials that change the two conductivities in two different ways. In

this paper we look only at the thermal conductivity and explore theoretically its changes due to mixing a homogeneous material with nano-size particles of different types, different shapes, and different sizes. Our investigation shows that the composition of the dispersion has indeed a strong influence on the thermal conductivity.

We use the same approach as we used in Refs. [1, 2]. The new challenge is to adapt to hybrid dispersions the Maxwell homogenization (providing the effective heat conductivity inside the Fourier heat theory) and the subsequent analysis in the context of the phonon kinetic theory. For the former we use two methods. One is an adaptation of the method that we introduced in Ref. [1] to investigate hybrid sphere&agglomerate dispersions and the other is an adaptation of the method developed in Refs. [5]. We show that both (very different) methods lead to essentially identical results. The adaptation of the subsequent phonon analysis to hybrid dispersions is straightforward.

This article was partially supported by Natural Sciences and Engineering Research Council of Canada.

Bibliographie

[1] A. Behrang, M. Grmela, C. Dubois, S. Turenne, and P. G. Lafleur, *J. Appl. Phys.*, **114**, 014305 (2013), (2013).

[2] A. Behrang, M. Grmela, C. Dubois, S. Turenne, P. G. Lafleur, and G. Lebon, *Appl. Phys. Lett.*, **104**, 063106 (2014).

[3] J.C. Maxwell, *Treatise on Electricity and Magnetism*, 2nd ed. (Clarendon, Oxford 1881)

[4] C.-Wen Nan, R. Birringer, David R. Clarke and H. Gleiter. *J. Appl. Phys.*, **81**, 6692 (1997).

[5] J. Wang, J. Carson, M. North, D. Cleland, *Int. J. Heat Mass Transfer*, **51**, 2389 (2008).

[6] A. J. Minnich and G. Chen, *Appl. Phys. Lett.*, **91**, 073105 (2007).

[7] A.D. Brailsford and K.G. Major. *British J. Appl. Phys.*, **15**, 313 (1964).

[8] R. Yang, G. Chen, and M. S. Dresselhaus, *Nano Lett.* **5**, 1111 (2005).

[9] R, Yang, G. Chen and M. S. Dresselhaus, *Phys. Rev. B.*, **72**, 125418 (2005).

[10] F. Hao, D. Fang, and Z. Xu, *Appl. Phys. Lett.* **100**, 091903 (2012).

[11] X. P. Huang, X. L. Huai, S. Q. Liang, and X. W. Wang, *J. Phys. D* **42**, 095416 (2009).

[12] V. Samvedi and V. Tomar, *J. Appl. Phys.* **114**, 034312 (2013).

[13] V. Samvedi and V. Tomar, *J. Eur. Ceram. Soc.* **33**, 615 (2013).

[14] E. S. Landry M. I. Hussein, A. J. H and McGaughey, *Phys. Rev. B.*, **77**, 184302 (2008).

[15] R. Prasher, *J. Appl. Phys.*, **100**, 034307 (2006).

[16] C. Dames and G. Chen, *J. Appl. Phys.* **95**, 682 (2004).

[17] G. Chen, *J. Heat Transfer* **118**, 539 (1996).

[18] A. Minnich, M. S. Dresselhaus, Z. F. Ren, and G. Chen,, *Energy Environ. Sci.* **2**, 466 (2009).

[19] A. I. Boukai, Y. Bunimovich, J. Tahir-Kheli, J. K. Yu, W. A. Goddard III, and J. R. Heath, *Nature* **451**, 168 (2008).

[20] M. S. Dresselhaus, G. Chen, M. Y. Tang, R. G. Yang, H. Lee, D. Z. Wang, Z. F. Ren, J. P. Fleurial, and P. Gogna,, *Adv. Mater.*, **19**, 1043 (2007).

CHAPTER 7

ARTICLE4 : Temperature dependence of thermal conductivity in hybrid nanodispersions

A. Behrang, M. Grmela, C. Dubois, S. Turenne and P. G. Lafleur

RSC Advances, 2014, DOI : 10.1039/C4RA12368A

Abstract

We derive first a formula for the overall heat conductivity for dispersions of cuboid nanowires and recall similar formulas derived previously in [Behrang *et al., Applied Physics Letters*, 2014, **104**, 233111 , **104**, 063106 and Behrang *et al., Journal of Applied Physics*,**114**, 014305], by using the same method, for several other morphologies (dispersions of nano-size spheres, nano-size spheres of different sizes, nano-wires, rectangular cuboid nano-wires, and nano-spheres and nano-wires). The temperature dependence of the microscopic quantities (like the phonon mean free path) entering the formulas is known from the phonon kinetic theory. The formulas thus provide a setting for investigating the temperature dependence of the overall heat conductivity of dispersions. In general, we see that the interface that is present in hybrid nanodispersions influences significantly the thermal conductivity only in lower temperatures. This then means that the possible benefit of hybrid nanodispersions in fabricating electronic devices diminishes with increasing the temperature.

7.1 Introduction

The heat and electric conductivities depend in heterogeneous materials on the nature of their homogeneous components, on the morphology, and on the nature of the interface among the components. Consequently, by varying these three elements a large family of materials with a wide spectrum of heat and electric conductivities can be created. Heterogeneous ma-

terials are therefore often used in the fabrication of electronic devices where such materials are needed.

In this paper we continue our investigation Refs. [1–3] of the heat conductivity in heterogeneous materials created by dispersing nano-size particles of various shapes and sizes in a homogeneous matrix. We follow the method pioneered by Minnich et al. in Ref. [4]. The Maxwell homogenization (Ref. [5]) made in the first step is followed by the second step in which the Peierls kinetic theory of phonons[6] is employed. The second step, needed due to the nano-size morphology, transforms the expressions for the effective overall heat conductivity obtained in the first step into expressions involving microscopic quantities (like for instance the phonon mean free paths, heat capacities, and the parameters characterizing interactions of phonons with the interface) entering the phonon kinetic theory. In this paper we concentrate in particular on one gain made in such transformation. We can theoretically predict the temperature dependence of the overall heat conductivity. This is because the kinetic theory provides a setting for investigating the temperature dependencies of the microscopic quantities entering it. Having known these dependencies, and having an expression for the overall heat conductivity in terms of the microscopic quantities, we obtain the temperature dependence of the heat conductivity of heterogeneous material.

The paper is organized as follows. First, we apply the method used in Refs. [1–3] to a new morphology, namely to dispersions of rectangular cuboid wires for which there is a large amount of microscopic simulation data with which our predictions can be compared. This first part gives us also an opportunity to recall general features of the setting that we have used for all the morphologies (namely for dispersions of nano-size spheres, nano-size spheres of different sizes, nano-wires, and nano-spheres & nano-wires). The temperature dependence of the overall heat conductivity is calculated and presented in the second part.

7.2 Dispersion of rectangular cuboid wires

The Maxwell homogenization in dispersions of nanowires of infinite length that are all oriented in one direction leads [7, 8] to the following expression for the overall Fourier heat conductivity

$$k_{eff} = \frac{\sum\limits_{i=m,p} k_i \phi_i \frac{\gamma\beta}{(\gamma-1)\beta+k_i}}{\sum\limits_{i=m,p} \phi_i \frac{\gamma\beta}{(\gamma-1)\beta+k_i}} \tag{7.1}$$

By the symbol ϕ we denote the volume fraction of the dispersed phase, k is the thermal conductivity, and subscripts "m" and "p" stand for matrix and dispersed phases respectively. Depending on the direction of the dispersed particles against heat flow, the parameters γ and β take different values. $\gamma \to \infty$ or $\beta = k_i$ for rectangular cuboid wires aligned in the direction of the heat flow (denoted by $\|$), and $\gamma = 2$ and $\beta = k_m$ for rectangular cuboid wires oriented in the direction that is perpendicular to the heat flow (denoted by $\perp$). In this paper we consider nano rectangular cuboid wires of thickness a_p, width b_p, and length L with the orientation characterized by the angle θ with respect to the orientation of the heat flow.

In order to take into account the nano-size of the wires, we pass now to the phonon kinetic theory. The thermal conductivity of the homogeneous component arises in the kinetic theory in the form

$$\begin{aligned} &k_i^{(j)}(s, a_p, b_p, L, \theta, T) = \\ &\frac{1}{3}\int C(T,\omega) v(T,\omega) \Lambda_i^{(j)}(s, a_p, b_p, L, \theta, T, \omega) d\omega \\ &j = spec,\ diff,\ \ i = m, p \end{aligned} \tag{7.2}$$

where ω is the phonon frequency, T is the temperature, C denotes the volumetric specific heat capacity per unit frequency at the frequency ω, v the phonon group velocity, and Λ the phonon mean free path. By $0 \le s \le 1$, we denote the probability of the specular scattering

of phonons on the particle-matrix interface is presented. The phonon scattering is diffuse if $s = 0$ and specular if $s = 1$. The angle between the direction of wires and the direction of heat flux is denoted by θ. Note that $\theta = 0$ if all the nanowires are oriented in the direction of the heat flow and $\theta = \pi/2$ if all the nanowires are aligned in the direction that is perpendicular to the direction of the heat flow. We assume in addition that $a_p - L$ face is exposed to heat flux when $\theta = \pi/2$

We now continue to investigate further the mean free paths. We begin with the matrix phase. The Matthiessen rule is employed to express the influence of boundary scattering :

$$\Lambda^{-1} = \Lambda_b^{-1} + \Lambda_{coll}^{-1} + \Lambda_{TBR}^{-1} \tag{7.3}$$

where Λ_b is the mean free path in the bulk, Λ_{coll} is the mean free path associated with the collision, and Λ_{TBR} the thermal boundary resistance mean free paths. We now adapt the method developed in Refs. [1–3] to rectangular cuboid wires of length L and thickness a_p and width b_p and arrive at

$$\frac{1}{\Lambda_m} = \frac{1}{\Lambda_{b,m}} + \phi(\frac{1-s}{1+s} + \frac{1}{\Gamma^{(j)}})(\frac{1}{\Xi^{(\|)}} + \frac{1}{\Xi^{(\perp)}}) \tag{7.4}$$

We point out that $1/\Xi^{(\|)} = (1/L + \xi/b_p + \zeta/a_p)\cos\theta$ and $1/\Xi^{(\perp)} = (1/b_p + \zeta/a_p)\sin\theta$ are the characteristic lengths of nanowires in $\|$ and $\perp$ directions respectively. Note that $\xi = a_p/(a_p + \sqrt{a_p b_p/\phi})$ and $\zeta = b_p/(b_p + \sqrt{a_p b_p/\phi})$ denote the probabilities of phonon-wire scattering when phonon scatters with faces $a_p - L$ and $b_p - L$, respectively. The diffuse and specular behaviour of phonons at the matrix-particle interface is defined by

$$\Gamma^{(diff)} = \frac{3t_{mp}^{(diff)}}{4(1-\frac{1}{2}(t_{mp}^{(diff)}+t_{pm}^{(diff)}))}$$
$$\Gamma^{(spec)} = \frac{3\int_0^{\mu_{crit}} t_{mp}^{(spec)}(\mu_m)\mu_m d\mu_m}{2(1-\int_0^{\mu_{crit}} t_{mp}^{(spec)}(\mu_m)\mu_m d\mu_m - \int_0^{\mu_{crit}} t_{pm}^{(spec)}(\mu_p)\mu_p d\mu_p)} \tag{7.5}$$

By the symbols t_{mp} and t_{pm} we denote probabilities of the transmission from matrix "m" to particles "p" and vice versa. Explicit expressions for these quantities in both specular and diffuse transmissions are given in Ref. [1].

Next, we direct our attention to dispersed particles and phonon scattering inside them. For nanowire in $\perp$ direction, we have

$$\frac{1}{\Lambda_p^{(\perp)}} = \frac{1}{\Lambda_{b,p}} + \frac{1}{a_p(s)} + \frac{1}{b_p(s)} \tag{7.6}$$

Note that $a_p(s) = a_p\frac{1+s}{1-s}$ and $b_p(s) = b_p\frac{1+s}{1-s}$ are the effective nanowire thickness and width respectively [9].

For $\parallel$ direction and when $L >> a_p, b_p$, the phonon kinetic theory provides (see [10]) the expression

$$\Lambda_p^{(\parallel)} = \Lambda_{b,p}(1-\frac{3}{2\pi}\int_0^{\pi}\sin\psi\cos^2\psi$$
$$[\int_{\arctan(-a_p/b_p)}^{\arctan(a_p/b_p)}(1-s)\frac{\exp(-\frac{b_p}{2\Lambda_{b,p}\sin\psi\cos\delta})}{1-s\exp(-\frac{b_p}{2\Lambda_{b,p}\sin\psi\cos\delta})}d\delta +$$
$$\int_{\arctan(a_p/b_p)}^{\pi-\arctan(a_p/b_p)}(1-s)\frac{\exp(-\frac{a_p}{2\Lambda_{b,p}\sin\psi\cos\delta})}{1-s\exp(-\frac{a_p}{2\Lambda_{b,p}\sin\psi\cos\delta})}d\delta]d\psi) \tag{7.7}$$

where ψ and δ are the polar and azimuthal angles respectively. In order to take into

account the influence of the length of nanowires, we modify the expression (7.7) (following [11]) into

$$\frac{1}{\Lambda_p^{(\|)}(L)} = \frac{1}{\Lambda_p^{(\|)}}\left(1 + \frac{\Lambda_p^{(\|)}}{2L(s)}\right) \tag{7.8}$$

Note that $L(s) = L\frac{1+s}{1-s}$.

When the angle between the orientation of wires and the heat flux is θ, then (7.6) and (7.8) combine to give

$$\Lambda(s, L, a_p, b_p, \theta) = \Lambda_p^{(\|)}(L)\cos^2\theta + \Lambda_p^{(\perp)}\sin^2\theta \tag{7.9}$$

Expressions (7.4) and (7.9) help us to show the influence of boundaries and their properties created by incorporating nanoscale particle sizes into the homogeneous matrix. Substituting these expressions into (7.2), the thermal conductivities of the matrix and dispersed phases which are function of (s, L, a_p, b_p, θ) are determined. Thus, recalling (7.1) in its appropriate form, the overall heat conductivity coefficient of the nanodispersion of rectangular cuboid wires is written as

$$\begin{aligned} k(s, L, a_p, b_p, \theta) &= s\left[k^{(\|,spec)}(s, L, a_p, b_p, \theta)\cos^2\theta\right. \\ &\left.+k^{(\perp,spec)}(s, L, a_p, b_p, \theta)\sin^2\theta\right] \\ &+(1-s)\left[k^{(\|,diff)}(s, L, a_p, b_p, \theta)\cos^2\theta\right. \\ &\left.+k^{(\perp,diff)}(s, L, a_p, b_p, \theta)\sin^2\theta\right] \end{aligned} \tag{7.10}$$

Next, we compare (qualitatively and quantitatively) our results with available results obtained by microscopic direct simulations. We make the comparison for $Bi_2Te_3 - Sb_2Te_3$ and then $SiGe$ which have been considered as candidates for nanostructure materials used in thermoelecteric applications. The material parameters are presented in Table(7.1). Note that for the sake of consistency between the structure of our nanodispersion and the nanodispersions

investigated previously in [12, 13], it is assumed that $a_p = b_p$.

Table 7.1 Material parameters used in calculations

Material	C $[\times 10^6 Jm^{-3}K^{-1}]$	v $[ms^{-1}]$	Λ_b $[nm]$	Density $[kgm^{-3}]$
Si (Ref. [13])	1.001	2403	172	2330
Ge (Ref. [13])	0.933	1308	133	5330
Bi_2Te_3 (Ref. [12])	0.5	212	31	-
Sb_2Te_3 (Ref. [12])	0.53	200	25.4	-

Figures (7.1)a-b show the influence of the volume fraction ϕ and the size a_p of dispersed Sb_2Te_3 particles on the thermal conductivity of $Bi_2Te_3 - Sb_2Te_3$ nanodispersion perpendicular to the heat flow direction. We note a good agreement with results obtained from the Boltzmann-Peirels transport equation for $Bi_2Te_3 - Sb_2Te_3$ nanodispersion [12].

In Figure (7.1)a, we see that an increase in the volume fraction ϕ leads to a decrease of $k^{(\perp)}$. This is due to the influence of the phonon-boundary scattering. For a fixed particle size, an increase in the volume fraction increases the chance of the phonon-boundary scattering which in turn causes the thermal conductivity to decrease.

Figure (7.1)b, shows that $k^{(\perp)}$ increases monotonically with increasing the size of dispersed Sb_2Te_3 particles. The reason behind this enhancement is the decrease of the probability of the phonon-boundary scattering with the increase of a_p leading to a weaker resistance against heat transfer. In other words, the role of the phonon-boundary interactions (i.e. boundary resistance) is suppressed at larger particle sizes and the phonon-phonon scattering (i.e. the internal resistance) dominates. Consequently, the thermal conductivities of the matrix and of the dispersed particles come close to their values in bulk where the boundary effects are absent and the macroscopic nature of the heat conduction prevails. Note that the boundary scattering is expressed in Λ_{coll} and Λ_{TBR} and the internal scattering in Λ_b. For large dispersed particles the obstacles to the motion of phonons caused by boundaries are smaller and consequently the thermal conductivity is higher.

We have also compared our results with the Monte Carlo simulations with $SiGe$ nanodispersions [13]. In Figure (7.2)a, Si wires are embedded in Ge matrix. The dispersion of Ge

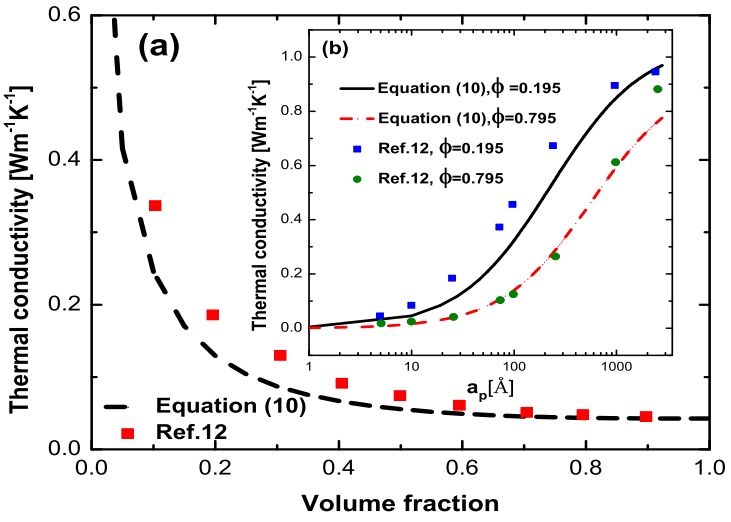

Figure 7.1 The effect of (a). volume fraction for $a_p = 25.4\text{Å}$, and (b). particle size on the thermal conductivity of $Bi_2Te_3 - Sb_2Te_3$ nanodispersion in $\perp$ direction.

particles in Si matrix is presented in Figure (7.2)b. For both cases, our results are in good agreement with results of the Monte Carlo simulation in particular for smaller particle sizes. Theses results confirm again that the boundary scattering, caused by the presence of nanoscale particles, create strong obstacles against phonon mean free path which then results in lower thermal conductivity of the dispersion. We can indeed anticipate that a simultaneous decrease of the particle size and increase of the volume fraction of the dispersed phase will intensify impact of the phonon-boundary scattering. In other words, the probability of phonon-boundary scattering will be greater than the probability of phonon-phonon scattering at higher volume fractions and smaller particle sizes. This then leads to a significant reduction in the thermal conductivity. In Figure (7.2)c, we show the agreement between our results and results presented in Ref[13] for the thermal conductivity of nanodispersion of Si embedded rectangular cuboid wires in Ge matrix where Si wires are oriented in $\parallel$ direction to the heat flow. Comparing to the thermal conductivity in $\perp$ direction, higher thermal conductivity is expected in $\parallel$ direction due to less phonon-boundary scattering events. As the final comment on Figures (7.1)a and (7.2), we can see a dramatic dependence of the thermal conductivity

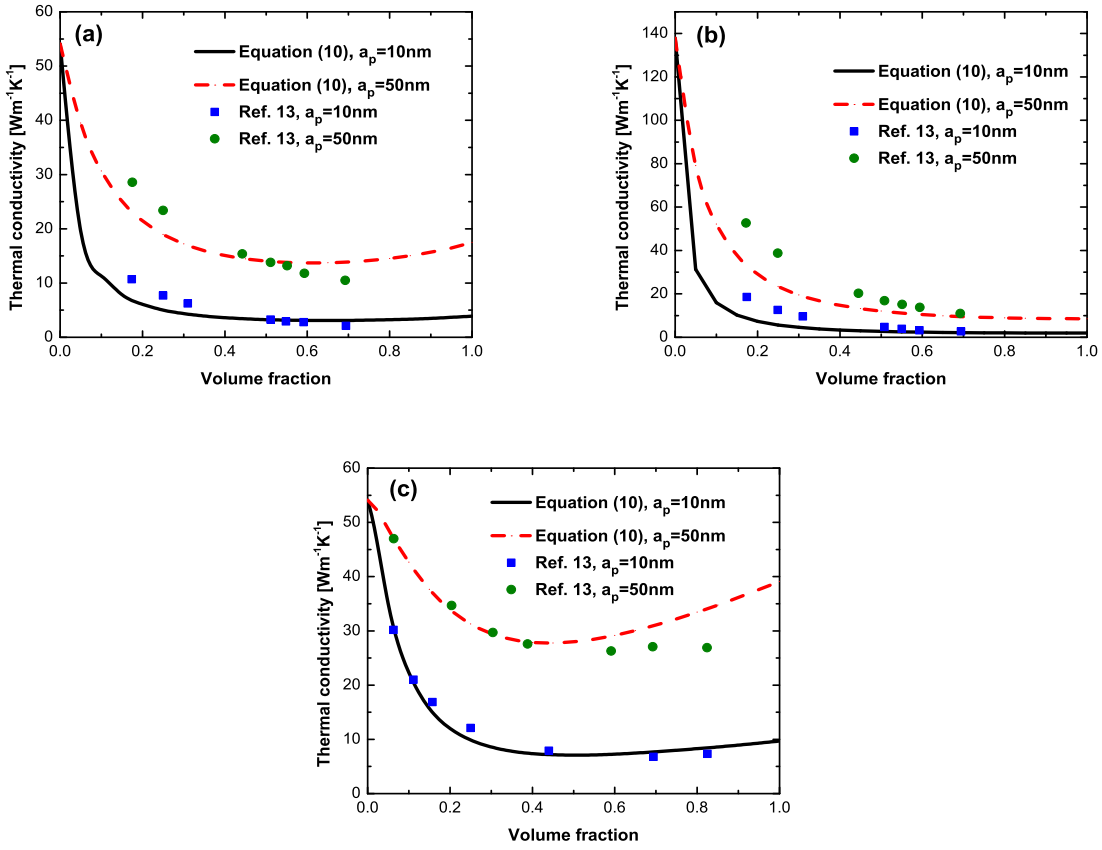

Figure 7.2 The sensitivity of the thermal conductivity of (a). Si nanowires embedded in Ge matrix for $\perp$ direction, (b). Ge nanowires embedded in Si matrix for $\perp$ direction, and (c). Si nanowires in Ge matrix for $\parallel$ direction.

on the degree of homogeneity of the dispersion. This means that in these graphs the thermal conductivity curves show an exponential decay behavior with high sensitivity to an incorporation of dispersed phase at low volume fractions where a small amount of dispersed particles results in a significant reduction in the thermal conductivity of dispersion. This sharp drop in the thermal conductivity can be interpreted by the concept of interparticle distance. In this region, a smaller change in the volume fraction of dispersed phase at a certain particle size induces an intense reduction in the interparticle distance which then dramatically increases the chance of the phonon-boundary scattering which then leads to a sharp reduction in the thermal conductivity. For the central region of the graph we note that the thermal conductivity is almost independent of ϕ. In this region the size of the dispersed particles influences more the thermal conductivity rather than the volume fraction (the behavior investigated in Refs. [14–17]).

Figure (7.3) depicts the influence of other parameters on the thermal conductivity. In order to take into account the role of the nanowire alignment, the orientation distribution function $f(\theta)$ presented in Ref. [18] is considered :

$$f(\theta) = \frac{(\sin\theta)^{2p-1}(\cos\theta)^{2q-1}}{\int_{\theta_{min}}^{\theta_{max}}(\sin\theta)^{2p-1}(\cos\theta)^{2q-1}d\theta} \tag{7.11}$$

where p and q are the shape parameters. We note that when $p = q = 1$ then the most probable orientation angle $\theta_{mod} = \pi/4$; $p = 1$ and $q > 1$ or $p > 1$ and $q = 1$, $\theta_{mod} > \pi/4$; when $p = 1/2$, $\theta_{mod} = 0$; $q = 1/2$, $\theta_{mod} = \pi/2$. The nanowires are distributed randomly if $p = q = 1/2$.

In Figure (7.3), the dispersion of Si nanowires of thickness a_p, width b_p and length L in the Ge matrix is shown. It is observed that the thermal conductivity of dispersion decreases when the orientation of nanowires changes from 0 toward $\pi/2$. This reduction arises due to an increase in the probability of phonon-boundary scattering. In other words, once the orientation of the nanowires tends toward $\pi/2$, the effective cross section for scattering of phonons

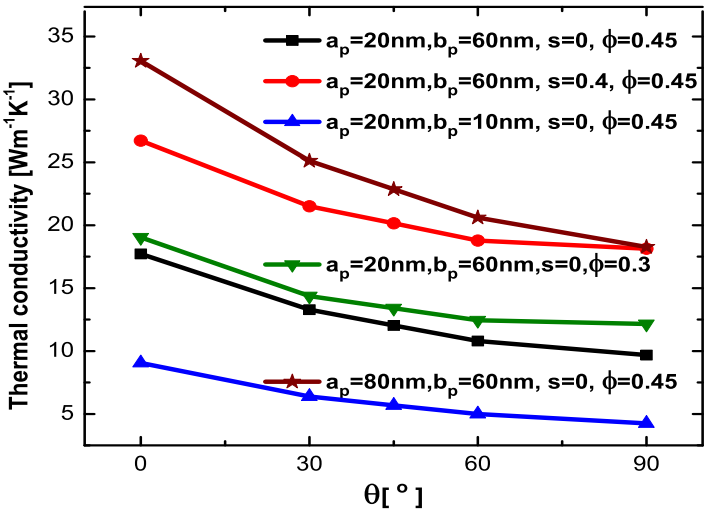

Figure 7.3 Sensitivity of the thermal conductivity of the Si nanowires incorporated in Ge matrix to orientation of nanowires.

by boundaries increases. Consequently, phonons experience more boundary scatterings and as the result the thermal conductivity decreases. We also point out that the thermal conductivity of dispersion increases with increasing the probability of the specular scattering of phonons on the particle-matrix interface (i.e. with the increase of the specularity parameter "s"). One can see that the higher is the specularity parameter, the lower is the phonon confinement at the interface and consequently the larger is the thermal conductivity. Finally, we note that phonons are encountered with more obstacles if the width of nanowire b_p decreases which then means that the thermal conductivity decreases.

7.3 Temperature dependence

Now we turn to the main objective of this paper. We use the expressions obtained in the previous section and similar expressions obtained in Refs. [1–3] to investigate the thermal dependency of the effective heat thermal conductivity of hybrid heterogeneous materials.

We begin by specifying the temperature dependence of all the microscopic quantities entering the expression (7.1) and similar expressions obtained in Refs. [1–3].

First, we assume (following Refs. [19, 20]) that the phonon group velocity is independent of the temperature.

For the specific heat capacity, we assume [21, 22]

$$C_i(T,\omega) = \frac{3\hbar^2}{2\pi^2 v_i^3 k_B T^2} \frac{\omega^4 \exp(\hbar\omega/k_B T)}{[\exp(\hbar\omega/k_B T)-1]^2} \quad i = m, p \tag{7.12}$$

where $\hbar$ is the reduced Planck's constant, k_B is the Boltzmann constant.

For the bulk mean free paths, we take

$$\Lambda_{b,i} = \frac{\exp(\theta_i/T)}{B_i T \omega^2}, \quad i = m, p \tag{7.13}$$

where B and θ are constant parameters determined by fitting experimental data[20, 21].

The temperature dependence of the transmission coefficients ($t_{mp}^{(diff)}$ and $t_{pm}^{(diff)}$) entering (7.5) is given in Ref. [1]

$$\begin{aligned} t_{il}^{(diff)} &= [\frac{3\hbar^2}{2\pi^2 v_l^2 k_B T^2} \int_0^{\omega_{D,l}} \frac{\omega^4 \exp(\hbar\omega/k_B T)}{[\exp(\hbar\omega/k_B T)-1]^2} d\omega]/ \\ &[\frac{3\hbar^2}{2\pi^2 v_l^2 k_B T^2} \int_0^{\omega_{D,l}} \frac{w^4 \exp(\hbar\omega/k_B T)}{[\exp(\hbar\omega/k_B T)-1]^2} d\omega \\ &+ \frac{3\hbar^2}{2\pi^2 v_i^2 k_B T^2} \int_0^{\omega_{D,i}} \frac{\omega^4 \exp(\hbar\omega/k_B T)}{[\exp(\hbar\omega/k_B T)-1]^2} d\omega] \\ &i, l = m, p; \ i \neq l \end{aligned} \tag{7.14}$$

By substituting the above expressions into (7.2) we obtain [19, 20]

$$\begin{aligned} &k_i(a_p, b_p, L, \theta, T) = \\ &\int_0^{\omega_{D,i}} \frac{\hbar^2}{2\pi^2 v_i^2 k_B T^2} \frac{\omega^4 \exp(\hbar\omega/k_B T)\Lambda_i(T,\omega)}{[\exp(\hbar\omega/k_B T)-1]^2} d\omega \\ &i = m, p \end{aligned} \tag{7.15}$$

As for the phonon-boundary scattering, we limit ourselves hereafter only to the diffuse scattering.

As the case study, we take the dispersion of Si wires in Ge matrix. This type of heterogeneous materials is widely used in thermoelectric applications. First, we need to identify the constants entering the expression (7.13). For silicon and germanium, we use (see Ref. [1]) where the constants have been found by making the best fit with experimental results reported in Ref. [23]. For Si the values are : $B = 5.753 \times 10^{-23} s^2 m^{-1} K^{-1}$ and $\theta = 199.2K$. For Ge the values are : $B = 1.655 \times 10^{-22} s^2 m^{-1} K^{-1}$ and $\theta = 78.92K$. Finally , we use the temperature dependence given in (7.4) and (7.9).

For the temperature dependence investigation we use the material parameters calculated by Debye model. This then means that the Debye frequency cutoff of Si and Ge are assumed to be $9.125 \times 10^{13} s^{-1}$ and $5.14 \times 10^{13} s^{-1}$ [24] and the phonon group velocities for Si and Ge $6400 ms^{-1}$ and $3900 ms^{-1}$[25], respectively.

Figures (7.4)a-b, depict $k^{(\perp)}$ as a function of the particle size (note that $a_p = b_p$) for $\phi = 0.05$ and $\phi = 0.4$ at four different temperatures. For lower temperatures, the thermal conductivity decreases monotonically with decreasing the particle size. This is due to the relative increasing of the boundary scattering area per unit volume. As the temperature increases, the sensitivity of the thermal conductivity to the particle size is weakened and we can observe a smooth trend at higher temperatures. We note that as the temperature increases, the impact of phonon-phonon scattering reflected by Λ_b term is strengthened and at the same time the influence of the phonon-boundary scattering expressed in Λ_{coll} and Λ_{TBR} terms becomes less significant. In other words, reduction of the thermal conductivity by creating more obstacles against phonon transport is smaller at higher temperatures.

In order to observe the dependence of $k^{(\perp)}$ on the temperature for different particle sizes and volume fractions, Figures (7.5)a-b are presented. In both figures we can observe the same scenario in which a decrease in the thermal conductivity is a consequence of an increase in the temperature. Note that the influence of the particle size (phonon-boundary

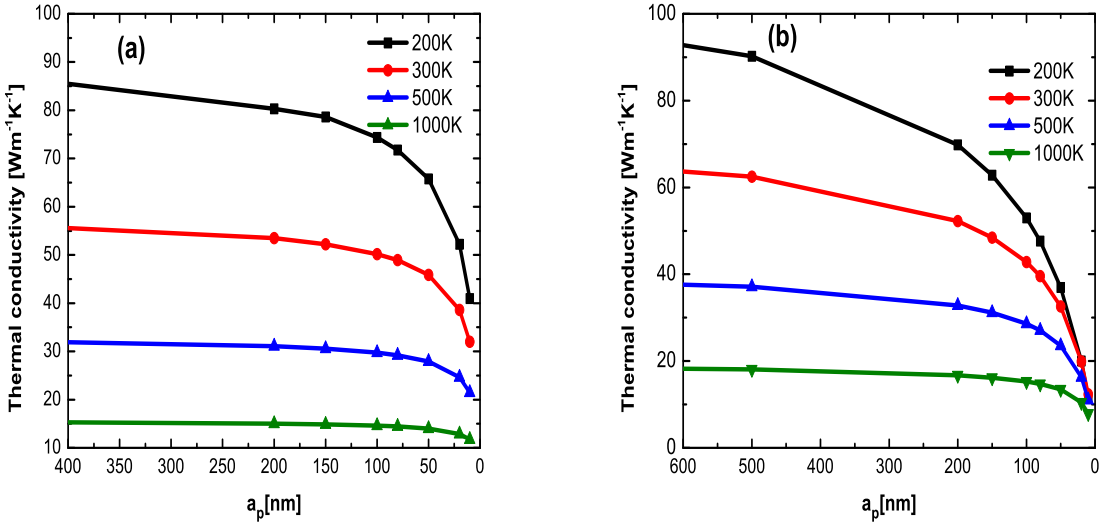

Figure 7.4 Size dependent thermal conductivity of nanodispersions of Si nanowires embedded in a Ge matrix for four different temperatures when $(a).\phi_p = 0.05$ and $(b).\phi_p = 0.4$, respectively.

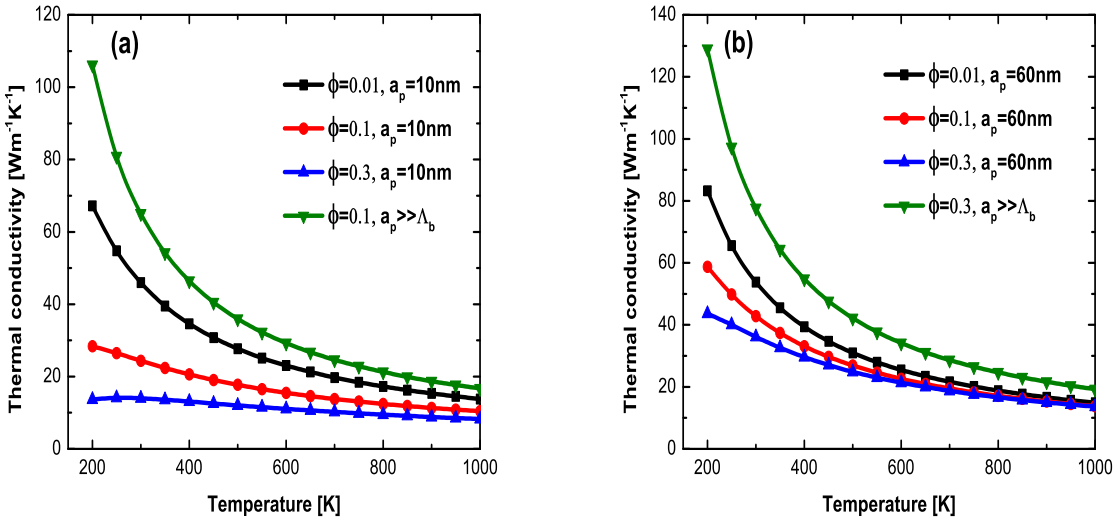

Figure 7.5 Effect of temperature on the thermal conductivity nanodispersions of Si nanowires within Ge matrix for three different volume fractions and particle sizes $(a).a_p = b_p = 10nm$ and $(b).a_p = b_p = 60nm$.

scattering) is not taken into account if $a_p >> \Lambda_b$. This means that the resistance against phonon transport caused by boundaries fades. This then implies that the mean free paths and consequently also the thermal conductivities of the matrix and dispersed particles tend toward their corresponding bulk values. At lower temperatures, one can see a strong dependence of the thermal conductivity on the particle size and the volume fraction, while, apart from particle size and volume fraction, almost the same thermal conductivities are observed at higher temperatures. To sum it up, the phonon-phonon scattering becomes more important and the phonon-boundary scattering less important as the temperature increases. We also see that the thermal conductivity of dispersion is almost independent of temperature for higher volume fractions and smaller particle sizes (see Figure (7.5)a for $a_p = 10nm$ and $\phi = 0.3$). In other word, the influence of the boundary scattering dominates and the contribution of phonon-phonon scattering (i.e. internal scattering) becomes even smaller than that of boundary scattering when the nanodispersion is fabricated with higher volume fraction and smaller size dispersed particles. Generally speaking, the lower is temperature, the higher is the contribution of phonon-boundary scattering (i.e. boundary resistance) while the higher is temperature, the more significant is the phonon-phonon scattering (i.e. the internal resistance).

Figure (7.6)a depicts the comparison between $k^{(\|)}$ and $k^{(\perp)}$. Since phonons experience less boundary scattering when they travel along L direction, the higher thermal conductivity is expected in $\|$ direction. $k^{(\|)} vs. \phi$ is illustrated in Figure (7.6)b. When the volume fraction increases, a significant reduction of thermal conductivity is observed for lower temperatures, while the sensitivity of the thermal conductivity to the volume fraction becomes reduced as the temperature is elevated. Such behavior again confirms the importance of the boundary scattering at lower temperatures and the internal scattering at higher temperatures. In other words, when temperature is low (say $200K$) and volume fraction increases monotonically, the boundary scattering plays the key role and the thermal conductivity of nanodispersion (apart from either in $\|$ or $\perp$ directions) experiences a significant reduction due to an increase of the

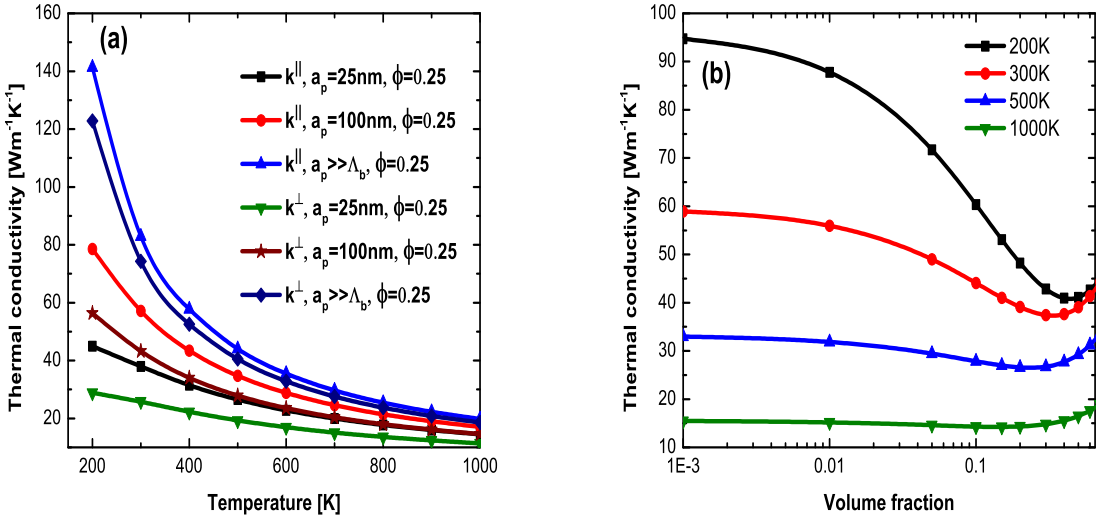

Figure 7.6 (a) Comparison between the thermal conductivity of nanodispersions in $\parallel$ and $\perp$ directions as the function of temperature for different particle sizes and $\phi_p = 0.25$ and (b). thermal conductivity of nanodispersions as a function of the volume fraction for $a_p = b_p = 25nm$ and different temperatures. Nanodisperions of Si nanowires/Ge matrix has been illustrated.

effective area for phonon-boundary scattering. Consequently, as the temperature increases (for example $1000K$) the scenario changes and the contribution of phonon-phonon scattering becomes important, thereby an increase in the volume fraction of the dispersed particles does not affect significantly the thermal conductivity. We see a weak sensitivity of the thermal conductivity of nanodispersion to changes in the volume fraction (note an almost plateau curve for $k^{\parallel \ or \ \perp}$ vs. ϕ).

We turn now our attention to our previous work (presented in Ref. [3]) where we have investigated hybrid dispersion of nanowires and nanospheres. We concentrate on the temperature dependence. The hybrid dispersion under investigation is composed of nanowires with radius of $a_p^{(w)}$, length of $L^{(w)}$ and volume fraction of $\phi_p^{(w)}$ and nanospheres with radius of $a_p^{(sph)}$ and volume fraction of $\phi_p^{(sph)}$. In Ref. [3], two different methods of homogenizations have been derived and performed on such hybrid dispersions. It was observed that the results of theses different approaches are in an excellent agreement. For the sake of simplicity, we take here

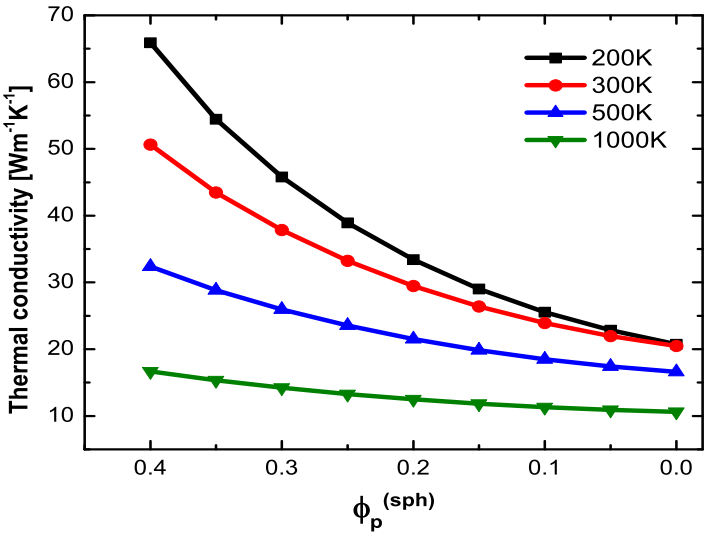

Figure 7.7 Thermal conductivity of hybrid dispersion of Si nanospheres and nanowires in Ge matrix against the volume fraction of nanospheres for different temperatures when $a_p^{(w)} = 10nm$, $a_p^{(sph)} = 100nm$, $L^{(w)} >> a_p^{(w)} \& a_p^{(sph)}$, $\theta = \pi/2$ and $\phi_p^{(t)} = 0.4$.

the second method of homogenization presented in Ref[3]. In the study the influence of temperature, we assume that only diffuse scattering of phonons on the interfaces takes place. In Figure (7.7), the thermal conductivity of hybrid dispersion in $\perp$ direction is plotted against the volume fraction of spheres, $\phi_p^{(sph)}$ for four different temperatures. Note that in this figure, $a_p^{(w)} = 10nm$, $a_p^{(sph)} = 100nm$, $L^{(w)} >> a_p^{(w)} \& a_p^{(sph)}$ and $\phi_p^{(sph)} + \phi_p^{(w)} = \phi_p^{(t)}$, where $\phi_p^{(t)}$ is the total volume fraction of the dispersed components. In Figure(7.7), $\phi_p^{(t)} = 0.4$. For lower temperatures, we note that the thermal conductivity of the hybrid dispersion becomes smaller when the volume fraction of nanospheres decreases ($\phi_p^{(sph)} \to 0$). Provided $a_p^{(w)} < a_p^{(sph)}$, such behavior is a consequence of the confinement of the phonon transport by boundaries when $\phi_p^{(w)} \to \phi_p^{(t)}$. When the temperature increases, another scenario emerges in which the sensitivity of the thermal conductivity to the composition of hybrid dispersion significantly decreases and almost a plateau line is observed (see Figure(7.7) for $1000K$). This behavior is observed because the possibility of phonon scattering at high temperatures is mostly the internal (phonon-phonon) scattering and subsequently the role of the boundary (the phonon-

boundary scattering) is smaller. Summing up, we note that fabrication of hybrid dispersions may not lead to a desired flexibility in influencing the thermal conductivity if the temperatures used in applications are high. We see that at higher temperatures, apart from the particle sizes, the thermal conductivity of the hybrid dispersion does not dramatically vary from those nanodispersions of single particle shape of nanowires ($\phi_p^{(w)} = \phi_p^{(t)}$) or nanospheres ($\phi_p^{(sph)} = \phi_p^{(t)}$). Figures (7.8) and (7.9) also confirm such observation.

The dependence of the thermal conductivity of hybrid dispersion in $\perp$ direction on the temperature is shown in Figure (7.8). One can see a notable difference between the thermal conductivity of hybrid dispersions at low temperatures, while apart from the size of nanoparticles, all curves converge at high temperatures. For lower temperatures, the lower thermal conductivity is expected for a situation in which the influence of phonon-boundary scattering is more significant. Note that for a fixed volume fraction, the smaller is the particle size, the stronger is phonon confinement by boundaries. In opposite situation when $a_p^{(w)}, a_p^{(sph)} >> \Lambda_b^{(w)}, \Lambda_b^{(sph)}$ (i.e. sign of macroscopic heat conduction where the boundary scattering is eliminated), the higher thermal conductivity of hybrid dispersion is achieved at lower temperatures.

Since the boundary scattering does not influence the thermal conductivity at higher temperatures, the advantage of nanostructuration is diminished. Accordingly, no remarkable difference is found between the thermal conductivities of hybrid dispersions with different particle sizes.

As shown in Figure(7.9)a-b, the thermal conductivity of hybrid dispersions versus particle size of wires have been depicted for two temperatures of $200K$ and $1000K$ in $\parallel$ and $\perp$ directions when $a_p^{(sph)} = 80nm$ and $L^{(w)} >> a_p^{(w)} \& a_p^{(sph)}$. In Figure (7.9)a, $\phi_p^{(t)} = 0.2$ and $\phi_p^{(sph)} = 0.15$ and $\phi_p^{(t)} = 0.6$ and $\phi_p^{(sph)} = 0.2$ are considered for Figure (7.9)b.

The illustrations show that the thermal conductivity of the hybrid dispersion is insensitive to the composition of hybrid dispersion (i.e. $\phi_p^{(t)}, \phi_p^{(sph)} \& \phi_p^{(w)}$), particle size of nanospheres, particle size and orientation (either in $\parallel$ or $\perp$ directions) of nanowires at higher temperatures

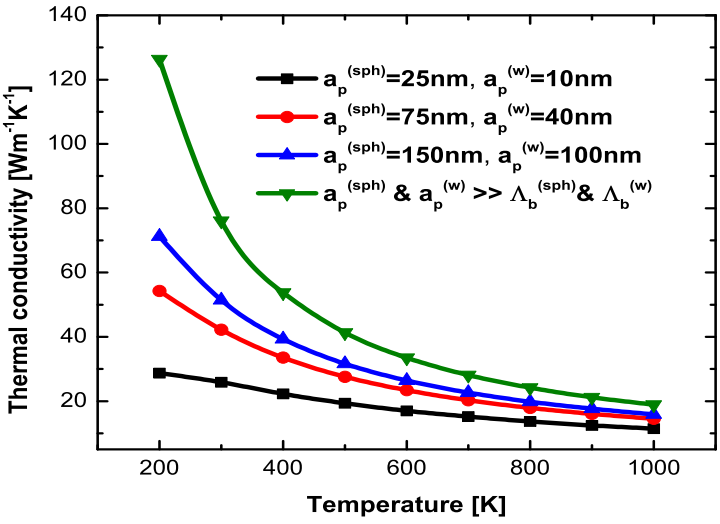

Figure 7.8 Sensitivity of the thermal conductivity of hybrid dispersion of Si nanospheres and nanowires in Ge matrix to temperature for different particle sizes when $L^{(w)} >> a_p^{(w)} \& a_p^{(sph)}$, $\theta = \pi/2$, $\phi_p^{(t)} = 0.3$ and $\phi_p^{(sph)} = 0.15$.

(see Figures (7.9)a-b for $1000K$). This means that the strength of phonon-boundary scattering created by incorporation of hybrid nanoparticles with different compositions, sizes, shapes and orientations within a homogeneous matrix reduces as temperature elevated. Therefore, for high temperature applications, we can not benefit from fabrication of hybrid dispersions.

On the other hand when the temperature is low, the influence of the phonon-boundary scattering is more significant than the influence of the phonon-phonon scattering and also the influence of changes in the composition, size, shape and orientation of hybrid nanoparticles.

7.4 Conclusion

In this paper we present two results.

First, we adapt the method used in Refs. [1–3] to nanodispersions of rectangular cuboid wires. The values of the coefficient of the overall heat conductivity calculated from the analytical formula derived in the paper agree well with results coming from direct simulations. We see that : (i) the smaller is the particle size and the higher is volume fraction, the hi-

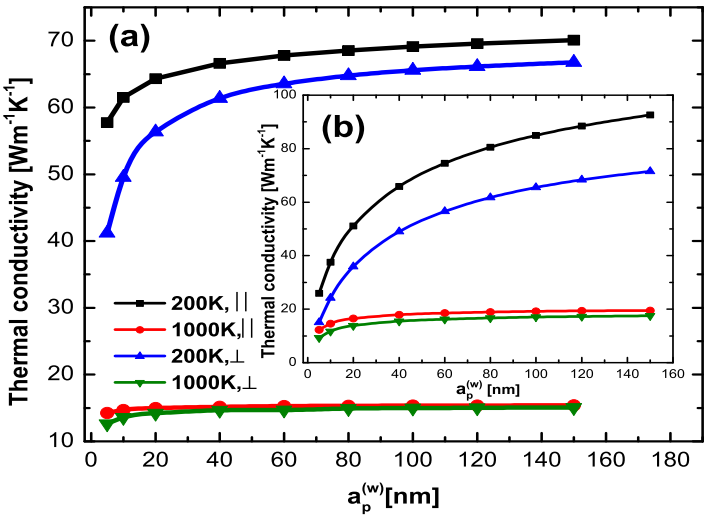

Figure 7.9 Thermal conductivity of hybrid dispersion of Si nanospheres and nanowires in Ge matrix as a function of the nanowire particle size for $a_p^{(sph)} = 80nm$, $L^{(w)} >> a_p^{(w)} \& a_p^{(sph)}$ and temperatures of $200K$ and $1000K$ in $\parallel$ and $\perp$ directions when $(a).\phi_p^{(t)} = 0.2$ and $\phi_p^{(sph)} = 0.15$ and $(b).\phi_p^{(t)} = 0.6$ and $\phi_p^{(sph)} = 0.2$.

gher is phonon-boundary scattering and the lower is the thermal conductivity. (ii) As the specularity of the interface increases, the confinement of phonons by boundaries decreases and the thermal conductivity increases. (iii) When more nanowires are aligned perpendicularly $(\theta \to \pi/2)$ to the direction of heat flow then the chance of phonon-boundary scattering increases and the thermal conductivity is lowered.

Second, we systematically study the temperature dependence of the thermal conductivity of hybrid dispersions of particles of various shapes (spheres, circular and rectangular cuboid wires) and sizes. This investigation is based on the formulas (derived in this and the previous papers Refs.[1–3]) in which the coefficient of the overall heat conductivity is expressed in terms of microscopic quantities (like the phonon mean free path) for which the temperature dependence is known from the phonon kinetic theory. As for the results, we see that at low temperatures the temperature dependence is sensitive to differences in dispersion morphologies. Such sensitivity disappears at higher temperatures.

Acknowledgement

This article was partially supported by Natural Sciences and Engineering Research Council of Canada. Authors thank Professor Lebon for valuable discussions and useful comments.

Bibliographie

[1] A. Behrang, M. Grmela, C. Dubois, S. Turenne, and P. G. Lafleur, *J. Appl. Phys.*, **114**, 014305 (2013), (2013).

[2] A. Behrang, M. Grmela, C. Dubois, S. Turenne, P. G. Lafleur, and G. Lebon, *Appl. Phys. Lett.*, **104**, 063106 (2014).

[3] A. Behrang, M. Grmela, C. Dubois, S. Turenne, P. G. Lafleur, and G. Lebon, *Appl. Phys. Lett.*, **104**, 233111 (2014).

[4] A. J. Minnich and G. Chen, *Appl. Phys. Lett.*, **91**, 073105 (2007).

[5] J.C. Maxwell, *Treatise on Electricity and Magnetism*, 2nd ed. (Clarendon, Oxford 1881).

[6] R. Peierls , *Ann. Phys.* **395**, 1055 (1929).

[7] C.-Wen Nan, R. Birringer, David R. Clarke and H. Gleiter. *J. Appl. Phys.*, **81**, 6692 (1997).

[8] J. Wang, J. Carson, M. North, D. Cleland, *Int. J. Heat Mass Transfer*, **51**, 2389 (2008).

[9] C. Dames and G. Chen, *J. Appl. Phys.* **95**, 682 (2004).

[10] X. L*ü*, *J. Appl. Phys.*, **106**, 064305 (2009).

[11] E. S. Landry M. I. Hussein, A. J. H and McGaughey, *Phys. Rev. B.*, **77**, 184302 (2008).

[12] A. Pattamatta and C. K. Madnia, *Int. J. Heat Mass Transfer*, **52**, 860-869 (2009).

[13] M-J. Huang and T-Y. Kang, *Int. J. Term. Sci.*, **50**, 1156-1163 (2011).

[14] N. Yang, G. Zhang and B. Li, *Nano Lett.*, **8**, 276-280 (2008).

[15] J. Garg, N. Bonini, B. Kozinsky and N. Marzari, *Phys. Rev. Lett.*, **106**, 045901 (2011).

[16] J. Shiomi, K. Esfarjani and G. Chen, *Phys. Rev. B*, **84**, 104302 (2011).

[17] R. Cheaito, J. C. Duda, T. E. Beechem, K. Hattar, J. F. Ihlefeld, D. L. Medlin, M. A. Rodriguez, M. J. Campion, E. S. Piekos, and P. E. Hopkins, *Phys. Rev. Lett.*, **109**, 195901 (2012).

[18] Shao-Yun Fu, B. Lauke, *Compos. Sci. Technol.*, **56**, 1179 (1996).

[19] J. Callaway, *J. Phys. Rev.* **113**,1046 (1959).

[20] N. Mingo, L. Yang, D. Li and A. Majumdar, *Nano Lett.* **3**,1713 (2003).

[21] G. Chen, *Nanoscale Energy Transport and Conversion : A Parallel Treatment of Electrons, Molecules, Phonons, and Photons : A Parallel Treatment of Electrons, Molecules, Phonons, and Photons* (Oxford University Press, Oxford, New York, 2005).

[22] Z. M. , *Nano/Microscale Heat Transfer* (Mc Graw-Hill, 2007).

[23] C. J. Glassbrenner and G. A. Slack, *Phys. Rev.* **134**, A1058 (1964).

[24] K. Kádas, L. Vitos and R. Ahuja, *Appl. Phys. Lett.* **92**, 052505 (2008).

[25] Chen, G., *Phys. Rev. B.* **57**, 14958 (1998).

CHAPTER 8

GENERAL DISCUSSION

From research, economic and engineering considerations, nanostructured materials have undergone a remarkable progress to manufacture materials for either electric power generation and solid-state cooling or thermal interface materials applications. It has been pointed out that performance improvement of these materials significantly depends on the thermal conductivity properties. It has been conceptually established and experimentally proven that boundaries produced in nanostructured materials can give the thermal conductivity a size dependence. In other words, the thermal conductivity of nanostructured materials significantly differ from their corresponding bulk thermal conductivities. Thus, the influence of dominant parameters on the thermal conductivity of nanodispersions should be determined. It is too expensive, difficult and time consuming to find experimentally an optimized nanostructure and optimized geometric factors for specific materials under different processing conditions. Meanwhile, several *ab initio* calculations have been used to study the thermal conductivity in nanostructures. However, it would be difficult to apply *ab initio* approaches to study the influence of different parameters such as orientation of anisotropic particles, agglomeration, and dispersion of hybrid nanoparticles on the thermal conductivity of nanodispersions.

Theoretical approaches are seemingly the best way to predict the thermal conductivity. However, for dispersion of nanostructured particles in a matrix, the effective thermal conductivity cannot be described by the conventional macroscopic heat transport models in which the importance of the size and time on the heat transport is not taken into account.

Despite the importance of nanodispersion materials for many practical applications, there are not many theoretical attempts which have been devoted to understand the heat carrier transport, and subsequently the thermal conductivity in nanodispersions.

Although theoretical studies can provide a reliable prediction about the thermal conductivity

of nanodispersions, the effect of some other parameters such as particle size distribution, irregularity of particle and agglomeration shapes would result in a difference between theoretical and experimental results.

The first part of this work is aimed at fundamentally understanding the possible scattering mechanisms that a heat carrier can undergo during its motion in a heterogeneous medium. For the matrix phase, it is assumed that the mean free path of the heat carrier is shortened due to multiple scattering events between the heat carrier and dispersed particles. Thus, collision and thermal boundary resistance mean free paths are defined as barriers to the heat carrier motion. The influence of particle size, volume fraction, and orientation can be clearly observed in the collision and thermal boundary resistance mean free path expressions. Also, effects of different types of scattering mechanisms including totally specular, totally diffuse, and partially specular-partially diffuse on the particle-matrix interface are explored. For the dispersed phase, the heat carrier mean free path is also significantly confined by boundaries. The collision mean free path for the dispersed phase is then defined as the distance traveled by the heat carrier before experiencing scattering at the boundary of the particle phase. Applying the Matthiessen's rule, the bulk mean free path of the heat carrier presented by the kinetic theory is modified to take the effect of different scattering mechanisms into account. Since the effective area for the heat carrier-particle scattering varies with particle geometry, for different particle shapes, different collision and thermal boundary resistance mean free paths are defined.

After making the framework, a homogeneous matrix consisting of nano spherical particles is considered as the first case study. For fully dispersion (no agglomeration) of nanoparticles in the matrix, reliability of the results is confirmed by available numerical simulation observations and experimental data. Over a wide range of temperature, the sensitivity of the thermal conductivity to the volume fraction and particle size is studied. For temperature dependent studies, specular scatterings on the matrix-particle boundary is not evaluated due to more complexity. Thus, we restrict ourself to cases where interfaces are totally diffuse. In

order to make the study more comprehensive, the sensitivity of the thermal conductivity to the dispersed particle aggregation is addressed. The importance of nonuniform dispersion of particles in nanodispersions for practical applications has been a motivation to see how the degree of agglomeration (from fully-dispersed to fully-agglomerated) can be influenced on the thermal conductivity. Depending on how compact are the agglomerates (the volume fraction of individual particles inside the agglomerate shows the degree of compaction), the thermal conductivity either decreases or increases.

After successful evaluation of the feasibility of the model for dispersion of nanospheres, the impact of anisotropic particles (nanowires) on the thermal conductivity is studied. The influence of the specularity of the nanowire-matrix interface is determined. Results show that an increase in the specularity of the interface is led to the thermal conductivity enhancement. The sensitivity of the thermal conductivity to the radius and volume fraction of nanowires is also illustrated. The analytical results are in good agreement with previous numerical results. The proposed framework is further modified to capture the influence of the nanowire length into account. It seems interesting to observe how the alignment of nanowires can control the thermal conductivity of dispersions. Results reveal that the thermal conductivity of nanodispersions decreases when the orientation of nanowires moves from parallel to the heat flow direction toward perpendicular to the heat flow direction.

The extension of the framework to include more complicated structures is sought. Thus, the thermal conductivity of the hybrid dispersion of nanospheres and nanowires is considered as the next case study. Two different methods of homogenizations are performed to determine the thermal conductivity of hybrid nanodispersions. The obtained results from both methods of homogenization are in good agreement. The importance of different governing elements such as particles size, volume fraction, orientation, specularity of the interface and etc, on the thermal conductivity of hybrid nanodispersions is illustrated.

Afterwards, the temperature dependent thermal conductivity of the hybrid dispersion of nanospheres and nanowires brings very interesting results which can be useful to design hybrid

nanodispersions for different applications. At higher temperatures, it is observed that size of particles and composition of the hybrid dispersion do not have a remarkable effect on the thermal conductivity, while in lower temperatures (room temperature) evidence of the opposite scenario is found. As another verification of the framework, thermal conductivity of nanodispersions when the cross section of nanowires changes from circle toward rectangular is taken into consideration. When compared with simulation observations of $Bi_2Te_3 - Sb_2Te_3$ and $SiGe$ nanodispersions, the presented results in this study show a good agreement over a wide range of particle size and volume fraction.

The presented framework cannot be performed on dispersion of metal nanoparticles in a non-

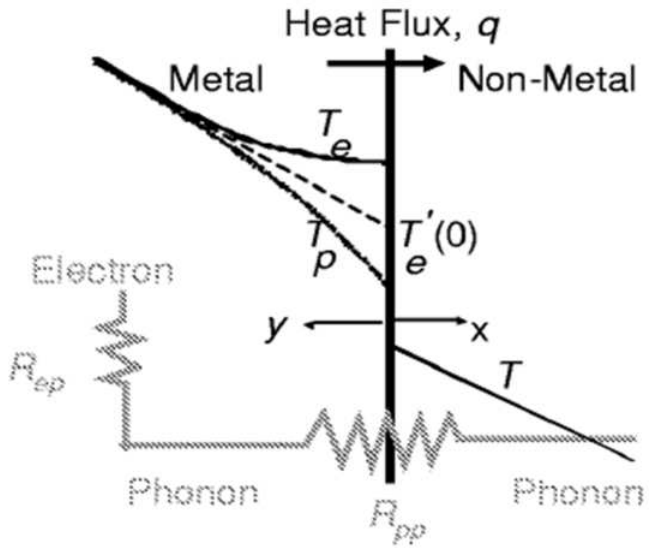

Figure 8.1 Illustration of coupling process to study heat transfer between metal and non-metal across the interface[98].

metal matrix due to domination of different types of heat carriers in metals and non-metals. Note that phonons dominate heat conduction in semiconductors and insulators whereas the heat carriers in metals are mainly electrons. This restriction can be solved by electron-phonon coupling inside the metal and subsequently considering interactions between phonons of metal and phonons of non-metal (see Figure(8.1)).

Further modifications on the framework will be required if the heat conduction in nanofluids

are desired to be included.

CONCLUSIONS AND RECOMMENDATIONS

8.1 Conclusions

In this dissertation we have developed a fundamental and comprehensive framework for investigating thermal conductivity in nanodispersions involving a large variety of particles of different sizes, volume fractions, geometries, and orientations as well as interface properties between matrix and particles. The study sheds light on how the temperature and dispersion of hybrid nanoparticles influences the thermal conductivity. The framework is based on the phonon viewpoint of heat conduction in nanostructured materials in which the phonon transport is influenced by several scattering mechanisms in the bulk and on boundaries. The following conclusions are drawn from this study :

i. For a certain volume fraction, the thermal conductivity decreases with decreasing the particle size due to strong phonon confinement effects. In other words, phonon confinement is gradually weakened as the particle size increases and consequently the thermal conductivity increases. For a specific particle size, two different scenarios can be observed for the evolution of thermal conductivity of nanodispersions as a function of particle volume fraction. For smaller particle sizes, the thermal conductivity decreases with increasing the volume fraction due to monotonic increase in effective area for phonon-boundary scattering. For large particle sizes, boundary scattering effects are gradually weakened and effective thermal conductivities of the matrix and dispersed particles tend toward their corresponding bulk values. In this condition, if the bulk thermal conductivity of dispersed phase is higher than the matrix, the thermal conductivity of dispersion will increase with increasing the volume fraction.

ii. It was observed that the thermal conductivity is very sensitive to the interface properties between matrix and dispersed particles. The larger is the specularity of the interface the lower is the phonon confinement at the interface and consequently the higher is the thermal conductivity of nanodispersion. For incorporation of anisotropic particles in a host matrix,

the thermal conductivity appears to be larger when all particles are aligned in heat flow direction. The thermal conductivity of nanodispersions monotonically decreases when the orientation of nanodispersed particles shifts from parallel to the direction of heat flux toward perpendicular to the direction of heat flux.

iii. Depending on degrees of agglomeration of the dispersed particles (from fully dispersed to fully aggregated) as well as degrees of compactness of the agglomerates, either an increase or a decrease in the thermal conductivity of nanodispersions was observed.

iv. Fabrication of dispersions consisting hybrid nanospheres and nanowires gives an opportunity to benefit from the properties of both nanospheres and nanowires.

It was also concluded that composition, size, shape and orientation of nanoparticles do not play a dominant role on the thermal conductivity of hybrid dispersions when the temperature is high. At higher temperatures, internal (phonon-phonon) scattering events are more likely and are more significant than boundary (phonon-boundary) scattering events. On the other hand, at lower temperatures, boundaries produced by nanoscale particles create strong obstacles against phonon transport which then implies the thermal conductivity reduction. Consequently, for high temperature applications, we can not benefit from fabrication of hybrid dispersions. A similar trend is observed for temperature evolution of the thermal conductivity for dispersions consisting uniform nanoparticles.

8.2 Recommendations

The following aspects are recommended for more exploration in future studies :

i. In view of the importance of the electrical conductivity particularly in thermoelectric materials, further studies on the influence of particle size, volume fraction, shape, orientation, degree of dispersion as well as temperature on the electrical conductivity of nanodispersions is recommended.

ii. To develop presented framework for nanoporous materials. Note that nanoporous materials with thermal insulating properties appear to be attractive candidates for sensor development.

iii. To extent the framework for the thermal and electrical conductivities of nanofluids by considering the influence of the Brownian motion of nanoparticles.

iv. To present an effective thermal conductivity expression in dispersion of nanometals in a non-metal matrix by gaining further insight into the heat conduction mechanism across interfaces between metal and non-metal materials.

v. To study the influence of some important parameters such as interparticle distance effect and tunnelling process between dispersed particles on the thermal conductivity of dispersions consisting nanoparticles with different shapes.

vi. To measure the thermal conductivity of nanodispersions in melt state by transient heat conduction method. To study the influence of the shear rate on the nanoparticle orientation and consequently on the thermal conductivity of nanodispersions.

REFERENCES

[1] Mildred S. Dresselhaus, Gang Chen, Ming Y. Tang, Ronggui Yang, Hohyun Lee, Dezhi Wang, Zhifeng Ren, Jean-Pierre Fleurial, and Pawan Gogna. New directions for low-dimensional thermoelectric materials. *Advanced Materials*, vol. 19 :pp. 1043–1053, 2007.

[2] A. J. Minnich, M. S. Dresselhaus, Z. F. Ren, and G. Chen. Bulk nanostructured thermoelectric materials : current research and future prospects. *Energy and Environmental Science*, vol. 2 :pp. 466–479, 2009.

[3] F. J. Disalvo. Thermoelectric cooling and power generation. *Science*, vol. 285 :pp. 703–706, 1999.

[4] J-F. Li, W-S. Liu, L-D. Zhao, and M. Zhou. High-performance nanostructured thermoelectric materials. *NPG Asia Materials*, vol. 2 :pp. 152–158, 2010.

[5] M. G. Kanatzidis. Nanostructured thermoelectrics : The new paradigm. *Chemistry of Materials*, vol. 22 :pp. 648–659, 2010.

[6] L. D. Hicks and M. S. Dresselhaus. Effect of quantum-well structures on the thermoelectric figure of merit. *Physical Review B*, vol. 47 :pp. 12727, 1993.

[7] M. Zebarjadi, K. Esfarjani, M. S. Dresselhaus, Z. F. Ren, and G. Chen. Perspectives on thermoelectrics : from fundamentals to device applications. *Energy and Environmental Science*, vol. 5 :pp. 5147–5162, 2012.

[8] C. J. Vineis, A. Shakouri, A. Majumdar, and M. G. Kanatzidis. Nanostructured thermoelectrics : Big efficiency gains from small features. *Advanced Materials*, vol. 22 : pp. 3970–3980, 2010.

[9] M. Martin-Gonzalez, O. Calballero-Calero, and P. Diaz-Chao. Nanoengineering thermoelectrics for 21st century : Energy harvesting and other trends in the field. *Renewable and Sustainable Energy Reviews*, vol. 24 :pp. 288–305, 2013.

[10] C. Kang, H. Kim, S-G Park, and W. Kim. Comparison of thermal conductivity in nanodot nanocomposites and nanograined nanocomposites. *Applied Physics Letters*, vol. 96 :pp. 213114, 2009.

[11] L. E. Bell. Cooling, heating, generating power, and recovering waste heat with thermoelectric systems. *Science*, vol. 321 :pp. 1457–1461, 2008.

[12] D. Rowe. *Thermoelectrics Handbook : Macro to Nano*. CRC Press, Boca Raton, 2006.

[13] J. Ma, O. Delaire, A. F. May, C. E. Carlton, M. A. McGuire, L. H. VanBebber, D. L. Abernathy, G. Ehlers, T. Hong, A. Huq, W. Tian, V. M. Keppens, Y. Shao-Horn, and B. C. Sales. Glass-like phonon scattering from a spontaneous nanostructure in $AgSbTe_2$. *Nature Nanotechnology*, vol. 8 :pp. 445–451, 2013.

[14] L-D. Zhao, V. P. Dravid, and G. Kanatzidis. The panasonic approach to high performance thermoelectrics. *Energy and Environmental Science*, vol. 7 :pp. 251–268, 2014.

[15] G. Jeffrey Snyder and Eric S. Toberer. Complex thermoelectric materials. *Nature Materials*, vol. 7 :pp. 105–114, 2008.

[16] A. I. Hochbaum, R. Chen, R. D. Delgado, W. Liang, E. C. Garnett, M. Najarian, A. Majumdar, and P. Yang. Enhanced thermoelectric performance of rough silicon nanowires. *Nature*, vol. 451 :pp. 163–167, 2008.

[17] B. Poudel, Q. Hao, Y. Ma, Y. Lan, A. Minnich, B. Yu, X. Yan, D. Wang, A. Muto, D. Vashaee, X. Chen, J. Liu, M. S. Dresselhaus, G. Chen, , and Z.F. Ren. High-thermoelectric performance of nanostructured bismuth antimony telluride bulk alloys. *Science*, vol. 320 : pp. 634–638, 2008.

[18] G. H. Zhu, H. Lee, Y. C. Lan, X.W. Wang, G. Joshi, D. Z. Wang, J. Yang, D. Vashaee, H. Guilbert, A. Pillitteri, M. S. Dresselhaus, G. Chen, and Z. F. Ren. Increased phonon scattering by nanograins and point defects in nanostructured silicon with a low concentration of germanium. *Physical Review Letters*, vol. 102 :pp. 196803, 2009.

[19] Joseph P. Feser, Emory M. Chan, Arun Majumdar, Rachel A. Segalman, and Jeffrey J. Urban. Ultralow thermal conductivity in polycrystalline cdse thin films with controlled grain size. *Nano Letters*, vol. 13 :pp. 2122–2127, 2013.

[20] Zong-Yue Li, Jing-Feng Li, Wen-Yang Zhao, Qing Tan, Tian-Ran Wei, Chao-Feng Wu, and Zhi-Bo Xing. Pbte-based thermoelectric nanocomposites with reduced thermal conductivity by sic nanodispersion. *Applied Physics Letters*, vol. 104 :pp. 113905, 2014.

[21] Alexander A. Balandin. Thermal properties of graphene and nanostructured carbon materials. *Nature Materials*, vol. 10 :pp. 569–581, 2011.

[22] Khan M. F. Shahil and Alexander A. Balandin. Graphene multilayer graphene nanocomposites as highly efficient thermal interface materials. *Nano Letters*, vol. 12 :pp. 861–867, 2012.

[23] Jan Felba. *Thermally Conductive Nanocomposites In Nano-Bio- Electronic, Photonic and MEMS Packaging*. 2010. See page 277-314, editor Wong, C.P. and Moon, Kyoung-Sik and Li, Yi.

[24] Y. Xu, D. D. L. Chung, and C. Mroz. Thermally conducting aluminum nitride polymer-matrix composites. *Composites Part A : Applied Science and Manufacturing*, vol. 32 : pp. 1749–1757, 2001.

[25] Y. Xu and D. D. L. Chung. Increasing the thermal conductivity of boron nitride and aluminum nitride particle epoxy-matrix composites by particle surface treatments. *Composite Interfaces*, vol. 7 :pp. 243–256, 2000.

[26] X. Huang, T. Iizuka, P. Jiang, Y. Ohki, and T. Tanaka. Role of interface on the thermal conductivity of highly filled dielectric epoxy/aln composites. *Journal of Physical Chemistry C*, vol. 116 :pp. 13629–13639, 2012.

[27] A. Yu, P. Ramesh, M. E. Itkis, E. Bekyarova, and R. C. Haddon. Graphite nanoplatelet-epoxy composite thermal interface materilas. *Journal of Physical Chemistry C*, vol. 111 : pp. 7565–7569, 2007.

[28] X. Tian, M. E. Itkis, E. B. Bekyrova, and R. C. Haddon. Anisotropic thermal and electrical properties of thin thermal interface layers of graphite nanoplatelet-based composites. *Scientific Reports*, vol. 3 :pp. 1710, 2013.

[29] A. Yu, P. Ramesh, X. Sun, E. Bekyarova, M. E. Itkis, and R. C. Haddon. Enhanced thermal conductivity in a hybrid nanoplatelet-caron nanotube filler for epoxy composites. *Advanced Materials*, vol. 20 :pp. 4740–4744, 2008.

[30] Zhoumin M. Zhang. *Nano/Microscale heat transfer*. New York ; Toronto : McGraw-Hill, 2007.

[31] T. M. Tritt. *Thermal Conductivity, Theory, Properties and Applications*. Kluwer Academic/Plenum Publishers, New York, 2004.

[32] Chen Gang. *Nanoscale energy transport and conversion : a parallel treatment of electrons, molecules, phonons, and photons*. New York : Oxford University Press, 2005.

[33] M. J. Fryer and H. Struchtrup. Moment model and boundary conditions for energy transport in the phonon gas. *Continuum Mechanics Thermodynamic*, vol. 26 :pp. 593–618, 2014.

[34] Gang Chen. Phonon heat conduction in nanostructures. *International Journal of Thermal Science*, vol. 39 :pp. 471–480, 2000.

[35] Gang Chen. Particularities of heat conduction in nanostructures. *Journal of Nanoparticle Research*, vol. 2 :pp. 199–204, 2000.

[36] G. H. Tang, Y. Zhao, G. X. Zhai, and C. Bi. Phonon boundary scattering effect on thermal conductivity of thin films. *Journal of Applied Physics*, vol. 110 :pp. 046102, 2011.

[37] S. Volz. *Microscale and NanoscaleHeat Transfer*. Springer, 2007.

[38] J. E. Turney, A. J. H. McGaughey, and C. H. Amon. In-plane phonon transport in thin films. *Journal of Applied Physics*, vol. 107 :pp. 024317, 2010.

[39] D. P. Sellan, J. E. Turney, A. J. H. McGaughey, and C. H. Amon. Cross-plane phonon transport in thin films. *Journal of Applied Physics*, vol. 108 :pp. 113524, 2010.

[40] R. Yang, G. Chen, and M. S. Dresselhaus. Thermal conductivity of simple and tubular nanowire composites in the longitudinal direction. *Physical Review B*, vol. 72 :pp. 125418, 2005.

[41] Xiaopeng Huang, Xiulan Huai, Shiqiang Liang, and Xinwei Wang. Thermal transport in si/ge nanocomposites. *Journal of Physics D : Applied Physics*, vol. 42 :pp. 095416, 2009.

[42] Feng Hao, Daining Fang, and Zhiping Xu. Thermal transport in crystalline si/ge nanocomposites : Atomistic simulations and microscopic models. *Applied Physics Letters*, vol. 100 :pp. 091903, 2012.

[43] R. Yang and G. Chen. Thermal conductivity modeling of periodic two-dimensional nanocomposites. *Physical Review B*, vol. 69 :pp. 195316, 2004.

[44] R. Yang, G. Chen, and M. S. Dresselhaus. Thermal conductivity of modeling of core-shell and tubular nanowires. *Nano Letters*, vol. 5 :pp. 1111–1115, 2005.

[45] W. Tian and R. Yang. Thermal conductivity modeling of compacted nanowire composites. *Journal of Applied Physics*, vol. 101 :pp. 054320, 2007.

[46] A. Pattamatta and C. K. Madnia. Modeling heat transfer in $Bi_2Te_3\breve{}Sb_2Te_3$ nanostructures. *International Journal of Heat and Mass Transfer*, vol. 52 :pp. 860–869, 2009.

[47] T-Y. Hsieh, J-Y. Yang, and Z-C. Hong. Thermal conductivity modeling of compacted type nanocomposites. *Journal of Applied Physics*, vol. 106 :pp. 023528, 2009.

[48] W. Tian, H. Hu, and Y. Sun. A molecular dynamic study of effective thermal conductivity in nanocomposites. *International Journal of Heat and Mass Transfer*, vol. 61 : pp. 577–582, 2013.

[49] David G. Cahill, Paul V. Braun, Gang Chen, David R. Clarke, Shanhui Fan, Kenneth E. Goodson, Pawel Keblinski, William P. King, Gerald D. Mahan, Arun Majumdar, Humphrey J. Maris, Simon R. Phillpot, Eric Pop, and Li Shi. Nanoscale thermal transport. ii. 2003–2012. *Applied Physics Reviews*, vol. 1 :pp. 011305, 2014.

[50] C. L. Tien, A. Majumdar, and F. M. Gerner. *Microscale Energy Transport*. Taylor and Francis, Washington,DC, 1997.

[51] M. Asheghi, K. Kurabayashi, R. Kasnavi, and K. E. Goodson. Thermal conduction in doped single-crystal silicon films. *Journal of Applied Physics*, vol. 91 :pp. 5079–5088, 2002.

[52] C. Dames and G. Chen. Theoretical phonon thermal conductivity of si/ge superlattice nanowires. *Journal of Applied Physics*, 95 :682, 2004.

[53] J. Callaway. Model for lattice thermal conductivity at low temperatures. *Physical Review*, vol. 113 :pp. 1046–1051, 1959.

[54] N. Mingo, L. Yang, D. Li, and A. Majumdar. Predicting the thermal conductivity of si and ge nanowires. *Nano Letters*, vol. 3 :pp. 1713–1716, 2003.

[55] W. Kim, J. Zide, A. Gossard, D. Klenov, S. Stemmer, A. Shakouri, and A. Majumdar. Thermal conductivity reduction and thermoelectric figure of merit increase by embedding nanoparticles in crystalline semiconductors. *Physical Review Letters*, vol. 96 :pp. 045901, 2006.

[56] C. Kittel. *Introduction to Solid State Physics*. John Wiley, 1996.

[57] J. Yang, D. T. Morelli, G. P. Meisner, W. Chen, J. S. Dyck, and C. Uher. Infuence of electron-phonon interaction on the lattice thermal conductivity of $Co_{1-x}Ni_xSb_3$. *Physical Review B*, vol. 65 :pp. 094115, 2002.

[58] Patrick E. Hopkins, Peter T. Rakich, Roy H. Olsson, Ihab F. El-kady, and Leslie M. Phinney. Origin of reduction in phonon thermal conductivity of microporous solids. *Applied Physics Letters*, vol. 95 :pp. 161902, 2009.

[59] C. B. Satterthwaite and J. R. W. Ure. Electrical and thermal properties of Bi_2Te_3. *Physical Review*, vol. 108 :pp. 1164–1170, 1957.

[60] B. Qiu and X. Ruan. Molecular dynamics simulations of lattice thermal conductivity of bismuth telluride using two-body interatomic potentials. *Physical Review B*, vol. 80 : pp. 165203, 2009.

[61] Ganesh Balasubramanian and Ishwar K. Puri. Heat conduction across a solid-solid interface : Understanding nanoscale interfacial effects on thermal resistance. *Applied Physics Letters*, vol. 99 :pp. 013116, 2011.

[62] E.-K. Kim, S.-I. Kwun, S.-M. Lee, H. Seo, and J.-G. Yoon. Thermal boundary resistance at $Ge_2Sb_2Te_5/ZnS : SiO_2$ interface. *Applied Physics Letters*, vol. 76 :pp. 3864, 2000.

[63] J. Alvarez-Quintana, J. L. Labar, and J. Rodriguez-Viejo. Ultra-low thermal conductivity in nanoscale layered oxides. *Journal of Heat Transfer*, vol. 132 :pp. 032402, 2010.

[64] Yee Kan Koh, Yu Cao, David G. Cahill, and Debdeep Jena. Heat-transport mechanisms in superlattices. *Advanced Functional Materials*, vol. 19 :pp. 610–615, 2009.

[65] Patrick E. Hopkins, Pamela M. Norris, and Robert J. Stevens. Influence of inelastic scattering at metal-dielectric interfaces. *Journal of Heat Transfer*, vol. 130 :pp. 022401, 2008.

[66] Sergei Shenogin, Liping Xue, Rahmi Ozisik, Pawel Keblinski, and David G. Cahill. Role of thermal boundary resistance on the heat flow in carbon-nanotube composites. *Journal of Applied Physics*, vol. 95 :pp. 8136, 2004.

[67] N. Khosravian, M. K. Samani, G. C. Loh, G. C. K. Chen, D. Baillargeat, and B. K. Tay. Molecular dynamic simulation of diamond/silicon interfacial thermal conductance. *Journal of Applied Physics*, vol. 113 :pp. 024907, 2013.

[68] W. A. Little. The transport of heat between dissimilar solids at low temperatures. *Canadian Journal of Physics*, vol. 37 :pp. 334–349, 1959.

[69] E. T. Swartz and R. O. Pohl. Thermal-boundary resistance. *Reviews of Modern Physics*, vol. 61 :pp. 605–668, 1989.

[70] Patrick E. Hopkins and Pamela M. Norris. Relative contributions of inelastic and elastic diffuse phonon scattering to thermal boundary conductance across solid interfaces. *Journal of Heat Transfer*, 131 :022402, 2009.

[71] Patrick E. Hopkins. Multiple phonon processes contributing to inelastic scattering during thermal boundaryconductance at solid interfaces. *Journal of Applied Physics*, 106 : 013528, 2009.

[72] F. X. Alvarez, J. Alvarez-Quintana, D. Jou, and J. Rodriguez Viejo. Analytical expression for thermal conductivity of superlattices. *Journal of Applied Physics*, 107 :084303, 2010.

[73] Gang Chen. Thermal conductivity and ballistic phonon transport in the cross plane direction of superlattices. *Physical Review B*, vol. 57 :pp. 14958, 1998.

[74] M. Szymanski. Calculation of the cross-plane thermal conductivity of a quantum cascade laser active region. *Journal of Physics D : Applied Physics*, vol. 44 :pp. 085101, 2011.

[75] C. Maxwell. *A Treatise on Electricity and Magnetism*. Clarendon, Oxford, 1904.

[76] Y. Benveniste. Effective thermal conductivity of composites with a thermal contact resistance between the constituents : Nondilute case. *Journal of Applied Physics*, vol. 61 : pp. 2840–2843, 1987.

[77] C-W Nan, R. Birringer, D. R. Clarke, and H. Gleiter. Effective thermal conductivity of particulate composites with interfacial thermal resistance. *Journal of Applied Physics*, vol. 81 :pp. 6692, 1997.

[78] D. P. H. Hasselman and L. F. Johnson. Effective thermal conductivity of composites with interfacial thermal barrier resistance. vol. 21 :pp. 508–515, 1987.

[79] Z. Hashin. Assessment of the self consistent scheme approximation : Conductivity of particulate composites. *Journal of Composite Materials*, vol. 2 :pp. 284–300, 1968.

[80] J. Ordonez-Miranda, R. Yang, and J. J. Alvarado-Gil. On the thermal conductivity of particulate nanocomposites. *Applied Physics Letters*, vol. 98 :pp. 233111, 2011.

[81] A. Minnich and G. Chen. Modified effective medium formulation for the thermal conductivity of nanocomposites. *Applied Physics Letters*, vol. 91 :pp. 073105, 2007.

[82] R. Prasher. Thermal conductivity of composites of aligned nanoscale and microscale wires and pores. *Journal of Applied Physics*, vol. 100 :pp. 034307, 2006.

[83] X. Lu. Longitudinal thermal conductivity of radial nanowire heterostructure. *Applied Physics Letters*, vol. 106 :pp. 064305, 2009.

[84] A. J. H. McGaughey, E. S. Lamdry, D. P. Sellan, and C. H. Amon. Size-dependent model for thin film and nanowire thermal conductivity. *Applied Physics Letters*, vol. 99 : pp. 131904, 2011.

[85] E. H. Sondheimer. The mean free path of electrons in metals. *Advances in Physics*, vol. 50 :pp. 499–537, 2001.

[86] A. Majumdar. Microscale heat conduction in dielectric thin films. *Journal of Heat Transfer*, vol. 115 :pp. 7–16, 1993.

[87] M. Maldovan. Micro to nano scale thermal energy conduction in semiconductor thin films. *Journal of Applied Physics*, vol. 110 :pp. 034308, 2011.

[88] A. Sellitto, F. X. Alvarez, and D. Jou. Phonon-wall interactions and frequency-dependent thermal conductivity in nanowires. *Journal of Applied Physics*, 109 :064317, 2011.

[89] F. X. Alvarez, D. Jou, and A. Sellitto. Phonon boundary effects and thermal conductivity of rough concentric nanowires. *Journal of Heat Transfer*, 133 :022402, 2010.

[90] F. X. Alvarez and D. Jou. Size and frequency dependence of effective thermal conductivity in nanosystems. *Journal of Applied Physics*, 103 :094321, 2008.

[91] F. X. Alvarez and D. Jou. Memory and nonlocal effects in heat transport : From diffuse to ballistic regimes. *Applied Physics Letters*, 90 :083109, 2007.

[92] H. Huang, C. Liu, Y. Wu, and S. Fan. Aligned carbon nanotube composites films for thermal management. *Advanced Materials*, vol. 17 :pp. 1652–1656, 2005.

[93] S. Ghose, K. A. Watson, D. C. Working, J. W. Connell, J. G. Smith Jr, and Y. P. Sun. Thermal conductivity of ethylene vinyl acetate copolymer/nanofiller belnds. *Composites Science and Technology*, vol. 68 :pp. 1843–1853, 2008.

[94] F. Gong, K. Bui, V. Papavassiliou, and H. M. Duong. Thermal transport phenomena and limitations in heterogeneous polymer composites containing carbon nanotubes and inorganic nanoparticles. *Carbon*, vol. – :pp. –, 2014.

[95] M. J. Huang and T. Y. Kang. A monte-carlo study of the phonon transport in nanowire-embedded composites. *International Journal of Thermal Sciences*, vol. 50 :pp. 1156–1163, 2011.

[96] S. J. Poon, A. S. Petersen, and D. Wu. Thermal conductivity of core-shell nanocomposites for enhancing thermoelectric performance. *Journal of Applied Physics*, vol. 102 : pp. 173110, 2013.

[97] S. J. Poon and K. Limtragool. Nanostructure model of thermal conductivity for high thermoelectric performance. *Journal of Applied Physics*, vol. 110 :pp. 114306, 2011.

[98] Majumdar A and P. Reddy. Role of electron-phonon coupling in thermal conductance of metal-nonmetal interfaces. *Applied Physics Letters*, vol. 84 :pp. 4768, 2004.